Constitutive Modeling of the Resilient Response of Granular Solids

Thesis by
Ertugrul Taciroglu

B.S., Istanbul Technical University, 1993
M.S., University of Illinois at Urbana−Champaign, 1995

In Partial Fulfillment of the Requirements
for the Degree of
Doctor of Philosophy

University of Illinois at Urbana − Champaign
Urbana, Illinois
1998

To my parents and my sisters
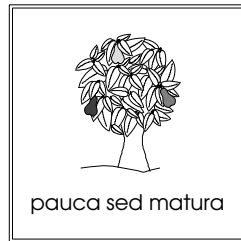
pauca sed matura

Acknowledgements

Abstract

A constitutive model is the mathematical relationship between load and displacements within the context of solid mechanics. The objective of this study is to investigate, to develop and to implement to finite element method, constitutive models of the resilient response of granular solids. These models are mainly used in analysis and design of airport and highway pavements; they characterize the response of granular layers in pavements under repeated wheel loads.

Two well known nonlinear elastic models, based on the concept of resilient modulus are investigated in detail. Due to their success in organizing the response data from cyclic triaxial tests and their success relative to competing material models in predicting the behavior observed in the field, these two models, namely the *K–* and the *Uzan–Witzcak* models, have been implemented to many computer programs used by researchers and design engineers. However, all of these implementations have been made to axisymmetric finite element codes which preclude the study of the effects of multiple wheel loads. This study provides a careful analysis of the behavior of these models and addresses the issue of effectively implementing them in a conventional 3–dimensional finite element analysis framework.

Also in this study, a new coupled constitutive model based on hyperelasticity is proposed to capture the resilient behavior granular materials. The coupling property of the proposed model accounts for the shear dilatancy and pressure–dependent behavior of the granular materials. This model is demonstrated to yield better fits to experimental data than the *K–* and the *Uzan–Witzcak* models.

Due to their particulate nature, granular materials usually cannot develop tensile stresses under applied loading. To this end, several modifications to the coupled hyperelastic model are developed with which the built up of tensile hydrostatic pressure is limited. Another model based on an elastic projection operator is formulated. This model effectively eliminates all tensile stresses. As opposed to the coupled hyperelastic model which is formulated using strain invariants, this model is based on a formulation in terms of principal stresses. The difficulties in achieving a robust implementation of this model to the finite element method are resolved.

Finally, a few sample boundary value problems are analyzed with the finite element method to demonstrate the response predicted by the models described above.

List of Figures

List of Tables

Table of Contents

Chapter 3. A Simple Coupled Hyperelastic Model   28

Chapter 4. Determination of Material Constants   45

Chapter 5. A Projection Operator for No–Tension Elasticity   52

Chapter 6. Finite Element Analysis of a Pavement System   70

Chapter 7. Closure   78

Bibliography   80

Appendix   84

Chapter 1

Introduction

1.1 Objective and Outline

A constitutive model is the mathematical relationship which relates the stresses (loads) to the strains (displacements) in a medium. A good constitutive model should be capable of capturing the essential aspects of load-deformation characteristics of the material which it intends to represent and the boundary value problem that it will be used for. The parameters (material constants) of a constitutive model should be measurable — directly or indirectly — via laboratory tests. It is also desirable that minor changes in the values of the material constants result in correspondingly minor changes in the solution of the boundary value problem. Furthermore, a good constitutive model should be amenable to large-scale computation. Perhaps the most important of all, a good constitutive model should obey the laws of thermodynamics.

The objective of this study is to investigate, to develop and to implement to finite element method constitutive models for the resilient response of granular solids. As it will be presented later in detail, such constitutive models are mainly used in analysis and design of airport and highway pavements. The aim of these models is to characterize the behavior of granular layers in pavement systems under repeated loads. Following is an outline of the contents of this study.

Chapter 2. A brief survey of analysis methods and state–of–the–art computer programs used in pavement analysis are presented. Two nonlinear elastic constitutive models, namely $K - \theta$ and *Uzan–Witzcak* models, are investigated in detail and a consistent implementation of these models to the finite element method is provided. These are two well known nonlinear elastic constitutive models used in analysis and design of airport and highway pavements. These models aim to characterize the response of granular layers in pavement systems under repeated loads. Numerous implementations of $K - \theta$ and *Uzan–Witzcak* models exist. However, all of these implementations have been made to axisymmetric finite element codes which preclude the study of the effects of multiple wheel loads, such as the tandems of trucks, automobiles or the landing gear of aircraft. In addition to this drastic shortcoming, these codes use –as will be investigated in detail– a *quasi–fixed–point iteration* technique for the solution of nonlinear field equations with ad hoc modifications to improve convergence, rendering the analyses of large scale boundary value problems virtually intractable. A strain–based formulation of these two models is obtained which allows their implementation in a conventional finite element

analysis framework and the convergence properties of various finite element solution techniques is studied.

Chapter 3. A coupled constitutive model based on hyperelasticity is proposed to capture the resilient behavior of granular materials. The coupling property of the proposed model accounts for shear dilatancy and pressure-dependent behavior of the granular materials. Also, a framework to derive similar (coupled hyperelastic) material models is provided. Due to their particulate nature, granular materials cannot bear tensile hydrostatic loads. To this end, several modifications to the proposed model is investigated with which the material fails when the volumetric strain becomes positive.

Chapter 4. This chapter dedicated to finding the material constants from experimental data. The calibration is done using triaxial resilient test data obtained from available literature (Allen 1973). A statistical comparison is made between the predictions of the models presented in Chapter 2, Chapter 3 and those of Linear Elasticity.

Chapter 5. In this chapter, a constitutive model based on a tensor–valued projection operator is presented. This model effectively eliminates all tensile stresses. As opposed to the model(s) presented in Chapter 3 which are formulated using stress and strain invariants, the formulation of this constitutive model is made in principal stress space. The difficulties in achieving a robust implementation are resolved and solutions to a few boundary value problems are obtained as a demonstration.

Chapter 6. The critical response of a multi–layered half–space structure, representative of a pavement, containing a layer whose behavior is governed by the models presented in Chapters 2, 3 and linear elasticity are obtained under applied (wheel) loads by finite element analysis.

Appendix. The implementations throughout this study are made to a commercial finite element analysis program (ABAQUS, 1994) by its user–defined subroutines (*UMAT*). A brief overview of the use of *UMAT* subroutine is presented in Appendix I. The source code of the implementation of the models presented in Chapter 2 is provided in Appendix II as an example. Finally, the experimental data (Allen, 1973) used in this study is presented in Appendix III.

1.2 Background

The mechanics of particulate (granular) media has been an important concern in many disciplines of engineering and science. Many civil engineering applications use granular materials as a construction material (pavements, foundation structures, dams, etc.), while some other applications require storing, containing, and transporting granular materials (silos, retaining walls, etc.). In fields like earthquake and geotechnical engineering accurate modelling of the behavior of granular materials (soils, sand, rock) under loading is crucial to determining stability of slopes and liquefaction potential. Occasion-

ally, simplified approaches to the representation of the complex and often unpredictable behavior of such materials has led to disaster (see, for example, Guterl 1997).

There are two major approaches to the mathematical characterization of the behavior of granular materials under applied loading (constitutive modelling):

1. *Particulate mechanics approach* in which the *"macroscopic"* (continuum) stress-strain relationships are studied in terms of *"microscopic"* interactions and behavior of the individual constituent elements of particulate media. This approach also makes use of probabilistic theory to capture the stochastic nature of inter-particle contact relationships (see for example Harr 1977).

2. *Phenomenological (continuum) approach* in which the *"microscopic"* effects are averaged and the particulate medium is idealized as a continuum (see for example Desai 1984, Chen 1994).

The first of these two approaches is rather complex and may not be particularly fruitful in most engineering applications, whereas the second approach may lead to gross miscalculations due to the stochastic nature of the behavior of granular materials. The constitutive models that are investigated in this report belong to the second category.

1.2.1 Granular Layers in Pavements

Since the constitutive models we are dealing with are to be used in analysis and design of pavements, let us define, in general terms, what a pavement is and why granular materials are used as components of pavement systems. From the perspective of continuum mechanics, pavements are multi-layered, half-space structures and the applied loadings are primarily wheel loads (Figure 1.1).
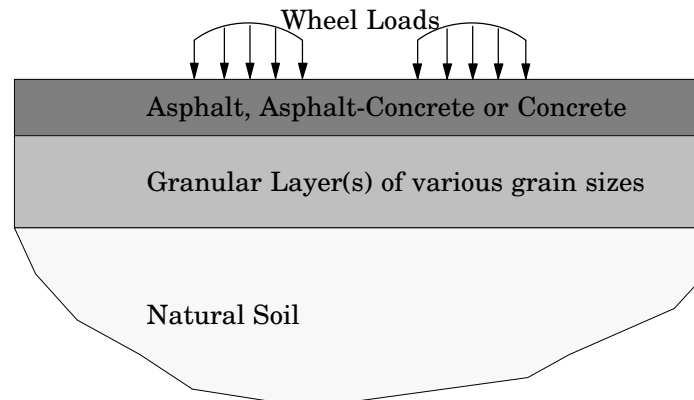
Figure 1.1. A Generic Pavement System

Granular materials are used as subgrade layers to transfer the loads from high quality (more expensive) top layers to the usually untreated and semi-infinite soil. From an eco-

nomical point of view, granular layers are used because they have better load bearing qualities than natural soil and are cheaper than high quality materials that constitute the top layers of a pavement system. The relatively larger grain size of granular layers help drain or safely contain the water that might be present within the structure. This attribute of granular materials also helps to control pumping, which is the loss of subgrade material via seepage through cracks and joints of a pavement under repeated loading when the water table is close to the surface (for other benefits of using granular materials see, for example, Huang 1993).

The earliest elasticity solution of a linear elastic half-space under surface loads can be traced back to Boussinesq (1885). Burmister (1945) offered a solution for multi-layered half-space structures composed of linear elastic materials under loads with cyclic symmetry . Westergaard (1947) provided an approximate solution for concrete pavements using plate theory . With the advent of computers, Burmister's and Westergaard's solutions were implemented to numerous computer codes and these codes are still being used as pavement design and analysis tools.

Increased traffic loads and advances in computational mechanics prompted researchers to investigate nonlinear material models to replace the linear elastic model used in pavement analysis and design. Since the mid-1970's, a variety of nonlinear models have been proposed and a number of them have been implemented to design and analysis codes. Almost exclusively, the proposed constitutive models in this area are based on elasticity theory, thus ignore inelastic deformations which accumulate in a pavement system due to repeated wheel loads and compaction. This trend is due to a hypothesis called *"resilient behavior"*. In the what follows, we will explain what is meant by *resilient behavior*, and later on, the formulation of a few resilient response models which are based on this hypothesis.

Chapter 2

An Analysis and Implementation of Resilient Modulus Models of Response of Granular Solids

2.1 Introduction

Resilient modulus models, like $K-\theta$ and Uzan–Witczak, are popular material models used in analysis and design of pavement systems. These constitutive models are motivated by the observation that the granular layers used in pavement construction shakedown quickly to elastic response under the repeated loading that is typically felt by these systems. Due to their simplicity, their great success in organizing the response data from cyclic triaxial tests, and their success relative to competing material models in predicting the behavior observed in the field, these models have been implemented into many computer programs used by researchers and design engineers. This chapter provides a careful analysis of the behavior of these models and addresses the issue of effectively implementing them in a conventional nonlinear 3–dimensional finite element analysis framework. Also, we develop bounds on the material parameters and present two competitive methods for global analysis with these models.

2.1.1 Resilient Behavior and Formulation

It is generally accepted that granular materials shake down to resilient (elastic) behavior under repeated loading (Allen 1973, Huang 1993). The response of a granular soil sample under repeated loading is shown schematically for a typical triaxial load test in Figure 2.1. Initially, the sample experiences inelastic deformations. The amount of plastic flow decreases with cycling until the response is essentially elastic. In the literature the "resilient modulus" M_r, which is the ratio of the deviator stress to the axial strain at shakedown, is recorded. Extensive efforts have been made to characterize the resilient modulus with the associated stress state. Perhaps the earliest model is the so-called $K-\theta$ model which suggests that the resilient modulus is proportional to the absolute value of the mean stress raised to a power, or

$$M_r(\theta) = K\theta^n \tag{2.1}$$

where $\theta \equiv \frac{1}{3}|\sigma_1 + 2\sigma_2|$ is the mean pressure acting on the sample in a triaxial test (Hicks and Monismith 1971). The $K-\theta$ model has become a very popular material model, partly

5

due to its simplicity, and has been widely used in practice since the late 1970s. Uzan (1985) observed that the $K-\theta$ model did not summarize measured data well when shear stresses were significant, and proposed a three parameter model of the form

$$M_r(\theta, \sigma_d) \;=\; K\theta^n \sigma_d^m \tag{2.2}$$

where $\sigma_d \equiv |\sigma_1 - \sigma_2|$ is the effective shear stress in a triaxial test configuration. Witczak and Uzan (1988) generalized the model of Eq. (2.2) by observing that σ_d coincided with the octahedral shear stress when the stress state is restricted to the triaxial test configuration. The generalized model was expressed as follows:

$$M_r(\theta, \tau) \;=\; K\theta^n \tau^m \tag{2.3}$$

where $\theta \equiv |\sigma|$ and $\sigma \equiv \frac{1}{3}\text{tr}(\mathbf{S})$ is the first invariant of the stress tensor $\mathbf{S}$ and τ is the octahedral shear stress, given in terms of the stress tensor through the expression

$$\tau^2 \;\equiv\; \frac{1}{3}\text{tr}(\overline{\mathbf{S}}^2) \tag{2.4}$$

where $\text{tr}(\overline{\mathbf{S}}^2) = \overline{S}_{ij}\overline{S}_{ij}$ is the second invariant of the deviator stress $\overline{\mathbf{S}} = \mathbf{S} - \sigma\mathbf{I}$. Note that for $m = 0$ the Uzan-Witczak model reduces to the $K-\theta$ model. Many alternatives and a number of modifications to this model, aimed at giving a better fit to resilient triaxial test data and field measured values, have been proposed by other researchers (May and Witczak 1981, Brown and Pappin 1981, and Boyce 1980).
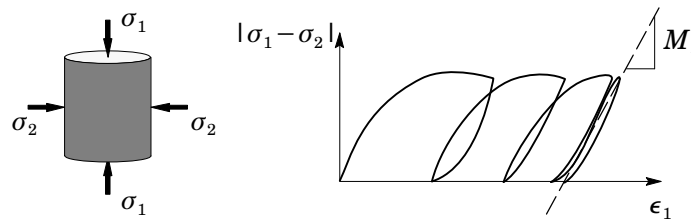
Figure 2.1. The triaxial test and the resilient behavior of granular materials.

Researchers have also used the notion of hypoelasticity to generate models with stress-dependent or strain-dependent elastic moduli (see, for example, Domaschuk and Valiappan 1975, Izumi et al. 1976, Chen and Saleeb 1994). The hypoelastic models take the general form

$$\dot{\mathbf{S}} \;=\; \mathbf{C}(\mathbf{S}, \mathbf{E})\dot{\mathbf{E}} \tag{2.5}$$

where $\mathbf{E}$ is the strain tensor and a dot indicates differentiation with respect to time. The beauty of the hypoelastic model is that the state-dependency of the moduli can be implemented directly. The drawback of hypoelasticity is that response to general loading is not path independent.

2.1.2 Current Approach to Implementation

There are a number of computer programs specifically developed to perform analyses of pavement systems and these can be listed under three main categories:

   i. Multi-layered linear elastic analysis programs based on elastic half-space solutions originally presented by Boussinesq (1885) and later generalized to multiple layers by Burmister (1945) like CHEVRON–ELP (Warren and Dieckman 1963), BISAR (De Jong, et al. 1972), and ELSYM5 (Kooperman et al. 1986).

  ii. Multi-layered nonlinear elastic half-space analysis programs like KENLAYER (Huang 1993).

 iii. Finite element analysis programs like *ILLIPAVE* (Raad and Figueroa 1980), MICHPAVE (Harichandran et al. 1971), GTPAVE (Tutumluer 1995), and SENOL (Brown and Pappin 1981).

The computer programs listed above under each category are very similar in all aspects but differ only in the way they handle specific issues such as treatment of the domain extent, tension in the granular layers, computation of resilient modulus, consideration of the self–weight of the pavement system, etc. (for detailed descriptions see references). The programs listed under categories 2 and 3 use $K - \theta$, Uzan–Witczak and similar constitutive models. These nonlinear material models have been traditionally implemented as fixed-point iterations wherein initial values of the resilient moduli are assumed, a linear analysis of the problem is performed using the current values of resilient moduli (as if they were constant), and the resulting displacements are used to compute strains, subsequently stresses, and subsequently new values of the resilient moduli. The process is repeated until the next computed resilient moduli are equal to the assumed resilient moduli of the previous iteration. In some of the programs (e.g., KENLAYER) the axisymmetric granular layers are divided into a rather arbitrary number of sublayers. This is done in order to take into account the hypothetical variation of resilient modulus with respect to depth, since as depth increases, the influence of the applied loading decreases. (KENLAYER also uses a scheme to take into account the horizontal variation of the resilient modulus within each layer). Several researchers have chosen to apply to load incrementally to overcome convergence problems (Huang 1993, Harichandran et al. 1971).

   The procedure outlined above is not efficient for several reasons. Every element in each layer is under a different state of stress, therefore a procedure that accounts for the continuous variation of resilient modulus is appropriate. Layered elastic system analysis programs cannot achieve this end without certain ad hoc modifications (Huang 1993). The convergence of a fixed point iteration is not guaranteed in general even if a unique solution to the nonlinear problem exists (Heath 1997) and may require ad hoc treatment of the problem at hand to obtain a solution. Indeed many researchers report of conver-

gence problems and some, for example, use damping factors when updating the resilient moduli (Brown and Pappin 1981, Tutumluer 1995).

In what follows, we will develop a strain–based formulation of $K-\theta$ and *Uzan–Witczak* models which can be implemented directly to a conventional finite element analysis program. We will then investigate the convergence properties of various implementations of these two models and make comparisons between the solution technique summarized above and more conventional techniques such as Newton's method.

2.2 Consistent Implementation

The conventional finite element analysis method is a natural setting for examining the issues associated with the implementation of the *K–* and *Uzan-Witczak* models in three dimensions. In this section we show how the typical extension of these types of models to three dimensions allows one to express the stress-dependent resilient moduli completely in terms of strain invariants, obviating the need to solve the nonlinear constitutive equations iteratively. We next find closed-form expressions for the eigenvalues of the material tangent tensor for the Uzan-Witczak model, and find bounds on the material parameters required for unique solutions to boundary value problems. We show that there are strain states where uniqueness of solution fails.

2.2.1 Notation

Consider a solid body $\mathcal{B}$ with boundary $\partial\mathcal{B}$, having normal vector field $\mathbf{n}$, subjected to applied tractions $\bar{\mathbf{t}}$ and body forces $\mathbf{b}$ with prescribed displacements $\bar{\mathbf{u}}$ over certain regions of the boundary. Let $\mathbf{S}$ represent the stress tensor field and $\mathbf{E}$ the strain tensor field in the interior of the body. The equations governing the response of the body constitute the boundary value problem (see, for example, Hjelmstad 1997)

$$
\begin{aligned}
\text{div}\mathbf{S} + \mathbf{b} &= \mathbf{0} && \text{in } \mathcal{B} \\
\mathbf{E} &= \tfrac{1}{2}\left(\nabla\mathbf{u} + \nabla\mathbf{u}^{T}\right) && \text{in } \mathcal{B} \\
\mathbf{S}\mathbf{n} &= \mathbf{t} && \text{on } \partial\mathcal{B}_{t} \\
\mathbf{u} &= \bar{\mathbf{u}} && \text{on } \partial\mathcal{B}_{u}
\end{aligned}
\tag{2.6}
$$

where the divergence is computed as $[\text{div}\mathbf{S}]_{i} = \partial S_{ij}/\partial x_{j}$ and the gradient as $[\nabla\mathbf{u}]_{ij} = \partial u_{i}/\partial x_{j}$. A superscript T indicates the transpose of the argument. To complete the statement of the boundary value problem we need only constitutive equations — the relationship between $\mathbf{S}$ and $\mathbf{E}$.

It will prove convenient to characterize the constitutive behavior of the material in terms of volumetric strains and deviatoric strains. For small strains the change in volume is equal to the trace of the strain tensor. Let us call the volumetric strain

$$\epsilon \equiv \mathrm{tr}(\mathbf{E}) \tag{2.7}$$

Note that ϵ is an invariant of the strain tensor. The strain deviator can then be defined as

$$\overline{\mathbf{E}} \equiv \mathbf{E} - \tfrac{1}{3}\epsilon\mathbf{I} \tag{2.8}$$

where $\mathbf{I}$ is the identity tensor. The octahedral shear strain γ is the second invariant of the deviatoric strain and is defined through the relationship

$$\gamma^2 \equiv \tfrac{1}{3}\mathrm{tr}(\overline{\mathbf{E}}^2) = \tfrac{1}{3}\overline{E}_{ij}\overline{E}_{ij} \tag{2.9}$$

The deviatoric stress can be defined as $\overline{\mathbf{S}} \equiv \mathbf{S} - \sigma\mathbf{I}$ and one can observe that the octahedral shear stress then obeys $3\tau^2 = \mathrm{tr}(\overline{\mathbf{S}}^2) = \overline{S}_{ij}\overline{S}_{ij}$.

As a point of departure, we note that the linear hyperelastic (Hookean) material has the following constitutive equations

$$\mathbf{S} = \frac{E}{1+\nu}(\alpha\epsilon\mathbf{I} + \mathbf{E}) \tag{2.10}$$

where E is Young's modulus, ν is Poisson's ratio, and $\alpha(\nu) \equiv \nu/(1-2\nu)$ is a parameter that depends only on Poisson's ratio.

2.2.2 Resilient Modulus in Terms of Strains

Both $K-\theta$ and Uzan–Witczak models describe only a stress dependent modulus of the material, and do not, per se, define a constitutive relationship. In the literature (see, for example, Hicks and Monismith 1971, Uzan 1985) a constitutive model is often postulated wherein the constant E of the classical Hookean material, Eq. (2.10), is simply replaced with the resilient modulus M_r. Letting $C(\theta, \tau) \equiv M_r(\theta, \tau)/(1+\nu)$ we can write this constitutive relation as

$$\mathbf{S} = C(\theta, \tau)(\alpha\epsilon\mathbf{I} + \mathbf{E}) \tag{2.11}$$

In the context of displacement-based finite element analysis, the constitutive equations can be viewed as strain driven in the sense that one iterates from an approximate displaced configuration $\mathbf{U}^i$ to the next $\mathbf{U}^{i+1}$, where the notation $\mathbf{U}^i$ means the nodal displacements on a finite element mesh at iteration i, by solving some global equations $\mathbf{U}^{i+1} = \mathbf{G}(\mathbf{U}^i)$. The specific issues associated with solving these global equations will be examined in a later section. For all of these approaches to solving the global problem one can observe that, upon estimating the new state $\mathbf{U}^{i+1}$, one can evaluate the strains in each element. At the local (element gauss point) level we view the solution of the constitutive equations as a problem of finding the stress state that corresponds with the strain state dictated by the global state $\mathbf{U}$. The stresses and the element constitutive matrix are

needed for the computations in the next iteration. For the strain driven problem, we can view the determination of the stress state as finding the roots, i.e., $\mathbf{g}(\mathbf{S}) = \mathbf{0}$, of the nonlinear function

$$\mathbf{g}(\mathbf{S}) \;\equiv\; \mathbf{S} - C(\theta, \tau)(\alpha \epsilon \mathbf{I} + \mathbf{E}) \tag{2.12}$$

for a given state of strain $\mathbf{E}$ (and hence given ϵ and γ). Note that the function $\mathbf{g}(\mathbf{S})$ is a nonlinear function of $\mathbf{S}$ through the nonlinear function $C(\theta(\mathbf{S}), \tau(\mathbf{S}))$.

Finding the stress state from Eq. (2.12) would be trivial if the resilient modulus $C(\theta, \tau)$ could be expressed as a function of strain rather than stress. For the given power law model of resilient modulus we can find such a function. Let us first decompose Eq. (2.12) into bulk and deviatoric parts by letting $\overline{\mathbf{g}} \equiv \mathbf{g} - \frac{1}{3}(\mathrm{tr}\mathbf{g})\mathbf{I}$ and observing that both $\mathrm{tr}\mathbf{g} = 0$ and $\overline{\mathbf{g}} = \mathbf{0}$, giving the equivalent equations

$$\sigma \;=\; \overline{\alpha} C(\theta, \tau)\epsilon, \quad \overline{\mathbf{S}} \;=\; C(\theta, \tau)\overline{\mathbf{E}} \tag{2.13}$$

where $\overline{\alpha} \equiv (1+\nu)/3(1-2\nu) = \alpha + 1/3$. If we define $\varrho \equiv |\epsilon|$ and observe that $\mathrm{tr}(\overline{\mathbf{g}}^2) = 0$ we get

$$\theta \;=\; \overline{\alpha} C(\theta, \tau)\varrho, \quad \tau \;=\; C(\theta, \tau)\gamma \tag{2.14}$$

Letting $k \equiv K/(1+\nu)$, substituting for $C(\theta, \tau)$ in Eqn. (2.14) we arrive at the two equations

$$\theta^{n-1}\tau^m \;=\; \frac{1}{k\overline{\alpha}\varrho}, \quad \theta^n \tau^{m-1} \;=\; \frac{1}{k\gamma} \tag{2.15}$$

These equations can be solved by observing that Eq. (2.15) implies that $\theta = (\overline{\alpha}\varrho/\gamma)\tau$. Substituting back into the two original equations and solving for θ and τ in terms of ϱ and γ we get

$$\begin{aligned}
\theta &\;=\; k^\mu (\overline{\alpha}\varrho)^{\mu(1-m)}\gamma^{\mu m} \\
\tau &\;=\; k^\mu (\overline{\alpha}\varrho)^{\mu n}\gamma^{\mu(1-n)}
\end{aligned} \tag{2.16}$$

where $\mu \equiv 1/(1-n-m)$. Substituting these results into the definition of the resilient modulus we find that

$$C(\theta, \tau) \;=\; \hat{C}(\varrho, \gamma) \;=\; (k\overline{\alpha}^n \varrho^n \gamma^m)^\mu \;\equiv\; \hat{k}\varrho^{\mu n}\gamma^{\mu m} \tag{2.17}$$

where $\hat{k} \equiv (k\overline{\alpha}^n)^\mu$ is the constant for the strain-based formulation of the stress-dependent moduli. Note that when the exponent m is set equal to zero we can recover the relevant expressions for the $K - \theta$ model. In terms of strains, the constitutive equation (2.11) becomes

$$\mathbf{S} \;=\; \hat{C}(\varrho, \gamma)(\alpha \epsilon \mathbf{I} + \mathbf{E}) \tag{2.18}$$

With this equation, the strain-driven constitutive equations are trivial to solve. We shall take Eq. (2.18) as the basic statement of the $K - \theta$ and *Uzan–Witczak* models for the remainder of this study.

2.2.3 Material Tangent Stiffness

The material tangent stiffness $\mathbf{C} \equiv \partial\mathbf{S}/\partial\mathbf{E}$ can be computed directly from Eq. (2.18) as

$$\frac{\partial\mathbf{S}}{\partial\mathbf{E}} = \hat{C}(\mathbf{1} + a\mathbf{I} \otimes \mathbf{I}) + (a\epsilon\mathbf{I} + \mathbf{E}) \otimes \nabla_E\hat{C} \tag{2.19}$$

where we have recognized that $\partial\epsilon/\partial\mathbf{E} = \mathbf{I}$ (with components $[\mathbf{I}]_{ij} = \delta_{ij}$) and that $\partial\mathbf{E}/\partial\mathbf{E} = \mathbf{1}$ (with components $[\mathbf{1}]_{ijkl} = \delta_{ij}\delta_{kl}$). Because $\varrho = |\epsilon|$, we can compute

$$\frac{\partial\varrho}{\partial\mathbf{E}} = \frac{\partial\varrho}{\partial\epsilon}\frac{\partial\epsilon}{\partial\mathbf{E}} = \mathrm{sgn}(\epsilon)\mathbf{I} \tag{2.20}$$

and because $\gamma^2 = \frac{1}{3}\overline{E}_{ij}\overline{E}_{ij}$, we can compute

$$\frac{\partial\gamma}{\partial\mathbf{E}} = \frac{1}{3}\frac{\overline{\mathbf{E}}}{\gamma} \tag{2.21}$$

With these definitions, we find that

$$\nabla_E\hat{C}(\mathbf{E}) = \frac{\partial\hat{C}}{\partial\varrho}\frac{\partial\varrho}{\partial\mathbf{E}} + \frac{\partial\hat{C}}{\partial\gamma}\frac{\partial\gamma}{\partial\mathbf{E}} = \mu\hat{C}\left(\frac{n}{\epsilon}\mathbf{I} + \frac{m}{3\gamma^2}\overline{\mathbf{E}}\right) \tag{2.22}$$

Letting $\mathbf{N} \equiv \overline{\mathbf{E}}/\gamma$ we arrive at the final expression for the material tangent stiffness $\mathbf{C}$ for the $K-\theta$ and Uzan–Witczak models

$$\mathbf{C} = \hat{C}(\varrho,\gamma)\left[\mathbf{1} + (\mu n\overline{a}+a)\mathbf{I} \otimes \mathbf{I} + \frac{\mu m}{3}\mathbf{N} \otimes \mathbf{N} + \frac{\mu\overline{a}\epsilon m}{3\gamma}\mathbf{I} \otimes \mathbf{N} + \frac{\mu\gamma n}{\epsilon}\mathbf{N} \otimes \mathbf{I}\right] \tag{2.23}$$

Notice that this tensor is not symmetric, and has skew part

$$\mathbf{C}^{skew} = \frac{\mu\hat{C}}{6\epsilon\gamma}(\overline{a}\epsilon^2 m - 3\gamma^2 n)[\mathbf{I} \otimes \mathbf{N} - \mathbf{N} \otimes \mathbf{I}] \tag{2.24}$$

The material tangent stiffness tensor is useful for both for finding bounds on the material parameters of the model and also for carrying out numerical computations. In particular, it can be used to find the tangent stiffness matrix. Using standard notions of assembly of the stiffness matrix, the tangent stiffness matrix can be computed as

$$\mathbf{K}_t(\mathbf{U}) \equiv \sum_{m=1}^{M}\int_{\mathcal{B}_m} \mathbf{B}_m^T(\mathbf{x})\mathbf{C}_m(\mathbf{U},\mathbf{x})\mathbf{B}_m(\mathbf{x})\,dV \tag{2.25}$$

where M is the number of elements, $\mathcal{B}_m$ is the region occupied by element m, and $\mathbf{C}_m(\mathbf{U},\mathbf{x})$ is the material tangent tensor for element m, which depends upon the displaced state $\mathbf{U}$ and varies with the spatial coordinates $\mathbf{x}$. The strain-displacement matrix $\mathbf{B}_m$ allows the computation of the strain tensor in element m from the nodal displacement $\mathbf{U}$ as

$$\mathbf{E}_m(\mathbf{x}) = \mathbf{B}_m(\mathbf{x})\mathbf{U} \tag{2.26}$$

2.2.4 Uniqueness and Path Independence

Uniqueness of the equilibrium configurations displayed by the constitutive models can be assessed with a simple argument using the principle of virtual work. The principle of virtual work states that, if the equation

$$\int_{\mathcal{B}} \mathbf{S} \cdot \hat{\mathbf{E}} \, dV \;=\; \int_{\partial\mathcal{B}} \mathbf{t} \cdot \hat{\mathbf{u}} \, dA \;+\; \int_{\mathcal{B}} \mathbf{b} \cdot \hat{\mathbf{u}} \, dV \tag{2.27}$$

holds for all arbitrary kinematically admissible virtual displacement fields $\hat{\mathbf{u}}$ and their corresponding strain fields $\hat{\mathbf{E}}$, then equilibrium is satisfied in the domain and on the boundary (see, for example, Hjelmstad 1997A). Therefore, if the traction forces $\mathbf{t}$ and body forces $\mathbf{b}$ acting on body $\mathcal{B}$ are incremented by amounts $\delta\mathbf{t}$ and $\delta\mathbf{b}$, respectively, with a resulting displacement increment $\delta\mathbf{u}$, then the resulting increments in stress $\delta\mathbf{S}$ and strain $\delta\mathbf{E}$.

Following Sokolnikoff (1956), let us assume that there are two distinct equilibrium states (I and II) corresponding to the increments $\delta\mathbf{t}$ and $\delta\mathbf{b}$ and given by $\delta\mathbf{S}^I$ and $\delta\mathbf{S}^{II}$. Substituting the stress states $\mathbf{S}+\delta\mathbf{S}^I$ and $\mathbf{S}+\delta\mathbf{S}^{II}$ into Eqn. (2.27), taking the difference, and particularizing to the virtual strain $\hat{\mathbf{E}} = \delta\mathbf{E}^I - \delta\mathbf{E}^{II}$, where $\delta\mathbf{E}^I$ and $\delta\mathbf{E}^{II}$ are the strains associated with the stress states $\delta\mathbf{S}^I$ and $\delta\mathbf{S}^{II}$, we find that

$$\int_{\mathcal{B}} \left(\delta\mathbf{S}^I - \delta\mathbf{S}^{II}\right) \cdot \left(\delta\mathbf{E}^I - \delta\mathbf{E}^{II}\right) dV \;=\; 0 \tag{2.28}$$

Denoting the differences in states as $\mathbf{S}^* \equiv \delta\mathbf{S}^I - \delta\mathbf{S}^{II}$ and $\mathbf{E}^* \equiv \delta\mathbf{E}^I - \delta\mathbf{E}^{II}$, and substituting the incremental constitutive equation $\mathbf{S}^* = \mathbf{C}\mathbf{E}^*$, Eqn. (2.28) becomes

$$\int_{\mathcal{B}} \mathbf{E}^* \cdot \mathbf{C}\mathbf{E}^* \, dV \;=\; 0 \tag{2.29}$$

Therefore if $\mathbf{C}$ is positive definite, then the strain state differences $\mathbf{E}^*$, and thus the stress state differences $\mathbf{S}^*$, are identically zero. Thus, uniqueness of solution depends upon the definiteness of the tensor $\mathbf{C}$. A positive definite tensor is one that has all positive eigenvalues. Hence, we must examine the eigenvalues of the material tangent tensor.

2.2.5 Eigenvalues of the Material Tangent Tensor

Eqn. (2.29) indicates that uniqueness of stress for a given strain state (or vice versa) is guaranteed if the material tangent stiffness tensor $\mathbf{C}$ is positive definite. This restriction imposes certain bounds on the material constants of the $K-\theta$ and Uzan–Witczak models.

Let us obtain the eigenvalues and eigenvectors, for a tensor of the form

$$\mathbf{T} \;=\; \mathbf{1} + a\mathbf{I} \otimes \mathbf{I} + b\mathbf{N} \otimes \mathbf{N} + c\mathbf{I} \otimes \mathbf{N} + d\mathbf{N} \otimes \mathbf{I} \tag{2.30}$$

where, a, b, c, and d are scalars. If φ is an eigentensor of $\mathbf{T}$, with eigenvalue λ, then

$$\mathbf{T}\varphi = \varphi + [a(\mathbf{I} \cdot \varphi) + c(\mathbf{N} \cdot \varphi)]\mathbf{I} + [d(\mathbf{I} \cdot \varphi) + b(\mathbf{N} \cdot \varphi)]\mathbf{N} = \lambda\varphi \tag{2.31}$$

The tensor φ is symmetric (it has the same character as the strain tensor). Therefore, there are 6 eigenvectors. Four of these tensors ($\varphi^{(3)}$, $\varphi^{(4)}$, $\varphi^{(5)}$, $\varphi^{(6)}$) correspond to a repeated eigenvalue because these tensors need only be orthogonal to $\mathbf{I}$ and $\mathbf{N}$. Therefore, $\lambda = 1$ is an eigenvalue of algebraic multiplicity 4

$$\lambda_3 = \lambda_4 = \lambda_5 = \lambda_6 = 1 \tag{2.32}$$

The remaining two eigentensors must lie in the subspace spanned by tensors $\mathbf{I}$ and $\mathbf{N}$. To wit, the remaining eigenvectors are of the form

$$\varphi = \mathbf{I} + \beta\mathbf{N} \tag{2.33}$$

Because $\mathbf{N} = \overline{\mathbf{E}}/\gamma$, we have $\mathbf{I} \cdot \mathbf{N} = \delta_{ij}N_{ij} = 0$. Hence, these tensors are orthogonal in this sense. Substituting Eq. (2.33) into Eq. (2.31), noting that $\mathbf{I} \cdot \mathbf{I} = 3$ and $\mathbf{N} \cdot \mathbf{N} = 3$ and equating the coefficients of $\mathbf{I}$ and $\mathbf{N}$, we get the following equations for λ and β

$$\lambda - 1 = 3a + 3\beta c$$
$$\beta(\lambda - 1) = 3d + 3\beta b \tag{2.34}$$

Multiplying the first of these by β and subtracting the result from the second we arrive at a quadratic equation for β

$$c\beta^2 + (a - b)\beta - d = 0 \tag{2.35}$$

Solution of this quadratic equation yields the two parameters β_1 and β_2

$$\beta_{1,2} = \frac{b - a \pm \sqrt{(a-b)^2 + 4cd}}{2c} \tag{2.36}$$

These values of β can be substituted back into Eq. (2.34)$_a$ to give the remaining eigenvalues

$$\lambda_{1,2} = 1 + \frac{3}{2}\left(b + a \pm \sqrt{(a-b)^2 + 4cd}\right) \tag{2.37}$$

From Eq. (2.23) we can identify the constants as

$$a = \mu n\overline{a} + \alpha, \quad b = \mu m/3, \quad c = \mu m\overline{a}\epsilon/3\gamma, \quad d = \mu n\gamma/\epsilon \tag{2.38}$$

With these values, and noting that $\mathbf{C} = \hat{C}\mathbf{T}$ we find the eigenvalues of $\mathbf{C}$ to be

$$\overline{\lambda}_{1,2} = \hat{C}\lambda_{1,2}, \quad \overline{\lambda}_{3,4,5,6} = \hat{C} \tag{2.39}$$

The tensor $\mathbf{C}$ is not symmetric, but it is easy to show that the eigenvalues of $\mathbf{C}^T$ are identical to the eigenvalues of $\mathbf{C}$.

For uniqueness of solution we must have $\bar{\lambda}_i > 0$, for $i = 1, \ldots, 6$, and from this require-ment bounds on the material constants can be established. It is interesting to note that $\lambda_{1,2}$ do not depend upon the state of strain because a, b, and c, d depend only upon the material parameters. Therefore, the dependence of the eigenvalues of $\mathbf{C}$ comes entirely from $\hat{C}(\varrho, \gamma)$, which is a multiplier for all six of the eigenvalues. Therefore, the form of the spectrum is constant and loss of uniqueness can occur only when $\hat{C}(\varrho, \gamma) = 0$. As a conse-quence, we can observe that bounds on the material parameters α, n, and m imposed by the requirement of uniqueness of solution are

$$\lambda_{1,2} = 1 + \tfrac{3}{2}\left(b + a \pm \sqrt{(a-b)^2 + 4cd}\right) > 0 \tag{2.40}$$

A somewhat lengthy, but straightforward, calculation shows that $\lambda_{1,2} > 0$ if and only if

$$\bar{\alpha}\mu > 0 \tag{2.41}$$

Clearly, then we must have $n + m < 1$ and $\bar{\alpha} > 0$, which implies $-1 < \nu < 1/2$. If the pa-rameters of the model are chosen to satisfy Eq. (2.41) then the solution can fail to be unique only for states of strain where $\epsilon = 0$ or $\gamma = 0$.

2.3 Solution Methods

In this section we analyze the iterative methods currently used for pavement analysis and show that, because the constitutive model hardens, these iterative methods are bound to eventually fail. Finally, we make some comparisons with Newton-type solution methods and modified Newton methods on some example problems.

As mentioned earlier, fixed-point iteration is traditionally the method of choice in solv-ing boundary value problems of pavement systems having layers that display nonlinear material behavior. In this section we will investigate the convergence properties of such a method on a single finite element with one integration (material) point. This is a very simple problem, however it will enable us to gain insight to the convergence properties of this iterative solution method when applied to a collection of material points (i.e., In-tegration points in a finite element mesh) which behave according to the constitutive relations given by $K - \theta$ or Uzan–Witczak Models.

The principle of virtual displacements suggests that equilibrium is satisfied if

$$\mathcal{G}(\mathbf{U}) \equiv \sum_{m=1}^{M} \int_{\mathcal{B}_m} \mathbf{B}_m^T \mathbf{S}_m(\mathbf{U})\, dV - \mathbf{P} = \mathbf{0} \tag{2.42}$$

where $\mathbf{U}$ are the nodal displacements, $\mathbf{P}$ are the work equivalent nodal loads, $\mathbf{B}_m$ is the strain-displacement operator for element m, defined in Eq. (2.26), and $\mathbf{S}_m(\mathbf{U})$ is the stress in element m, which depends upon the nodal displacements through the strains. The summation in Eq. (2.42) is the usual assembly procedure and the element integrals are

generally carried out with numerical quadrature. The subscript m on the stress tensor $\mathbf{S}_m(\mathbf{U})$ indicates that the stress field is localized to element m. The stress field is said to depend upon the nodal displacements because, for a given displacement state, the strains are computed from the displacements in accord with Eq. (2.26) and the invariants ϱ and γ are computed from the strains. In this sense, the computation is strain driven. In the following sections we shall discuss and analyze various methods for solving two and three dimensional problems using this constitutive model.

2.3.1 Secant Method

One can define a secant stiffness matrix at a given state $\mathbf{U}$ by computing

$$\mathbf{K}_s(\mathbf{U}) \equiv \sum_{m=1}^{M} \int_{\mathcal{B}_m} \mathbf{B}_m^T \mathbf{D}_m(\mathbf{U}) \mathbf{B}_m \, dV \tag{2.43}$$

where the material secant stiffness is defined as

$$\mathbf{D} = \hat{C}(\varrho, \gamma)[\mathbf{1} + a\mathbf{I} \otimes \mathbf{I}] \tag{2.44}$$

The only difference between the tangent stiffness and the secant stiffness matrix of Eq. (2.43) is that in the tangent stiffness we used the consistent material tangent modulus $\mathbf{C}$ defined in Eq. (2.23) whereas in the secant stiffness we use the surrogate modulus $\mathbf{D}$ defined in Eq. (2.44)

Perhaps the simplest version of the fixed-point iteration is

$$\mathbf{U}^{i+1} = \mathbf{K}_s^{-1}(\mathbf{U}^i)\mathbf{P} \tag{2.45}$$

which can be started with an initial displacement vector $\mathbf{U}^0$. In practice one does not specify an initial guess of displacements, but rather an initial distribution of the modulus $\hat{C}_0$. Using this initial modulus the first iteration gives the initial displacement approximation and the iteration proceeds as given above. We shall refer to the algorithm of Eq. (2.45) from here on as the *total (original) secant method*.

The fixed-point iteration described by Eq. (2.45) is in the form $\mathbf{U}^{i+1} = \mathbf{G}(\mathbf{U}^i)$, and will converge if the spectral radius of $\nabla\mathbf{G}(\mathbf{U}^*)$ is less than unity at the solution $\mathbf{U}^*$. Noting that that at the solution we have $\mathbf{K}_s^{-1}(\mathbf{U}^*)\mathbf{P} = \mathbf{U}^*$ we find that

$$\nabla\mathbf{G}(\mathbf{U}^*) = -\mathbf{K}_s^{-1}(\mathbf{U}^*)\nabla\mathbf{K}_s(\mathbf{U}^*)\mathbf{U}^* \tag{2.46}$$

where the gradient of the inverse of a matrix was computed by noting $\mathbf{K}^{-1}\mathbf{K} = \mathbf{I}$. The gradient of the secant stiffness matrix can be computed from Eq. (2.43), noting that $\mathbf{B}_m\mathbf{U} = \mathbf{E}_m$, by noting that

$$\nabla\mathbf{K}_s(\mathbf{U})\mathbf{U} = \frac{\partial\mathbf{K}_s}{\partial\mathbf{U}}\mathbf{U} = \sum_{m=1}^{M} \int_{\mathcal{B}_m} \mathbf{B}_m^T[\nabla_U\mathbf{D}_m(\mathbf{U})]\mathbf{E}_m \, dV \tag{2.47}$$

where $\nabla_U \mathbf{D}$ can be computed via the chain rule for differentiation as

$$\nabla_U \mathbf{D} \;\equiv\; \frac{\partial \mathbf{D}}{\partial \mathbf{U}} \;=\; \frac{\partial \mathbf{D}}{\partial \mathbf{E}}\frac{\partial \mathbf{E}}{\partial \mathbf{U}} \;=\; \frac{\partial \mathbf{D}}{\partial \mathbf{E}}\mathbf{B} \tag{2.48}$$

Noting that we can compute the stress from the secant relationship $\mathbf{S} = \mathbf{DE}$, we can observe that

$$\mathbf{C} \;=\; \frac{\partial \mathbf{S}}{\partial \mathbf{E}} \;=\; \frac{\partial (\mathbf{DE})}{\partial \mathbf{E}} \;=\; \frac{\partial \mathbf{D}}{\partial \mathbf{E}}\mathbf{E} + \mathbf{D} \tag{2.49}$$

It therefore follows that

$$\frac{\partial \mathbf{D}}{\partial \mathbf{E}}\mathbf{E} \;=\; \mathbf{C} - \mathbf{D} \tag{2.50}$$

Therefore, combining Eqn.'s (2.47), (2.48), and (2.50), we find that

$$\nabla \mathbf{K}_s(\mathbf{U})\mathbf{U} \;=\; \sum_{m=1}^{M} \int_{\mathcal{B}_m} \mathbf{B}_m^T [\mathbf{C}_m(\mathbf{U}) - \mathbf{D}_m(\mathbf{U})]\mathbf{B}_m \, dV \tag{2.51}$$

Thus, $\nabla \mathbf{K}_s(\mathbf{U})\mathbf{U} = \mathbf{K}_t(\mathbf{U}) - \mathbf{K}_s(\mathbf{U})$ and the gradient of the fixed-point iteration function of Eq. (2.46) reduces to

$$\nabla \mathbf{G}(\mathbf{U}^*) \;=\; \mathbf{I} - \mathbf{K}_s^{-1}(\mathbf{U}^*)\mathbf{K}_t(\mathbf{U}^*) \;\equiv\; \mathbf{A} \tag{2.52}$$

The spectral radius of $\mathbf{A}$ is the largest eigenvalue of $\mathbf{A}$. Let the eigenvalue problem be denoted as $\mathbf{Aa} = \omega \mathbf{a}$, where ω is the (possibly complex valued) eigenvalue and $\mathbf{a}$ is the associated eigenvector. Then the criterion for convergence of the fixed-point iteration is

$$r(\mathbf{A}) \;=\; \omega_{max} \;<\; 1 \tag{2.53}$$

where $r(\cdot)$ is the spectral radius of $(\cdot)$, and where ω_{max} is the modulus of the largest eigenvalue of $\mathbf{A}$. Observe that when the secant stiffness is close the the tangent stiffness $\omega_{max} \approx 0$ and convergence of the iteration is very rapid (nearly quadratic). As the secant and tangent stiffness grow apart, as they do with increasing deformation, the eigenvalues of $\mathbf{A}$ get increasingly negative because the tangent is always steeper than the secant for this model. Therefore, the fixed-point iteration is eventually bound to diverge if the load level is high enough.

2.3.2 Damped Secant Method

Researchers have observed that the fixed-point iteration described in the previous section has poor convergence properties (Brown and Pappin 1981, Tutumluer 1995). The convergence properties of this method were observed to improve with the introduction of a "damped" fixed-point iteration in which a secant modulus is formed from the current state and the previous state using an effective modulus

$$\overline{C} \equiv \beta\hat{C}(\mathbf{U}^i) + (1-\beta)\hat{C}(\mathbf{U}^{i-1}) \tag{2.54}$$

where the damping parameter $\beta \in [0, 1]$ is selected a priori. Tutumluer (1995) has reported that a value of $\beta = 0.8$ gives good results. Note that, for notational convenience, we consider $\hat{C}$ to be a function of the state $\mathbf{U}$. Using $\overline{C}$ in the definition of the secant material modulus, Eq. (2.44), and using that in the definition of the global secant stiffness, Eq. (2.43), we find that the result is a modified secant stiffness

$$\overline{\mathbf{K}}(\mathbf{U}^i, \mathbf{U}^{i-1}) \equiv \beta\mathbf{K}_s(\mathbf{U}^i) + (1-\beta)\mathbf{K}_s(\mathbf{U}^{i-1}) \tag{2.55}$$

This modified stiffness is then used to define a modified fixed-point iteration as

$$\overline{\mathbf{K}}(\mathbf{U}^i, \mathbf{U}^{i-1})\mathbf{U}^{i+1} \equiv \left[\beta\mathbf{K}_s(\mathbf{U}^i) + (1-\beta)\mathbf{K}_s(\mathbf{U}^{i-1})\right]\mathbf{U}^{i+1} = \mathbf{P} \tag{2.56}$$

We shall refer to the algorithm of Eq. (2.56) from here on as the *total damped secant method*.

To examine the convergence properties of this fixed-point iteration it is convenient to put it into the form $\mathbf{Z} = \mathbf{G}(\mathbf{Z})$, from which we can observe that $r(\nabla_Z\mathbf{G}) < 1$ is the criterion for convergence. The two-step iteration for Eq. (2.56) can be converted to a one-step iteration by introducing the variable $\mathbf{W}^{i+1} \equiv \mathbf{U}^i$. Now we can write the iteration as

$$\begin{bmatrix} \overline{\mathbf{K}}(\mathbf{U}^i, \mathbf{W}^i) & \mathbf{0} \\ \mathbf{0} & \mathbf{I} \end{bmatrix} \begin{bmatrix} \mathbf{U}^{i+1} \\ \mathbf{W}^{i+1} \end{bmatrix} = \begin{bmatrix} \mathbf{P} \\ \mathbf{U}^i \end{bmatrix} \tag{2.57}$$

If we define $\mathbf{Z}^i \equiv \{\mathbf{U}^i, \mathbf{W}^i\}$ then we can identify the function $\mathbf{G}(\mathbf{Z})$ from Eq. (2.57) as

$$\mathbf{G}(\mathbf{Z}^i) \equiv \begin{bmatrix} \left[\overline{\mathbf{K}}(\mathbf{U}^i, \mathbf{W}^i)\right]^{-1}\mathbf{P} \\ \mathbf{U}^i \end{bmatrix} \tag{2.58}$$

The gradient of $\mathbf{G}$ can be computed as

$$\nabla_Z\mathbf{G}(\mathbf{Z}^i) \equiv \begin{bmatrix} -\beta\overline{\mathbf{K}}^{-1}[\nabla_U\mathbf{K}_s]\overline{\mathbf{K}}^{-1}\mathbf{P} & -(1-\beta)\overline{\mathbf{K}}^{-1}[\nabla_W\mathbf{K}_s]\overline{\mathbf{K}}^{-1}\mathbf{P} \\ \mathbf{I} & \mathbf{0} \end{bmatrix} \tag{2.59}$$

The convergence criterion is expressed in terms of the spectral radius of $\nabla_Z\mathbf{G}$ evaluated at the solution $\mathbf{U} = \mathbf{W} = \mathbf{U}^*$. At this point, $\overline{\mathbf{K}}^{-1}\mathbf{P} = \mathbf{U}^*$ and $\overline{\mathbf{K}} = \mathbf{K}_s$. Consequently,

$$\nabla_Z\mathbf{G}(\mathbf{Z}^*) \equiv \begin{bmatrix} \beta\mathbf{A} & (1-\beta)\mathbf{A} \\ \mathbf{I} & \mathbf{0} \end{bmatrix} \tag{2.60}$$

where $\mathbf{A} \equiv \mathbf{I} - \mathbf{K}_s^{-1}\mathbf{K}_t$, from Eq. (2.51). The eigenvalues λ of $\nabla_Z\mathbf{G}$ are determined from the eigenvalue problem

$$\begin{bmatrix} \beta\mathbf{A} & (1-\beta)\mathbf{A} \\ \mathbf{I} & \mathbf{0} \end{bmatrix} \begin{bmatrix} \mathbf{a} \\ \mathbf{b} \end{bmatrix} = \lambda \begin{bmatrix} \mathbf{a} \\ \mathbf{b} \end{bmatrix} \tag{2.61}$$

17

The bottom partition of this equation gives $\mathbf{a} = \lambda\mathbf{b}$. Substituting this into the top partition we find that

$$\left(\beta + \tfrac{1}{\lambda}(1-\beta)\right)\mathbf{A}\mathbf{a} \;=\; \lambda\mathbf{a} \tag{2.62}$$

Thus, we can observe that $\mathbf{a}$ is an eigenvector of $\mathbf{A}$. If ω is the corresponding eigenvalue of $\mathbf{A}$, i.e., it satisfies the eigenvalue problem $\mathbf{A}\mathbf{a} = \omega\mathbf{a}$, then the eigenvalue of the system in Eq. (2.61) is related to ω as

$$\omega \;=\; \frac{\lambda^2}{\lambda\beta + (1-\beta)} \tag{2.63}$$

Observe that when $\beta = 1$ the system reverts to the undamped fixed-point iteration of the previous section and the eigenvalues are the same. Solving Eq. (2.63) for λ in terms of ω gives

$$\lambda \;=\; \tfrac{1}{2}\left[\omega\beta \pm \sqrt{\omega^2\beta^2 + 4\omega(1-\beta)}\right] \tag{2.64}$$

Since the matrix $\mathbf{A}$ is not necessarily symmetric its maximum eigenvalue ω will generally be complex valued. Consequently, the eigenvalue of the damped system will also be complex valued. The spectral radius of the damped system (i.e., the modulus of λ) is shown as a function of the damping parameter β in Fig. 2.2 for values values of the eigenvalue $\omega = \overline{\omega}e^{i\theta}$. It is apparent from this figure that a damped secant method will converge in cases where an undamped case will not (up to $\overline{\omega} = 3$ in the best case) and that it will improve the convergence characteristics in all cases where the undamped secant method will converge. Furthermore, the presence of an imaginary part to the eigenvalue of $\mathbf{A}$ will always blunt the ability of the damped method to improve convergence. For example, with $\overline{\omega} = 1.5$ no improvement can be achieved through damping if $\theta > 0.5$. The optimal value of damping depends on both the magnitude and phase of the eigenvalue of the undamped case, which is not known a priori.
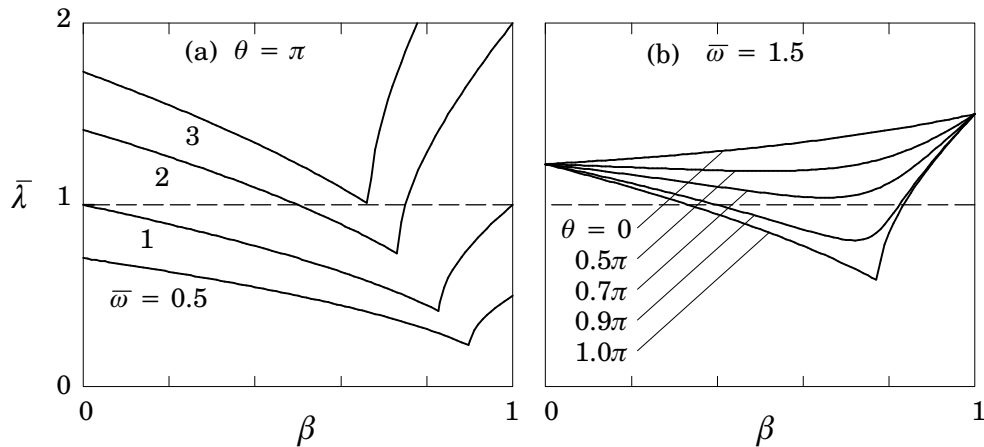
Fig. 2.2 Variation of the modulus of the spectral radius of damped system with damping parameter β (a) for various values of the spectral radius of the undamped system with purely real values $\theta = \pi$, and (b) for a spectral radius of the undamped system of 1.5 with different imaginary parts

2.3.3 Newton Methods

There are many ways to organize the computation associated with solving $\mathbf{G}(\mathbf{U}) = \mathbf{0}$, where $\mathbf{G}(\mathbf{U})$ is defined by Eq. (2.42). Among the most effective means are Newton-like methods. We can compute the linear part of $\mathbf{G}(\mathbf{U})$ and use the linearized equation to develop the estimate of the next state. Let us assume that we know the state $\mathbf{U}^i$ and we want to estimate $\mathbf{U}^{i+1}$. We can compute an incremental state by solving

$$\mathbf{K}_t(\mathbf{U}^i)\Delta\mathbf{U} = -\mathcal{G}(\mathbf{U}^i), \quad \mathbf{U}^{i+1} = \mathbf{U}^i + \Delta\mathbf{U} \tag{2.65}$$

where $\mathbf{K}_t(\mathbf{U})$ is the tangent stiffness matrix. The difference between the Newton iteration of Eq. (2.65) and the fixed-point iteration of Eq. (2.45) is that the right side of the Newton iteration is the residual force, which should go to zero as the iteration converges, while the right side of the fixed-point iteration is the total force. The Newton iteration computes the displacement by adding an increment to the previous estimate while the fixed-point iteration computes a completely new estimate of the total displacement at each iteration. In the neighborhood of the solution $\mathbf{U}^*$ Newton's method converges quadratically while the fixed-point iteration converges linearly. Although Newton's method is not guaranteed to converge from any starting point, one can easily modify the iteration to do a load incrementation scheme or implement a univariate line search (Fletcher 1987), solving the first of Eqn.'s (2.65) for the increment $\Delta\mathbf{U}$, but then updating to the new state as $\mathbf{U}^{i+1} = \mathbf{U}^i + s\Delta\mathbf{U}$, where the line search parameter s is determined by solving a one-dimensional problem like

$$\min_{s} \ \| \mathcal{G}(\mathbf{U}^i + s\Delta\mathbf{U}) \| \tag{2.66}$$

Another popular line search criterion is to solve $\Delta\mathbf{U}^T\mathcal{G}(\mathbf{U}^i + s\Delta\mathbf{U}) = 0$ for the line search parameter s (Crisfield 1991).

A modified Newton iteration can be established by replacing the tangent stiffness with the secant stiffness in Eq. (2.65) to give

$$\mathbf{K}_s(\mathbf{U}^i)\Delta\mathbf{U} = -\mathcal{G}(\mathbf{U}^i), \quad \mathbf{U}^{i+1} = \mathbf{U}^i + \Delta\mathbf{U} \tag{2.67}$$

where $\mathbf{K}_s$ is defined in Eq. (2.43). The stiffness matrix used in Newton-like iterations affects *only* the convergence properties of the algorithm *not* the converged solution. A straightforward analysis of this algorithm as a fixed-point iteration shows that its convergence properties are exactly the same as the original (total) secant method. Further, one can show that using the damped secant does not improve the convergence characteristics like it did for the original (total) secant method. On the other hand, a line search can be used in the modified Newton method of Eq. (2.67), but not in the secant method of Eqn. (2.45) or the damped secant method of Eq. (2.56).

From here on we shall refer to the finite element formulation based on Eqn. (2.65) as the *incremental tangent formulation* and the finite element formulation based on Eqn. (2.67) as the *incremental secant formulation*.

In what follows, we will investigate convergence properties of the solution techniques described so far on example problems and try to identify the best strategies for the solution of nonlinear finite element equations.

2.4 Simulations and Convergence Studies

We have implemented the algorithms discussed earlier to the commercial finite element package ABAQUS (1994) with the help of user defined subroutine UMAT. The program ABAQUS supports both symmetric and non-symmetric tangent formulations as well as line searches. A brief overview of ABAQUS UMAT routines and the source code of the implementation of the methods described above can be found in Appendix I and Appendix II.

2.4.1 Triaxial Test Simulation

In order to compare the various algorithms presented in this chapter we shall use them to compute the response of the simulated triaxial test configuration shown in Fig. 2.4. The model was constrained against vertical movement at the bottom, but allowed frictionless sliding on the top and bottom faces. Tractions were applied on the lateral surfaces of the test piece. The material properties were $K = 118.6$ MPa, $n = 0.4$, and $m = 0.3$, which are representative of a moderate to loose granular material. The extent of nonlin-

earity can be observed from the plot of the proportional load factor versus average strain in Figure 2.3. In particular, this degree of nonlinearity should be sufficient to exhibit the differences among the various algorithms.

The results of analysis of the triaxial sample under five different load levels are shown in Table 2.1. In each case the total load was applied in a single step and the state was iterated to convergence until default ABAQUS criteria were satisfied (ABAQUS, 1994). The algorithms used either secant stiffness matrix or a tangent stiffness matrix. The secant was either damped ($\beta = 0.8$) or original ($\beta = 1$). The tangent was either the unsymmetrical consistent or symmetrized consistent tangent. For each of these four choices the computation was done with and without line search. The table gives the number of iterations required for convergence at each load level. The typical convergence characteristics for the convergent methods are shown in Fig. 2.5.

The original secant method without line search failed to converge for all load levels. The beneficial effects of line search and damping can be seen in methods 2 and 3. Line search is considerably better than damping, but requires additional effort. Interestingly, damping and line search together is actually worse than line search alone. The symmetrized tangent stiffness method failed to converge at all load levels, while the unsymmetrical tangent stiffness method converged well at all load levels. It is interesting to note that the lowest load level was the most difficult for the consistent tangent, possibly because stiffness levels are so low for that load level (the secant being greater than the tangent there). Line search helped both tangent methods. The unsymmetrical tangent method appears to be competitive with the original secant method with line search in terms of number of iterations to convergence, but is considerably more expensive per iteration to compute. It would appear that the best strategy in this example is the original
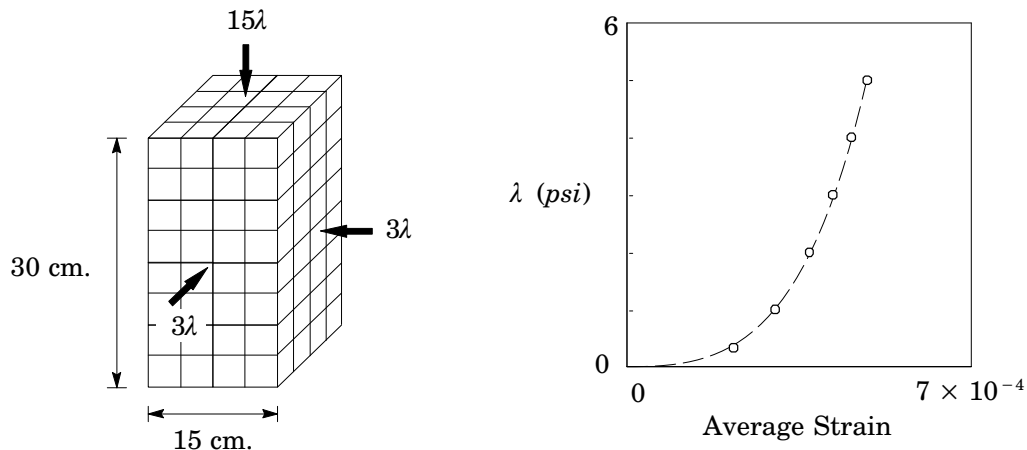
Figure 2.3. Finite element mesh and material response of example triaxial test.

Table 2.1. Results of example triaxial test computation for various solution algorithms

Method	LS	Stiffness Matrix				Load Factor λ				
		Secant		Tangent						
		Orig	Damp	Sym	Unsym	0.33	1	2	3	4
1	–	Yes	–	–	–	nc	nc	nc	nc	nc
2	Yes	Yes	–	–	–	2	3	3	2	2
3	–	–	Yes	–	–	5	7	5	5	4
4	Yes	–	Yes	–	–	4	5	4	3	3
5	–	–	–	Yes	–	nc	nc	nc	nc	nc
6	Yes	–	–	Yes	–	8	10	10	9	9
7	–	–	–	–	Yes	6	4	3	3	3
8	Yes	–	–	–	Yes	3	3	2	3	3

nc = no convergence

secant method with line search. The damped secant method without line search performs reasonably well also.

2.4.2 Axisymmetric Pavement Analysis

For the purpose of demonstration, an axisymmetric finite element analysis was performed on a flexible pavement system consisting of three layers of materials. The top layer of the system was 20 cm. of asphalt concrete, the second layer was 112 cm. of high density crushed rock, designated as HD1 by Allen (1973) (see Chapter 4), and the bottom layer was natural soil extending to a depth of 9 m. In the various analyses, the asphalt concrete layer was assumed to be linear elastic with Young's modulus $E = 1380$ MPa and Poisson's ratio of $v = 0.35$. The natural soil was also assumed to be linearly elastic with Young's modulus $E = 40$ MPa and Poisson's ratio of $v = 0.45$. The second layer was modeled using one of the following models: (a) linear elasticity with $E = 240$ MPa and $v = 0.34$, (b) K– with $k = 420$ MPa, $n = 0.29$, and $v = 0.33$ and (c) Uzan–Witczak with $k = 425$ MPa, $n = 0.22$, $m = 0.07$, and $v = 0.32$. The values of the material constants for the high density crushed rock material were established by fitting the given model (one of the three), using a weighted nonlinear least-squares curve fitting technique (as discussed in Chapter 4), to the laboratory test data measured by Allen (1973). Thus, although the models are quite different, they are each an attempt to best fit the given test data. The
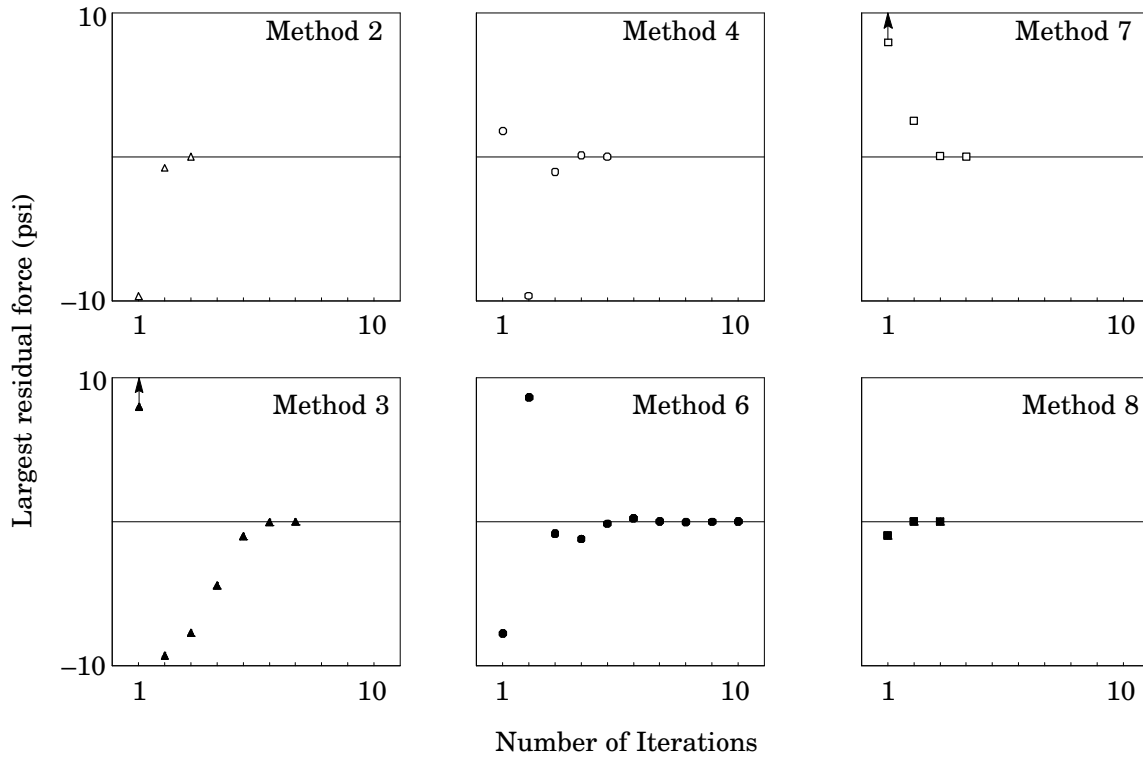
Figure 2.5. Convergence characteristics of various solution methods

densities of the materials were taken to be 0.0024 kgf/cm³ for the asphalt concrete, 0.0022 kgf/cm³ for the crushed rock, and 0.0017 kgf/cm³ for the natural soil.

Axisymmetric model/mesh consists of 3048 elements and 3157 nodes (Fig. 2.6). The circular load is representative of a single wheel of the B777–200 type aircraft with 24.6 cm. (9.7 in.) radius and 1.5 MPa (215 psi) tire pressure. For the axisymmetric mesh the the domain extent was taken as 50 load radii in both the lateral and vertical directions. The distribution of the bending stress and the vertical strain through the depth of the top and second layers directly under the center of the wheel are shown in Fig. 2.7. The analyses with the nonlinear material models are performed using both the *tangent* and *secant* formulations. The gravity loads are applied in one step and the wheel loading is applied afterwards. The solution statistics for the axisymmetric analyses are shown in Table 2.2.

Again in these analyses the *tangent* method is favored since it takes slightly fewer iterations to convergence and *secant* requires additional residual evaluations over the usual equilibrium iterations.
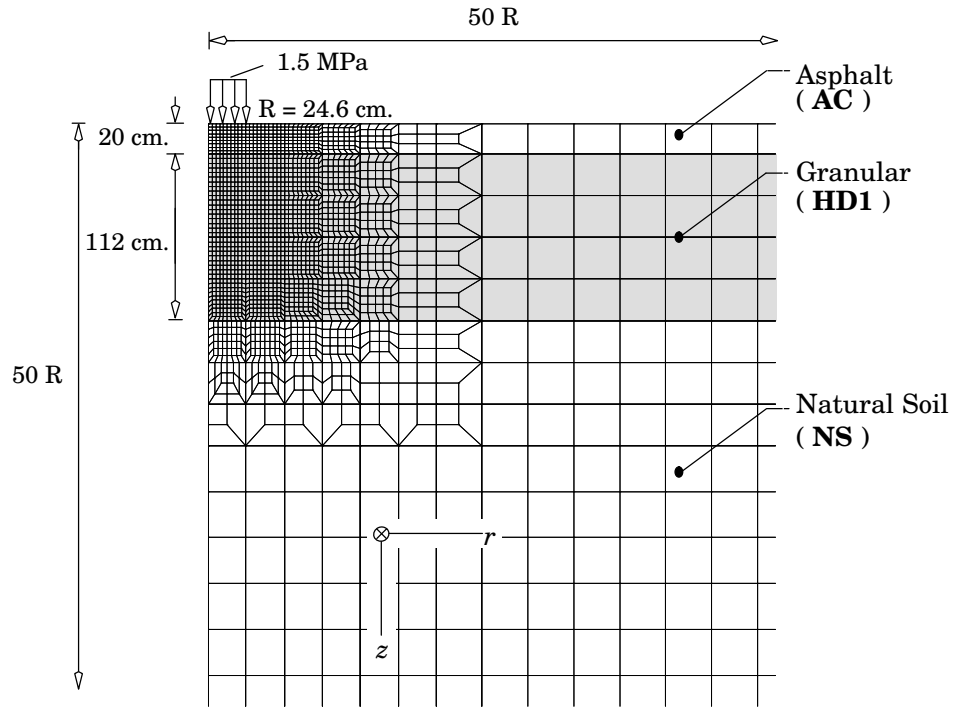
Figure 2.6. Axisymmetric mesh and geometry.
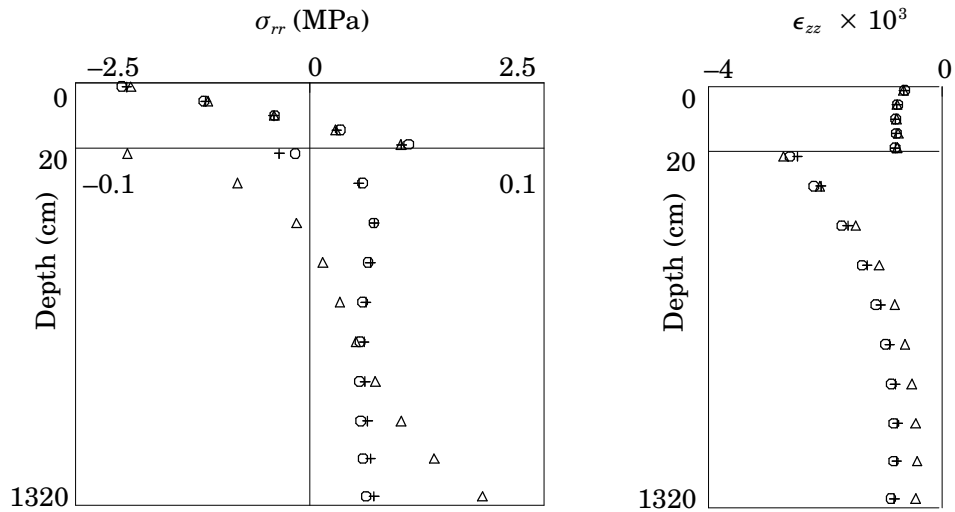
Figure 2.7. Bending stress and vertical strain under the wheel for the axi-symmetric mesh: ○ K–Θ model, + Uzan-Witczak model, Linear elasticity

MATERIAL MODEL	SOLUTION METHOD	EQUILIBRIUM ITERATIONS	
		LOAD STEP 1 (Grav. Loads)	LOAD STEP 2 (Wheel Loads)
Linear Elastic	–	1	1
K–	Tangent (7)	4	3
	Secant (2)	3	5
Uzan–Witzcak	Tangent (7)	4	5
	Secant (2)	3	6

Table 2.2. Solution Statistics for the Axisymmetric Mesh

2.4.3 Three Dimensional Pavement Analysis

For the purpose of demonstration, a 3–dimensional finite element analysis was performed on a flexible pavement system consisting of a layer of asphalt concrete on a layer of high density crushed rock, on top of natural soil as shown in Fig. 6.1 (see Chapter 6). The pavement system was subjected to a loading representative of a B777–200 type aircraft tridem gear (FAA 1995). The footprint of the loading is also shown in the same figure. The 55 cm. × 35 cm. rectangular tire prints are assumed to have a uniform pressure loading of 1.5 MPa. The loading was applied to the center of a 32 m × 32 m region. The finite element mesh of this analysis is described in Chapter 6 (see Figure 6.2).

The loading was applied in three steps with the gravity loads induced by the weight of materials first followed by two equal increments of the applied gear loads. Equilibrium under gravity loads was iterated to convergence prior to application of the wheel loads. Obviously, for the linear elastic model, one iteration was needed for each load application. For the nonlinear models the number of iterations required depends upon the solution strategy used. For this problem we considered only the consistent (unsymmetrical) tangent method without line search (method 7 in Table 2.1) and the original secant method with line search (method 2 in Table 2.1). Solution statistics of these analyses are shown in Table 2.3.

This three–dimensional example shows that the convergence results appear to favor the consistent tangent without line search over the original secant with line search, but not by much. The presentation of the stress and strain results for this analysis are def-

erred to appear in Chapter 6 in which we compare the predictions of various other resilient models as well as the ones that are presented in this chapter.

MATERIAL MODEL	SOLUTION METHOD	EQUILIBRIUM ITERATIONS		
		LOAD STEP 1 (Grav. Loads)	LOAD STEP 2 (Wheel Loads) Increment 1	Increment 2
Linear Elastic	–	1	1	1
K–	Tangent (7)	4	3	2
	Secant (2)	5	6	6
Uzan–Witzcak	Tangent (7)	4	3	5
	Secant (2)	5	5	9

Table 2.3. Solution Statistics for the Three–Dimensional Mesh

2.5 Conclusions

The $K-\theta$ and Uzan–Witczak constitutive models are widely used in pavement analysis to characterize the resilient response of granular materials. The models possess a resilient modulus C that depends upon the state of stress. These models have traditionally been implemented in finite element programs primarily with the original and damped secant methods. Success in computing with these models has been modest at best, and it appears that there has never before been a full three dimensional implementation of these models.

In this chapter we have presented a three dimensional analysis and implementation of the Uzan-Witczak constitutive model. We have shown that the resilient modulus, traditionally expressed as a function of stress invariants, can be equivalently cast in terms of strain invariants, thereby simplifying element level computations of the stress state. We have derived the consistent material tangent tensor, which has relevance both in implementing the ordinary Newton iteration and in proving that this model can suffer from loss of uniqueness of solution at various states of stress and strain. We have presented closed form expressions for the eigenvalues and eigenvectors of the material tangent tensor, from which bounds on the material constant required for uniqueness of solution were derived. We have presented a careful analysis of the convergence properties of the original and damped secant methods and have proven that it is possible for damping

to improve convergence and that there is good reason why a value of the damping parameter in the neighborhood of $\beta = 0.8$, mentioned by other researchers, works well. We have shown that the modified Newton algorithm using the secant stiffness in place of the tangent stiffness has the same convergence properties as the original (total) secant method and that convergence of the modified Newton method is not improved by damping the stiffness matrix. We have also presented a reformulation of the damped secant method that allows implementation of the method in a standard nonlinear finite element analysis package. This reformulation also has the benefits that the method can take advantage of load incrementation and line searches.

We illustrated the tradeoffs among eight versions of these algorithms with an example triaxial test configuration and a three dimensional analysis of a layered pavement system. These example suggests that the two best algorithms are ones that have not been used by other researchers concerned with these constitutive models — the original secant method with line search and Newton's method with a consistent tangent stiffness matrix. While the effort per iteration of these two methods is quite different they appear to be competitive overall.

Chapter 3

A Simple Coupled Hyperelastic Model

3.1 Introduction

Granular materials comprise discrete grains, air voids and water. These attributes lead to complex and often unpredictable behavior of these materials under applied loading. Unlike metals, granular materials tend to change their volume under deviatoric straining, and the shear stiffness of granular materials is affected by the applied mean (compressive) stress. Thus, there is a coupling effect between the volumetric and deviatoric response of granular materials. Stress induced anisotropy and inability to bear tensile hydrostatic loads are also important characteristics of granular materials to be considered when developing constitutive models to represent their behavior under loading. A thorough discussion of these important features and the accompanying experimental evidence can be found elsewhere (see for example, Lade 1988).

The triaxial test data indicate a strong stress dependence of the final shakedown slope of the cyclic response. Efforts to characterize this elastic behavior, as we have discussed earlier, go back at least to Hicks and Monismith (1971). As noted earlier, there have been many subsequent efforts to improve the description of the resilient behavior within the context of the resilient modulus and within the framework of hypoelasticity (where a stress-dependent modulus is easily implemented). The drawback of these formulations is that they do not lead to path independent elastic response and some of the models require some leaps of faith when extending them to three dimensional response.

In this chapter we propose a coupled hyperelastic constitutive model to characterize the resilient behavior of granular materials. The model is developed by adding a simple coupling term and a nonlinear shear response to the ordinary strain energy density function of linear elasticity. The resulting model is a four parameter model that can be fit to triaxial test data. The model is extended to limit the tensile response of the material under the assumption that the pressure should reach a (presumably small) limiting value as the volumetric strain takes on positive values. The model is implemented in a finite element context and compared to other models for a plate loaded pavement and as will be presented in Chapter 6, for an airport pavement containing a layer whose behavior is governed by the proposed model under applied loading.

3.2 Formulation

The framework of hyperelasticity provides a good foundation for developing constitutive models to represent the resilient behavior of granular materials. For a hyperelastic material, the stress is related to the strain through the strain energy density function $\mathcal{W}(\mathbf{E})$ by

$$\mathbf{S} = \frac{\partial \mathcal{W}(\mathbf{E})}{\partial \mathbf{E}} \tag{3.1}$$

which, in turn, guarantees path independent response. The hyperelastic model is capable of representing resilient behavior and is suited to large-scale finite element computation.

An uncoupled isotropic hyperelastic constitutive model can be derived from a strain energy density function of the form $\mathcal{W}(\epsilon, \gamma) = \mathcal{U}(\epsilon) + \mathcal{V}(\gamma)$. In particular, linear isotropic elasticity has the strain energy

$$\mathcal{W}(\epsilon, \gamma) \equiv \tfrac{1}{2} K \epsilon^2 + 3 G \gamma^2 \tag{3.2}$$

Noting that the relationships $\partial \epsilon / \partial \mathbf{E} = \mathbf{I}$ and $\partial(3\gamma^2)/\partial \mathbf{E} = 2\overline{\mathbf{E}}$, the linear elastic constitutive relationship takes the form

$$\mathbf{S} = K \epsilon \mathbf{I} + 2 G \overline{\mathbf{E}} \tag{3.3}$$

where K and G are usually called the bulk and shear moduli, respectively. This relationship between stress and strain is the familiar Hooke's Law. The mean pressure and octahedral shear stress can be computed from Eqn. (2.10) as

$$\sigma = K \epsilon, \quad \tau = 2 G \gamma \tag{3.4}$$

It is obvious from Eqns. (3.2) and (3.4) that the volumetric and deviatoric responses are uncoupled.

3.2.1. Coupled Hyperelastic models

A coupling effect can be introduced via a strain energy density function of the form

$$\mathcal{W}(\epsilon, \gamma) \equiv \tfrac{1}{2} K \epsilon^2 + 3 G \gamma^2 + \tfrac{3}{2} b \gamma^4 - 3 c \epsilon \gamma^2 \tag{3.5}$$

where K, G, b, and c are material constants. One can see the remnants of linear elasticity in this strain energy function with two additional nonlinear terms. The fourth term gives the coupling effect. It has been observed experimentally that the response in shear is nonlinear even when bulk effects are fixed. Thus, the third term enhances the primary shear response strain energy to include a quartic term. Using the definition given in Eqn. (3.1) with the strain energy function given in Eqn. (3.5) we obtain the stress-strain relationship

$$\mathbf{S} = (K\epsilon - 3c\gamma^2)\mathbf{I} + (2G + 2b\gamma^2 - 2c\epsilon)\overline{\mathbf{E}} \qquad (3.6)$$

The mean pressure and octahedral shear stress are related to the volumetric and octahedral shear strain as

$$\sigma = K\epsilon - 3c\gamma^2, \quad \tau = \left[2G + 2b\gamma^2 - 2c\epsilon\right]\gamma \qquad (3.7)$$

The coupling in Eqn. (3.7) is evident. To keep the volume constant under shearing, the pressure must increase. Because Eqn. (3.7) is linear in ϵ, one can relate shear stress to shear strain and mean stress as

$$\tau = 2G\left(1 - \frac{c}{KG}\sigma\right)\gamma + 2b\left(1 - \frac{3c^2}{Kb}\right)\gamma^3 \qquad (3.8)$$

From this relationship one can observe two important things. First, the first-order coupling feature that leads to increase shear stiffness is evident in the first term. (Remember that mean stress is negative in compression). Second, the nonlinear effect represented by the second term suggests that including the term $b\gamma^4$ in the strain energy function is essential for the reason that, since the parameter c will be determined by the primary coupling effect, the nonlinear shear response is dictated by the primary coupling without the freedom provided by b.

As we are going to develop variations of the basic formulation presented above, for clarity we shall refer to the constitutive relationship defined by Eqns. (3.5) and (3.6) as *the original coupled model.*

   Remark. It is interesting to note that $-3c\epsilon\gamma$, the bilinear function, might be considered the simplest coupling term. However, it is not a suitable choice for the coupling term in the present context of granular materials. Taking $b = 0$, for simplicity, one can show that this model leads to the linear relationships

$$\sigma = K\epsilon - 3c\gamma, \quad \tau = 2G\gamma - c\epsilon \qquad (3.9)$$

This model has the undesirable feature that shear stress can develop in absence of shear strain. Clearly, the model of Eqn. (3.7) does not have this peculiar feature.

3.2.2 Effects of Coupling

   Figure 3.1 displays the results of a numerical experiment in which octahedral shear stress τ is applied to the specimen under various values of constant (compressive) pressure (i.e., 0, −70, −350, −700 kPa or 0, −10, −50, −100 psi, respectively) for the HD1 material parameter values described in the next Chapter. The first graph (a) on Figure 3.1 shows the variation of volumetric strain ϵ with respect to octahedral shear stress. As indicated by this graph, purely deviatoric loading (i.e., octahedral shear) causes an increase
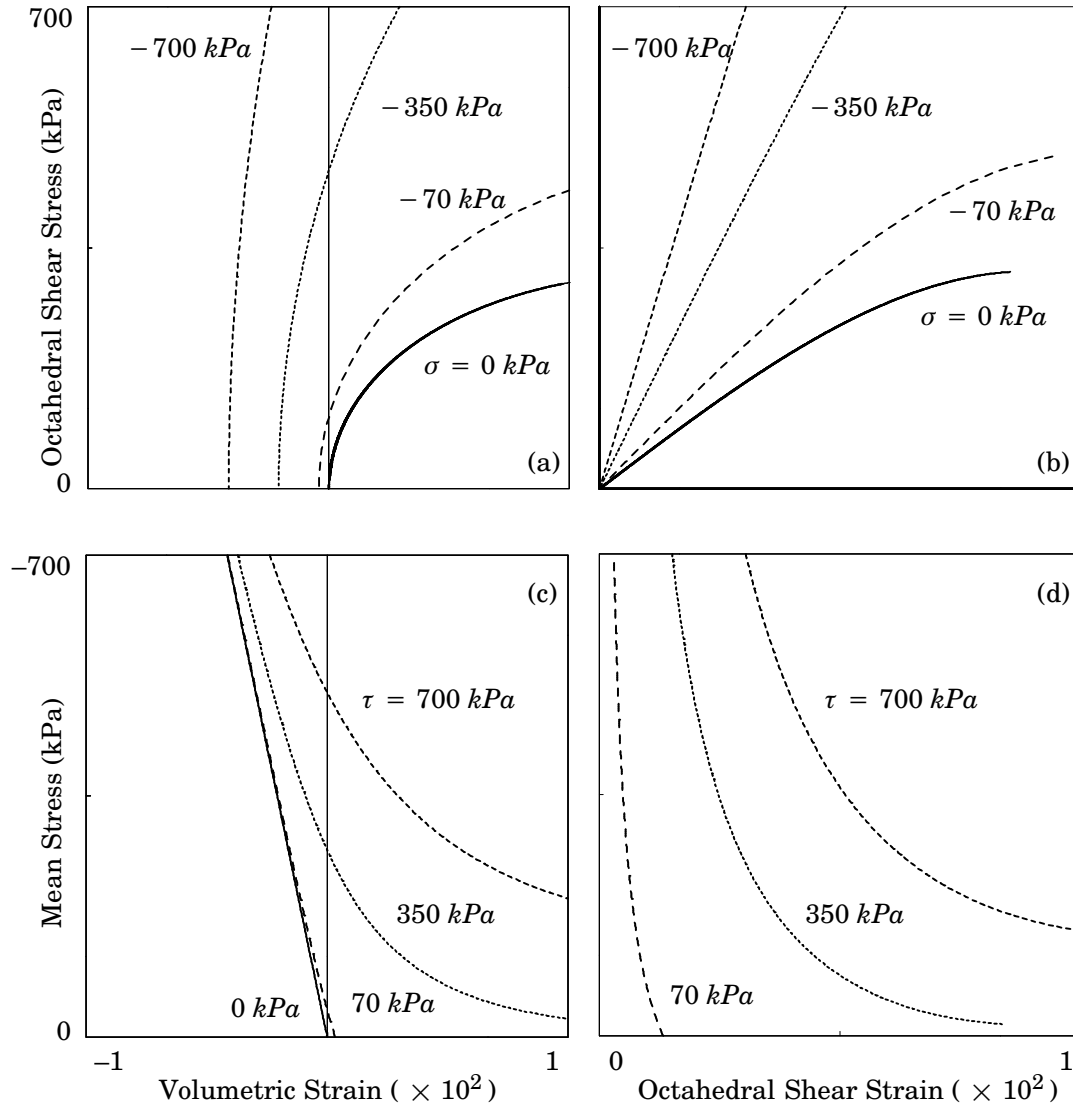
Figure 3.1. Coupling Effect Between Volumetric and Deviatoric
Responses of HD1 Specimen.

in the volume of the specimen. The behavior predicted by an uncoupled model (e.g., the linear elastic model) would yield straight (vertical) lines instead of the curved ones displayed in this graph. Furthermore, as indicated by the same graph, the rate of volume increase with respect to octahedral shear stress, decreases for higher values of constant pressure. In other words, the higher the applied pressure, the less is the volume change for a given level of octahedral shear stress. The second graph (b) in Figure 3.1 indicates that the material becomes stiffer in its deviatoric response for higher values of applied pressure.

The results of the dual experiment to the one described above in which pressure σ is applied to the specimen under various values of constant octahedral shear stress (i.e., 0, 70, 350, 700 kPa) is displayed again in Figure 3.1. Graphs (c) and (d) indicate that as the pressure is decreased from –700 kPa to 0 kPa (–100 psi to 0 psi), material becomes less stiff in its deviatoric response and may eventually fail for low values of hydrostatic pressure.

3.3 Limiting the Tensile Resistance

The stresses in a particulate medium are transferred through contact and friction between the grains. Therefore, when there is no confinement, granular materials have no means of transferring the forces between the grains. Confinement can be quantified by using the volumetric stress (hydrostatic pressure) or volumetric strain as a measure. Intuitively, granular materials should have no capacity to bear tensile hydrostatic loading. This phenomenon can be approximated within the context of hyperelasticity.

3.3.1 A Multiplicative Modification to the Strain Energy Density Function (MD)

To limit the tensile response we modify the strain energy function by multiplying an additional term $p(\epsilon)$ with the original strain energy density function that will limit the mean tensile stress when $\epsilon > 0$. Thus, the modified strain energy density is defined as

$$\mathcal{W}^{+}(\epsilon,\gamma) \equiv \mathcal{W}(\epsilon,\gamma)p(\epsilon) \tag{3.10}$$

where $\mathcal{W}(\epsilon,\gamma)$ is the strain energy given by Eqn. (3.5) and $p(\epsilon)$ is yet to be determined. The modified stress is given by the derivative of the modified strain energy density with respect to the strain as

$$\mathbf{S}^{+} = \left[(K\epsilon{-}3c\gamma^{2})p(\epsilon) + \mathcal{W}(\epsilon,\gamma)p'(\epsilon)\right]\mathbf{I} + \left(2G + 2b\gamma^{2} - 2c\epsilon\right)p(\epsilon)\overline{\mathbf{E}} \tag{3.11}$$

The modified mean stress and octahedral stress are, therefore, given by

$$\sigma^{+} = \left(K\epsilon - 3c\gamma^{2}\right)p(\epsilon) + \mathcal{W}(\epsilon,\gamma)p'(\epsilon)$$

$$\tau^{+} = \left(2G\gamma + 2b\gamma^{3} - 2c\epsilon\gamma\right)p(\epsilon) \tag{3.12}$$

We shall construct the function p so that the modified mean stress σ^{+} and octahedral shear stress τ^{+} decay as the tensile volumetric strain increases, i.e. $\epsilon \to +\infty$. Keeping this in mind, let us define a family of functions,

$$q_{n}(\epsilon) \equiv 1 - (1 - e^{-a\epsilon})^{n} \tag{3.13}$$

that depend upon the volumetric strain ϵ and proceed asymptotically to zero for all values of n. The constant a controls the rate at which the functions $q_{n}(\epsilon)$ ramp down. Note that the first and second derivatives of $q_{n}(\epsilon)$ are given by,

$$q_n'(\epsilon) \equiv -n\alpha e^{-\alpha\epsilon}(1 - e^{-\alpha\epsilon})^{n-1}$$

(3.14)

$$q_n''(\epsilon) \equiv -n\alpha^2 e^{-\alpha\epsilon}(1 - ne^{-\alpha\epsilon})(1 - e^{-\alpha\epsilon})^{n-2}$$

Let us denote, for $\epsilon < 0$, the mean stress and octahedral stress given by Eqn. (3.7) as

$$\sigma^- = \left(K\epsilon - 3c\gamma^2\right)$$

(3.15)

$$\tau^- = \left(2G\gamma + 2b\gamma^3 - 2c\epsilon\gamma\right)$$

Thus, upon comparing Eqns. (3.12) and (3.15), we see that, to enforce the continuity of stresses and –as we shall see later– the continuity of the material tangent stiffness at $\epsilon = 0$, the function $p(\epsilon)$ has to satisfy,

$$p(0) = 1, \ p'(0) = p''(0) = 0$$

(3.16)

Note that, the function $q_n(\epsilon)$ satisfies these same conditions for $n \geqq 3$. Since for $\epsilon > 0$, the term $1 - e^{-\alpha\epsilon} \leqq 1$, we see that among the family of functions $q_n(\epsilon)$, the function $q_3(\epsilon)$ is the fastest decaying one for a given α. Thus we may choose,

$$p(\epsilon) = q_3(\epsilon)$$

(3.17)

so that $\sigma^+(0,\gamma) = \sigma^-(0,\gamma)$ and $\tau^+(0,\gamma) = \tau^-(0,\gamma)$. Also note that the continuity requirements $\sigma^+(0,0) = \sigma^-(0,0)$ and $\tau^+(0,0) = \tau^-(0,0)$ are satisfied automatically.

As Eqn. (3.12) indicates, the parameter α controls the rate of decay of stresses under positive volumetric strain. Since the rate of decay cannot be determined from experiment one can simply choose it to be *sufficiently* large. This parameter can be interpreted as a *penalty* parameter: the larger the value of this parameter, the less is the resistance of the material to tension and shear. As one may anticipate, for extremely large values of α, one may suffer numerical difficulties because the material tangent stiffness has to take a sharp turn around where $\epsilon = 0$. As we shall see in the following sections, this value of α can typically be chosen in the range of 10^3–10^5 which is appropriate for very fast decay of the response with positive volumetric strain.

The strain energy density is therefore given by different equations in compression and tension, which we will designate as

$$\mathcal{W}_M(\epsilon,\gamma) = \begin{cases} \mathcal{W}(\epsilon,\gamma) & \epsilon \leq 0 \\ \mathcal{W}(\epsilon,\gamma)p(\epsilon) & \epsilon > 0 \end{cases}$$

(3.18)

We shall refer to this formulation as *coupled hyperelastic model with multiplicative decay* or *MD* for short for the remainder of this study.

3.3.2 An Additive Modification to the Strain Energy Density Function (AD)

Similarly, to limit the tensile response we can modify the strain energy function by adding an additional term $h(\epsilon,\gamma)$ that will limit the mean tensile stress when $\epsilon > 0$. The modified strain energy density is defined as

$$\mathscr{W}^+(\epsilon,\gamma) \equiv \mathscr{W}(\epsilon,\gamma) + h(\epsilon,\gamma) \tag{3.19}$$

where $\mathscr{W}(\epsilon,\gamma)$ is the strain energy given by Eqn. (3.5) and $h(\epsilon,\gamma)$ is yet to be determined. The modified stress is given by the derivative of the modified strain energy density with respect to the strain as

$$\mathbf{S}^+ = \left(K\epsilon - 3c\gamma^2 + \frac{\partial h}{\partial \epsilon}\right)\mathbf{I} + \left(2G + 2b\gamma^2 - 2c\epsilon + \frac{1}{3\gamma}\frac{\partial h}{\partial \gamma}\right)\overline{\mathbf{E}} \tag{3.20}$$

The modified mean stress and octahedral stress are, therefore, given by

$$\sigma^+ = K\epsilon - 3c\gamma^2 + \frac{\partial h}{\partial \epsilon} \tag{3.21}$$

$$\tau^+ = 2G\gamma + 2b\gamma^3 - 2c\epsilon\gamma + \frac{1}{3}\frac{\partial h}{\partial \gamma}$$

We shall construct the function h so that the modified mean stress σ^+ approaches a constant limiting value σ_o as the tensile volumetric strain increases. The transition from compressive to limiting tensile response can be accomplished by ramping up the constant term σ_o and ramping down the term $K\epsilon - 3c\gamma^2$ with complementary sigmoid functions as

$$\sigma^+ = \sigma_o[1 - d_0(\epsilon)] + \left[K\epsilon - 3c\gamma^2\right]d_0(\epsilon) \tag{3.22}$$

where $d_0(\epsilon)$ is the zeroth member of the family of functions

$$d_n(\epsilon) \equiv \frac{1}{(2a)^n}\left[4^n - (2^n - e^{-a\epsilon})^2\right] \tag{3.23}$$

that depend upon the volumetric strain ϵ and proceed asymptotically to zero for all values of n. The constant a controls the rate at which the functions $d_n(\epsilon)$ ramp down. Note that this family of functions has the special property

$$d_n' = -d_{n-1} \tag{3.24}$$

Let us assume, for the moment, that $\epsilon > 0$, thus, comparing Eqn. (3.22) with Eqn. (3.12) we find that

$$\frac{\partial h}{\partial \epsilon} = (\sigma_o - K\epsilon + 3c\gamma^2)[1 - d_0(\epsilon)] \tag{3.25}$$

If we integrate Eqn. (3.16) with respect to ϵ we get

$$h(\epsilon,\gamma) = (\sigma_o + 3c\gamma^2)[\epsilon + d_1(\epsilon)] - K\left[\tfrac{1}{2}\epsilon^2 + \epsilon d_1(\epsilon) + d_2(\epsilon)\right] + k(\gamma) \tag{3.26}$$

where $k(\gamma)$ denotes the integration constant. The veracity of Eqn. (3.17) is easily verified by differentiation, noting the property given by Eqn. (3.24). We can now compute

$$\frac{\partial h}{\partial \gamma} = 6c\gamma[\epsilon + d_1(\epsilon)] + k'(\gamma) \tag{3.27}$$

The octahedral shear stress, when $\epsilon > 0$ is given by Eqns. (3.12) and (3.27) as

$$\tau^+ = 2G\gamma + 2b\gamma^3 + 2c\gamma d_1(\epsilon) + \tfrac{1}{3}k'(\gamma) \tag{3.28}$$

There is some flexibility in determining the function $k(\gamma)$. The third term vanishes as $\epsilon \to +\infty$. Since the function $d_1(\epsilon)$ is not zero at $\epsilon = 0$, the term $2c\gamma d_1(\epsilon)$ causes a jump in the shear modulus at $\epsilon = 0$. To assure the continuity of octahedral shear stress, the constant has to be

$$k(\gamma) \equiv k_o - c\gamma^2 d_1(0) \tag{3.29}$$

where the value of k_o is immaterial and can be taken as zero and $d_1(0) = 3/2a$. This choice of the function $k(\gamma)$ results in the expression

$$\tau^+ = \left[2G + 2b\gamma^2 - 2c(d_1(0)-d_1(\epsilon))\right]\gamma \tag{3.30}$$

The shear stress is nonlinear in the shear deformation γ with initial stiffness $(2G + 2b\gamma^2)$ decaying to a final stiffness of $2G + 2b\gamma^2 - 2cd_1(0)$. Since $d_1(0) = 3/2a$, ignoring for the moment, the higher order term $2b\gamma^2$, we must have

$$G \geq \frac{3c}{2a} \tag{3.31}$$

Since the rate of decay cannot be determined from experiment one can simply choose it again to be sufficiently large while satisfying Eqn. (3.31). As we shall see in the following section, this value of a can typically be chosen within the range of 10^3–10^5, which is appropriate for very fast decay of the response with positive volumetric strain. Note that for very large values of the parameter a the shear response of the material becomes uncoupled from the volumetric response. The final form of the constitutive relationship for $\epsilon > 0$ can be written as

$$\mathbf{S}^+ = \left[\sigma_o(1-d_0(\epsilon)) + (K\epsilon - 3c\gamma^2)d_0(\epsilon)\right]\mathbf{I} + \left[2G + 2b\gamma^2 - 2c(d_1(0)-d_1(\epsilon))\right]\overline{\mathbf{E}} \tag{3.32}$$

where $d_n(\epsilon)$ is given by Eqn. (3.13). As we shall demonstrate later, this modification limits the pressure while allowing for the granular medium to dilate under deviatoric loading. Note that the continuity requirements for the stress, i.e. $\sigma^+(0,\gamma) = \sigma^-(0,\gamma)$ and $\tau^+(0,\gamma) = \tau^-(0,\gamma)$ are satisfied. Also note that the continuity requirements at zero strain $\sigma^+(0,0) = \sigma^-(0,0)$ and $\tau^+(0,0) = \tau^-(0,0)$ are satisfied as well.

The strain energy density is therefore given by different equations in compression and tension, which we will designate as

$$\mathcal{W}_A(\epsilon,\gamma) = \begin{cases} \mathcal{W}(\epsilon,\gamma) & \epsilon \leq 0 \\ \mathcal{W}(\epsilon,\gamma) + h(\epsilon) & \epsilon > 0 \end{cases} \tag{3.33}$$

We shall refer to this formulation as *coupled hyperelastic model with additive decay* or *AD* for short for the remainder of this study.
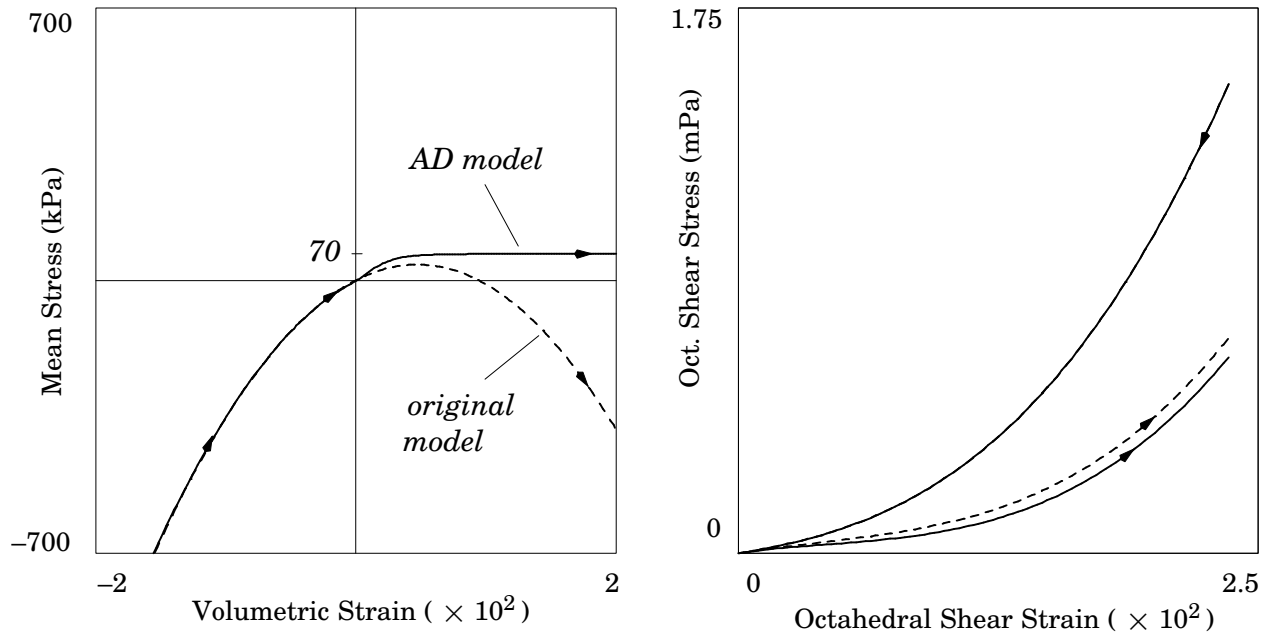
Figure 3.2. Response of HD1 for original and additive decay (AD) models under prescribed strains.

Remark. Eqn. (3.30) implies that the octahedral shear stress grows with octahedral shear strain, independent of the volumetric strain. This artifact is undesirable, however, for very large values of the parameter a, the shear stiffness of the material under positive volumetric strain will be considerably less than its response under compression. Keeping in mind that both modifications (AD and MD) are merely attempts to assess the material behavior close to failure, and the actual behavior of the material under positive volumetric straining can not properly be characterized without the consideration of plastic deformations, we shall nevertheless proceed with the AD formulation, treating it as a simple approximation of the response of the material near failure.

3.3.3 A Numerical Experiment

In order to display the behavior the constitutive models presented earlier in this chapter (i.e. original model, model with additive decay (AD) and model with multiplicative decay (MD)), we shall conduct a numerical experiment. In this experiment a single material point is proportionally loaded with a prescribed volumetric and octahedral shear strains. The material constants are those of the granular material designated as HD1 by Allen (1973) (see Chapter 4).

Figure 3.2 displays the results for the original formulation and the AD model. Arrows in the figure indicate the direction of loading. For the AD model, the additional material constants were chosen as $\sigma_o = 70$ kPa (or 10 psi) and $a = 5000$. As expected, for the AD
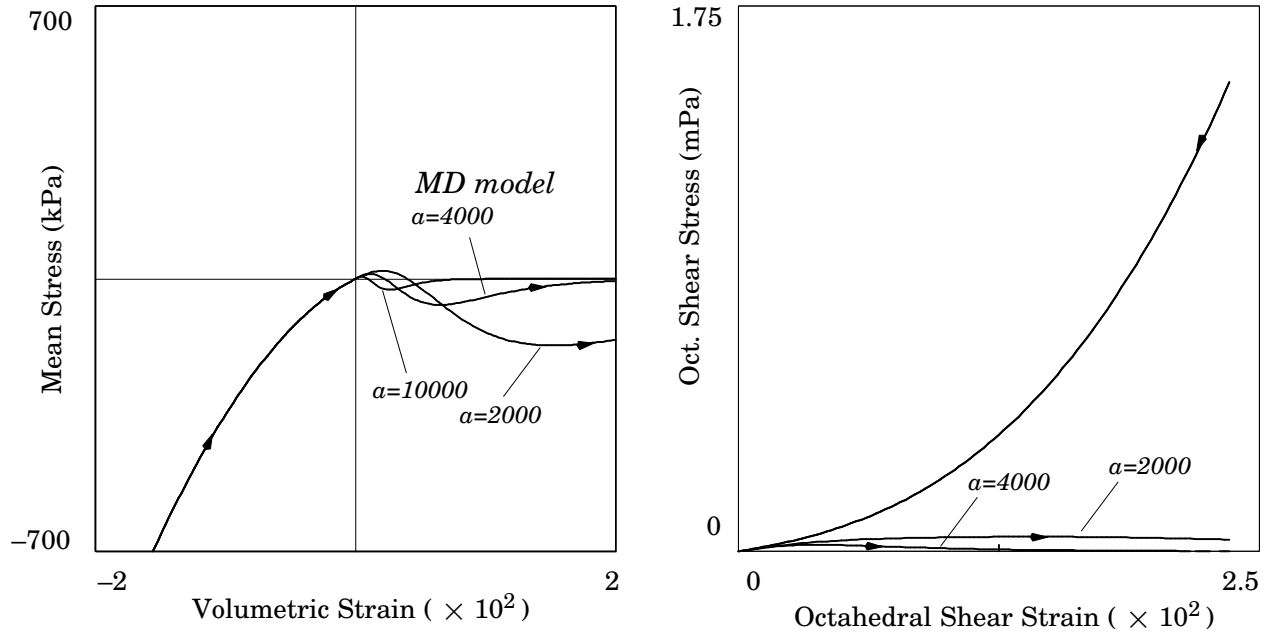
Figure 3.3. Response of HD1 for the multiplicative decay model (MD) under prescribed strains.

formulation, the maximum allowed hydrostatic pressure is limited to 70 kPa. For both the *original* and the *AD* models the material became less stiff in its deviatoric (shear) response when under tensile hydrostatic loading. The behavior of the material given by the *AD* model in the volumetric stress/strain space resembles that of an elastoplastic material, however, all deformations in this case are fully recoverable, unlike elastoplasticity. Also note that the original formulation (i.e. coupled hyperelastic model without the modifications) strain–softens under positive volumetric strain due to coupling. Thus, for large enough shear strains, compressive pressure develops in the material even though it has dilated. This is certainly a violation of the second law of thermodynamics. However it may still yield reasonable results for the behavior of the pavement systems under applied loading, provided that nowhere throughout the granular layer, such stress and strains occur.

Figure 3.3 displays the results for the *MD* model only, for different values of the parameter a (see Eqn (3.13)) which controls the rate of decay. The remaining material constants are, again, taken from HD1 material. As this figure indicates, the *AD* model also has the undesirable feature as the original model does: it develop compressive pressure even though the material has dilated. However, unlike the original formulation this built up of pressure is limited and as the value of the parameter a grows, this limit decreases. Thus as $a \rightarrow \infty$, we get a reasonable model. Note that, for this specific loading

$a = 4000$ yields a reasonable response for the behavior of the HD1 material under positive volumetric strains.

3.4 Material Tangent Stiffness

To perform numerical computations with nonlinear material models one must evaluate the material tangent stiffness $\mathbf{C}$. The material tangent stiffness $\mathbf{C}$ for the proposed model can easily be computed as

$$\mathbf{C} = \frac{\partial \mathbf{S}}{\partial \mathbf{E}} \tag{3.34}$$

The stress is given by different equations in compression and tension, which we will designate as

$$\mathbf{S} = \begin{cases} \mathbf{S}^- & \epsilon \leq 0 \\ \mathbf{S}^+ & \epsilon > 0 \end{cases} \tag{3.35}$$

where the tensor $\mathbf{S}^-$ is given by Eqn. (3.6) for all of the models discussed in this chapter. For the *original coupled model* $\mathbf{S}^+$ is the same as $\mathbf{S}^-$. For the *coupled model with multiplicative decay* (*MD*), $\mathbf{S}^+$ is given by Eqn. (3.11) and for the *coupled model with additive decay* (*AD*) $\mathbf{S}^+$ is given by Eqn. (3.32). The material tangent stiffness $\mathbf{C}$ can also be expressed as

$$\mathbf{C} = \begin{cases} \mathbf{C}^- & \epsilon \leq 0 \\ \mathbf{C}^+ & \epsilon > 0 \end{cases} \tag{3.36}$$

Material tangent stiffness tensor for the original model. From Eqn. (3.6) one can compute the material tangent modulus in compression to be

$$\begin{aligned}
\mathbf{C}^-(\epsilon,\gamma) = {} & K\mathbf{I} \otimes \mathbf{I} + 2[G + b\gamma^2 - c\epsilon]\mathbf{1} \\
& - 2c[\overline{\mathbf{E}} \otimes \mathbf{I} + \mathbf{I} \otimes \overline{\mathbf{E}}] + 2b\overline{\mathbf{E}} \otimes \overline{\mathbf{E}}
\end{aligned} \tag{3.37}$$

This is also the material tangent stiffness tensor for the *original model* in tension.

Material tangent stiffness for the MD model. From Eqn. (3.11) one can compute the material tangent modulus in tension to be

$$\begin{aligned}
\mathbf{C}^+(\epsilon,\gamma) = {} & \left[Kq(\epsilon) + 2(K\epsilon - 3c\gamma^2)q'(\epsilon) + \mathcal{W}(\epsilon,\gamma)q''(\epsilon)\right]\mathbf{I} \otimes \mathbf{I} \\
& + \left[(2G + 2b\gamma^2 - 2c\epsilon)q'(\epsilon) - 2cq(\epsilon)\right]\left[\overline{\mathbf{E}} \otimes \mathbf{I} + \mathbf{I} \otimes \overline{\mathbf{E}}\right] \\
& + \tfrac{4}{3}b\overline{\mathbf{E}} \otimes \overline{\mathbf{E}} + (2G + 2b\gamma^2 - 2c\epsilon)q(\epsilon)\mathbf{1}
\end{aligned} \tag{3.38}$$

Material tangent stiffness for the AD model. From Eqn. (3.32) one can compute the material tangent modulus in tension to be

$$\mathbf{C}^{+}(\epsilon,\gamma) = \left[Kd_0(\epsilon) + (\sigma_o - K\epsilon + 3c\gamma^2)d_{-1}(\epsilon)\right]\mathbf{I} \otimes \mathbf{I} \tag{3.39}$$
$$- 2cd_o(\epsilon)\left[\overline{\mathbf{E}} \otimes \mathbf{I} + \mathbf{I} \otimes \overline{\mathbf{E}}\right] + \tfrac{4}{3}b\overline{\mathbf{E}} \otimes \overline{\mathbf{E}}$$
$$+ \left[2G + 2b\gamma^2 - 2c(d_1(0) - d_1(\epsilon))\right]\mathbf{1}$$

where $\mathbf{I} \otimes \mathbf{I}$ is the fourth order identity tensor with components $[\mathbf{I} \otimes \mathbf{I}]_{ijkl} = \delta_{ij}\delta_{kl}$, $\mathbf{1}$ is the fourth order tensor with components $\mathbf{1}_{ijkl} = \delta_{ik}\delta_{jl} - \tfrac{1}{3}\delta_{ij}\delta_{kl}$, and the components of the tensor $\mathbf{I} \otimes \overline{\mathbf{E}}$ are $\left[\mathbf{I} \otimes \overline{\mathbf{E}}\right]_{ijkl} = \delta_{ij}\overline{E}_{kl}$. The functions $d_n(\epsilon)$ are given by Eqn. (3.23). One can see that the tangents for all the models satisfy the continuity relationships

$$\mathbf{C}^{+}(0,\gamma) = \mathbf{C}^{-}(0,\gamma), \quad \mathbf{C}^{+}(0,0) = \mathbf{C}^{-}(0,0) \tag{3.40}$$

Also note that the material tangent stiffness for all the models at zero strain is

$$\mathbf{C}(\epsilon,\gamma) = K\mathbf{I} \otimes \mathbf{I} + 2G\mathbf{1} \tag{3.41}$$

3.5 Plate Loading Test

The constitutive models described earlier are implemented to a finite element analysis code (ABAQUS, 1994) and a plate loading test is performed. The circular plate which is 20.3 cm. (8 inches) thick and has a radius of 380 cm. (150 inches) is made of asphalt concrete. It is loaded with a distributed load of 700 kPa (100 psi) with a radius of 24.6 cm. (9.7 inches). In addition to the wheel load, gravity loads (i.e. self weight of the structure) are include in the analyses. The plate stands on top of a 76.2 cm. (30 inches) thick layer of HD1 material. The bottom layer is natural soil. The lateral and vertical extent of the finite element model are chosen to be 40 times the radius of the wheel load, sufficiently remote so that the stresses and strains of interest (i.e. values within the vicinity of the load) are not significantly effected by the remote boundary conditions. The boundary conditions at the remote vertical boundary were chosen such that the displacements in the vertical (z) direction were fixed. The geometry and the axisymmetric finite element mesh are displayed on Figure 3.4.

The densities of the materials were taken to be 0.0024 kgf/cm³ for the (asphalt consrete) plate, 0.0022 kgf/cm³ for the crushed rock, and 0.0017 kgf/cm³ for the natural soil. The plate was assumed to be linearly elastic with Young's modulus $E = 2070$ MPa (300 ksi) and Poisson's ratio of $v = 0.15$. The natural soil was also assumed to be linearly elastic with Young's modulus $E = 40$ MPa (6 ksi) and Poisson's ratio of $v = 0.45$. The second layer was modeled using one of the following four models: (a) linear elasticity with $E = 240$ MPa (34.9 ksi) and $v = 0.34$, (b) *original* model with $K = 166$ MPa (24 ksi), $G = 52.4$ MPa (7.6 ksi), $b = 3.2 \times 10^7$ MPa (4.63×10^9 ksi) and $c = 4.3 \times 10^4$ MPa (6.3×10^3 ksi) (c) *AD* model with all material constants same as the original model with its additional constants a=5000 and $\sigma_o = 0$ MPa.and finally (d) *MD* model, again with all material constants same as the original model and with its additional constant $a = 4000$. The values of these material constants are for the high density crushed rock material designated as HD1 by Allen (1973) (see Chapter 4).
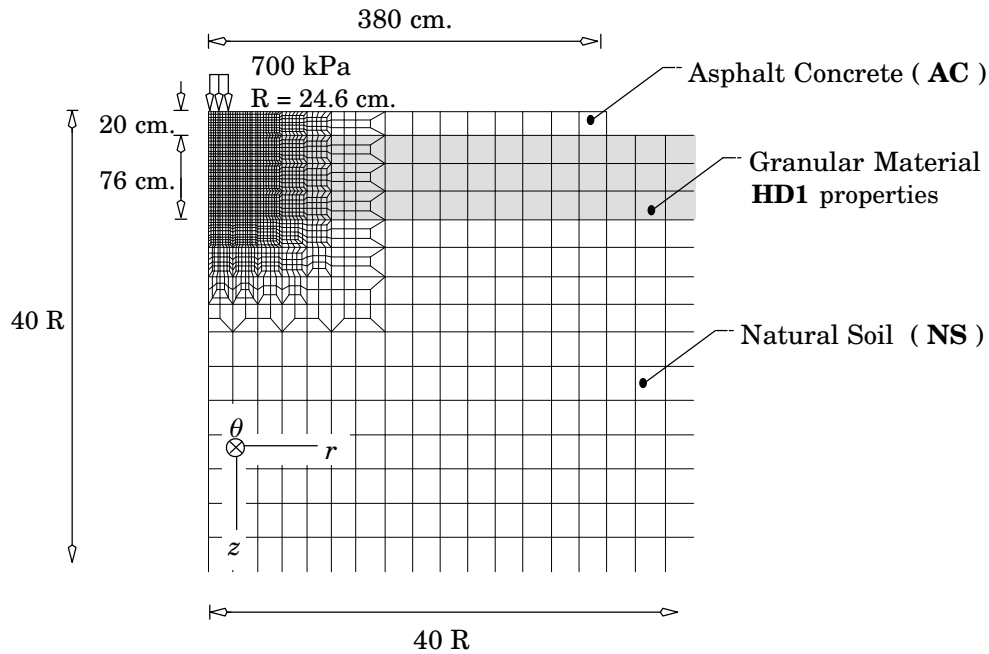
Figure 3.4. Plate Loading Test: Axisymmetric mesh and geometry.

Figure 3.5 shows the variation of the bending stress and vertical strain with respect to depth along the axis of symmetry. It can be seen that the *AD*, *MD* and *original* models predict a significantly larger bending stress –an important design parameter– at the bottom of the plate compared to the linear elastic model. However, *AD*, *MD* and *original* models all yield almost the same value for this bending stress. Also note that the *AD* and the *original* models yield almost identical values for the bending through the depth of the HD1 layer. Limiting the pressure, nevertheless, still yields tensile stresses in the granular layer which is unrealistic. However, it can be seen from Figure 3.5 that the *MD* model is trying to reduce this built–up of tensile stress as well. This is clearly due to the fact that both *AD* and *original* models allow the shear stress to grow independent of the dilation while the *MD* model limits both the pressure and the shear stress.

Figure 3.6 shows the variation of pressure, volumetric strain octahedral shear stress and strain for *MD* model and *linear elasticity*. This figure also includes results for the material a=2000. Note that while the use of *MD* model effectively eliminates tensile pressure, it predicts compressive pressure for positive volumetric strains. This, as mentioned before, can be eliminated by using a larger value for the parameter a. However, as a becomes larger, convergence difficulties may prevent one to obtain a solution. In such cases, the use of well known techniques such as line–searches and arc–length continuation methods may be a remedy (see, for example, Crisfield 1993).
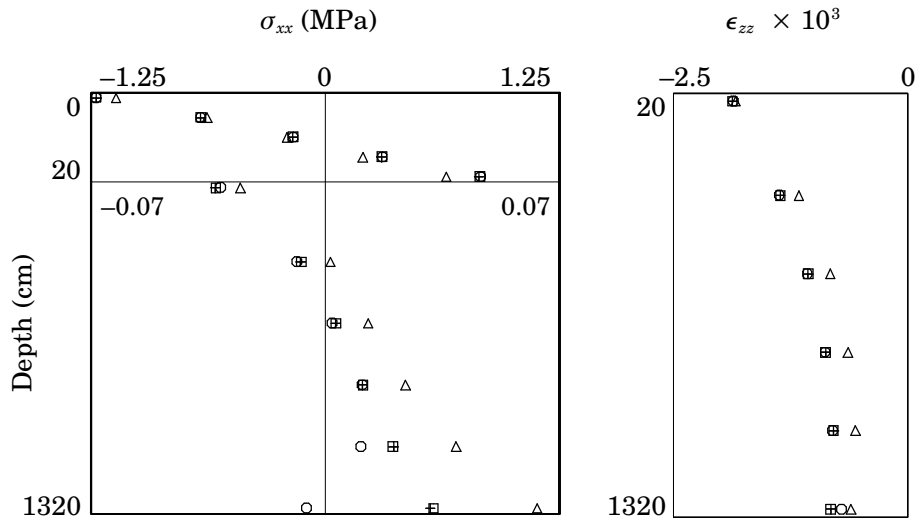
Figure 3.5. Bending stress and vertical strain under the wheel for the 3–dimensional mesh: ○ *MD* model, + *AD* model,   Linear elasticity, □ *Original* model

Figure 3.7 shows the variation of pressure, volumetric strain octahedral shear stress and strain for *AD* model and the *original* model. Both models yield no tensile volumetric stress (pressure) through the granular layer as expected. For the plate bending test under the given loads, both models yielded identical results. This is due to the fact that load was not high enough to reveal the differences of these two models. When we analyze a 3–dimensional pavement model later on in Chapter 5, the differences between them will become more evident.

3.6 Conclusions

A coupled hyperelastic constitutive model for predicting the behavior of granular materials along with a methodology to develop similar models has been proposed. The model predicts the dependency of deviatoric response on the hydrostatic pressure and the change in volume under deviatoric loading, the phenomenon that are deemed important in modeling granular materials. The proposed model can easily be implemented in a finite element analysis program and it is amenable to large scale computation. This feature of the proposed model is particularly important since for consideration of non–axisymmetric loads and for studying the effects of wheel load interaction large scale computation is inevitable. The proposed model can also be used to model the elastic behavior of soils provided that it is calibrated with appropriate tests. Since the constitutive model is based on the thermodynamically consistent hyperelasticity, the stress state for given strains is unique, and the response of the material is path independent. However,
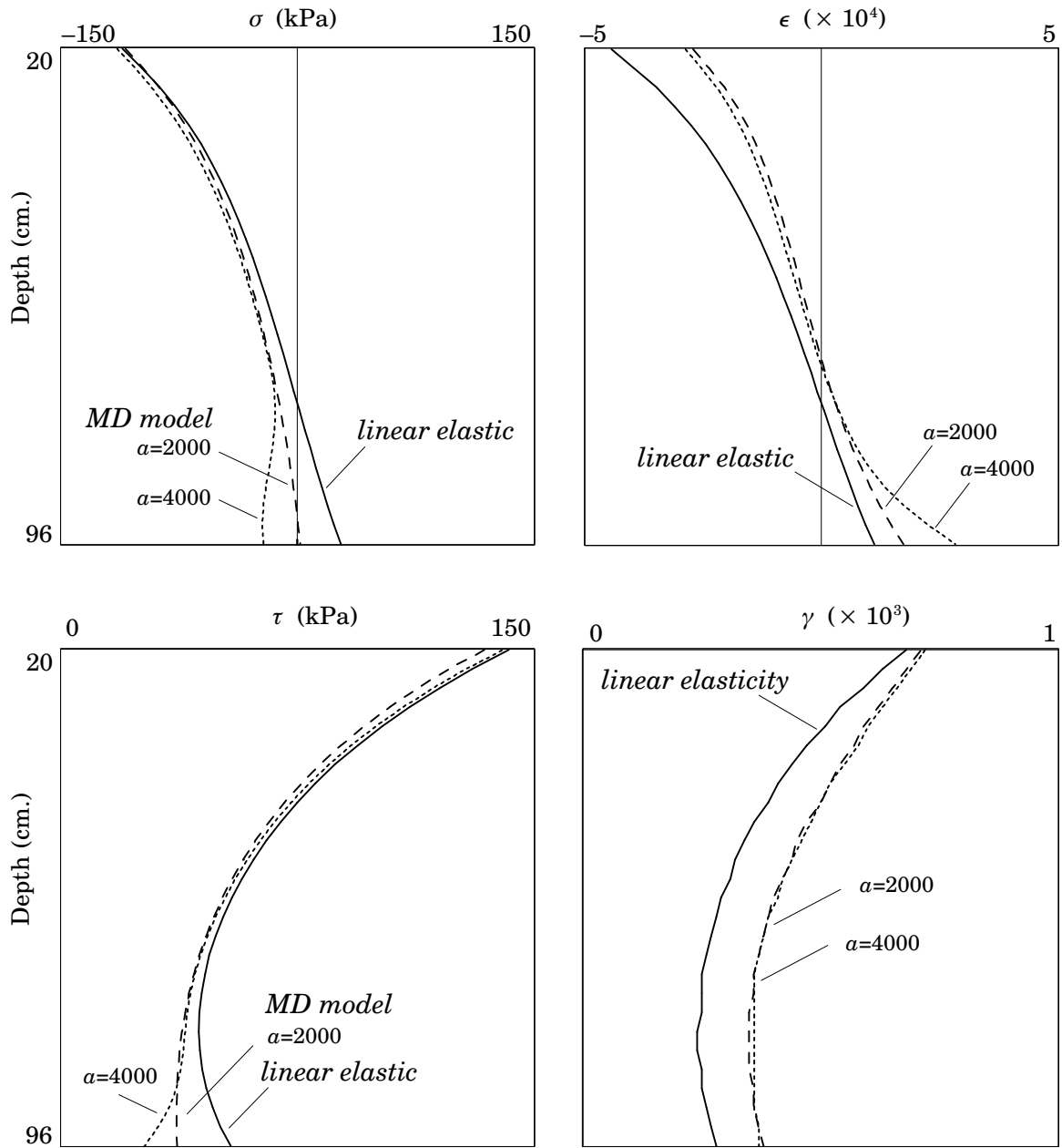
Figure 3.6. Variation of volumetric and octahedral shear stress
and strain through depth for *MD* model and linear elasticity.

the bounds on the material constants within which the constitutive model is stable and
unique are not established.
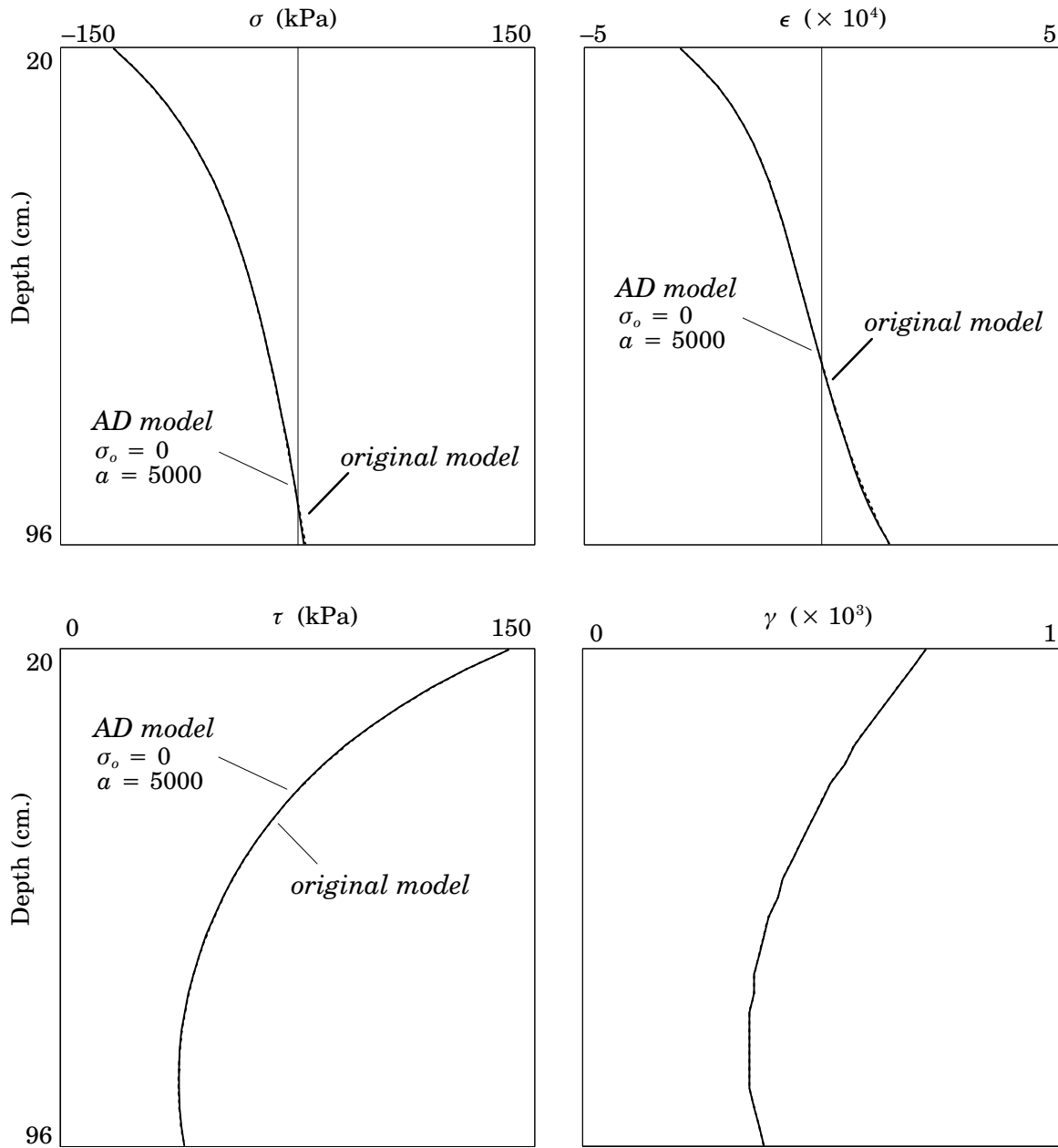
Figure 3.7. Variation of volumetric and octahedral shear stress and strain through depth for *original* and *AD* models.

The proposed model has been calibrated using resilient test data obtained from literature, and as we shall present in the following chapter it gives better fits to the test data than linear elasticity, $K - \theta$ model and Uzan model.

The fact that the granular materials have no or little tensile stress bearing capability has important implications to the design of pavement systems. To this end, we have proposed two alternative modifications to the original coupled hyperelastic model which effectively allows the control of the maximum hydrostatic tensile stress value and the way the tension-limited state is achieved can easily be manipulated and changed by using different forms of the auxiliary energy density functions, $p(\epsilon, \gamma)$ for the *model with additive decay* (*AD*) and $q(\epsilon)$ for the model with *multiplicative decay* (*MD*).

Chapter 4

Determination of Material Constants

Determination of material constants from experimental data is an important part of constitutive modelling. This chapter deals with the calibration of the K–θ, *Uzan–Witzcak* models and the coupled hyperelastic model (i.e. the *original model*) described in Chapter 3 from experimental data. Experimental data is obtained from available literature and statistical comparison of the success of K–θ, *Uzan–Witzcak*, coupled model and Linear Elasticity models in predicting the experimental values is presented.

4.1 Experimental Data

The resilient triaxial test data was obtained by Allen and Thompson at the University of Illinois (1973). They conducted tests on nine different specimens, and measured both vertical and lateral strains during each test. A brief description of these materials are shown in Table 4.1.

Specimen	Material	Density, kg/m^3	
HD1	Crushed Stone	2240	High
MD1	Crushed Stone	2170	Intermediate
LD1	Crushed Stone	2110	Low
HD2	Gravel	2260	High
MD2	Gravel	2170	Intermediate
LD2	Gravel	2125	Low
HD3	Blend	2260	High
MD3	Blend	2180	Intermediate
LD3	Blend	2125	Low

Note: 1 kg/m^3 = 0.0617 lbs/ft^3

Table 4.1. Test Specimens of Allen–Thompson Resilient Tests (Allen 1973).

The samples were first subjected to several cycles of certain stress patterns to achieve resilient behavior (i.e. shakedown). This phase is called *preconditioning*. Preconditioning simulates the actual response of granular layers in pavements at very early stages of their service life. Allen and Thompson report that after 10 to 20 cycles the samples were

almost entirely shaken down and the response after this stage was essentially nonlinear elastic. The samples were then subjected to repeated stress pulses with levels anticipated in granular layers of pavements under wheel loads. The data set of these experiments can be found in Appendix III.

4.2 A Weighted Nonlinear Least Squares Procedure

The values of the material constants were determined through a weighted nonlinear least squares curve fitting procedure. In a triaxial test the axial stress σ_1 and the lateral stress σ_2 are measured. From these measured values the mean and octahedral stresses can be computed as

$$\sigma = \tfrac{1}{3}(\sigma_1 + 2\sigma_2), \quad \tau = \tfrac{\sqrt{2}}{3}(\sigma_1 - \sigma_2) \tag{4.1}$$

The axial strain ϵ_1 and lateral strain ϵ_2, are also measured. From these measured values the mean and octahedral strains can be computed as

$$\epsilon = (\epsilon_1 + 2\epsilon_2), \quad \gamma = \tfrac{\sqrt{2}}{3}(\epsilon_1 - \epsilon_2) \tag{4.2}$$

Let us define the mean and deviatoric residual functions as,

$$r_i(\boldsymbol{x}) \equiv \hat{\sigma}_i - \sigma_i(\boldsymbol{x}, \hat{\epsilon}_i, \hat{\gamma}_i), \quad s_i(\boldsymbol{x}) \equiv \hat{\tau}_i - \tau_i(\boldsymbol{x}, \hat{\epsilon}_i, \hat{\gamma}_i) \tag{4.3}$$

where $\{\hat{\sigma}_i,\ \hat{\tau}_i,\ \hat{\epsilon}_i,\ \hat{\gamma}_i\}$ are the measured stresses and strains for observation i and for the coupled hyperelastic model described in Chapter 3, for example, $\boldsymbol{x} = \{K, G, b, c\}$ is the vector of unknown material constants. To determine the constitutive parameters from triaxial measurements we minimize the weighted least-squares residual function

$$g(\boldsymbol{x}) \equiv \tfrac{1}{2}\left(\lambda \sum_{i=1}^{N} r_i^2(\boldsymbol{x}) + (1-\lambda) \sum_{i=1}^{N} s_i^2(\boldsymbol{x})\right) \tag{4.4}$$

where the weight parameter λ can be specified to have a value between 0 and 1. By varying the value of λ we can apply different weights to the volumetric and deviatoric components of the test data. This is done to take into account the relative difference in the magnitudes of the volumetric and deviatoric stress and strain, with the hope of obtaining a better fit for values of λ other than 0.5.

The gradient and the Hessian of the objective function are given by,

$$\nabla g(\boldsymbol{x}) = \lambda \mathbf{J}_m^T \mathbf{r} + (1-\lambda)\mathbf{J}_d^T \mathbf{s}$$

$$\mathbf{H}_g(\boldsymbol{x}) \cong \lambda \mathbf{J}_m^T \mathbf{J}_m + (1-\lambda)\mathbf{J}_d^T \mathbf{J}_d \tag{4.5}$$

respectively. The ij th components of the Jacobian matrices are computed with the following convention $[\mathbf{J}_m]_{ij} \equiv \partial r_i/\partial x_j$ and $[\mathbf{J}_d]_{ij} \equiv \partial s_i/\partial x_j$. Beginning with an initial guess $\boldsymbol{x}^{(o)}$ one can generate a sequence of approximations $\{\boldsymbol{x}^{(k)}\}$ according to the recursion formula
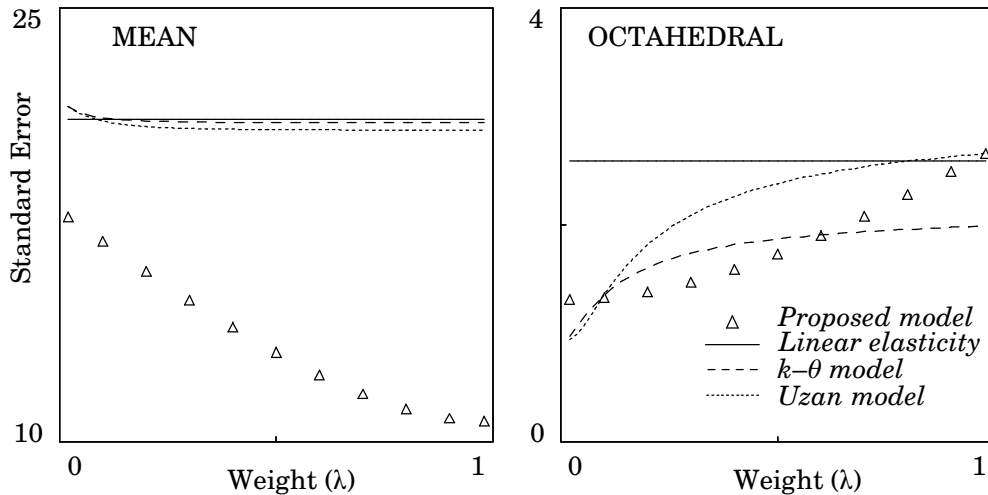
Figure 4.1. Standard Error versus Weight Parameter (λ) for HD1 Material.

$$\boldsymbol{x}^{(k+1)} \;=\; \boldsymbol{x}^{(k)} - \mathbf{H}_g^{-1}\!\big(\boldsymbol{x}^{(k)}\big)\,\nabla g\!\big(\boldsymbol{x}^{(k)}\big) \tag{4.6}$$

This method is the well-known Gauss–Newton method. Provided that we start with an appropriate initial guess $\boldsymbol{x}^{(o)}$, the sequence of iterates converge with a subquadratic rate, since the Hessian matrix given by Eqn. (4.5) is an approximation to the actual one (Heath 1997), to the desired parameter values.

A more elaborate curve fitting procedure and statistical evaluation of the test data may yield better fits for any of the models examined in this paper. For example, one can include the weight parameter λ among the unknowns, and minimize the objective function accordingly. However, we use only the value $\lambda = 0.5$, unless specifically noted otherwise. For different values of the weight parameter λ, it is possible to obtain a better fit between the predicted and measured responses of the test specimens, with the exception of the linear elastic model.

A plot of the variation of the standard error between predicted and measured mean stress σ and octahedral shear stress τ with respect to the weight parameter λ is shown in Figure 4.1 for the HD1 material. It is apparent from this figure that the proposed model does a better job in predicting the mean stress values and, as $\lambda \rightarrow 1$, the accuracy of the predictions increase considerably. Also, Figure 4.1 reveals that the other material models show little sensitivity with respect to parameter λ, for mean stress values. Clearly, the proposed model can be made to achieve greater accuracy in predicting the volumetric (mean) response of the material at the expense of sacrificing the accuracy in its prediction of the deviatoric response. Figure 4.2 shows the predicted versus measured mean stress (σ) and octahedral shear strain (τ) values.
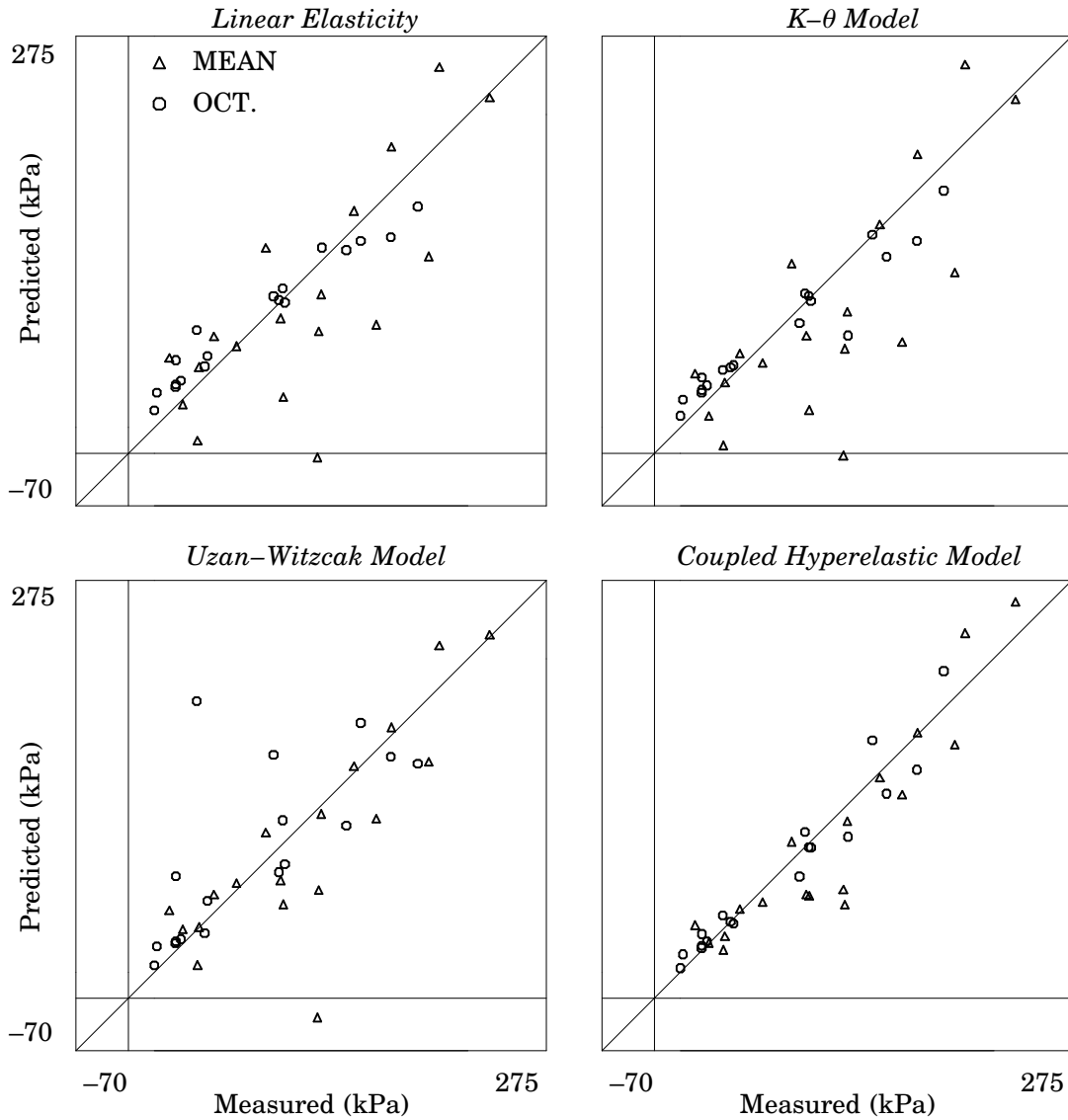
Figure 4.2. Predicted vs. Measured Response of HD1 Specimen
(Test Allen, Thompson 1976).

Figure 4.3 shows the distribution of standard error between the predicted and measured values of volumetric and octahedral shear stress values for all the specimens. As this figure indicates, the proposed coupled hyperelastic model generally did better than the other three models in predicting the measured volumetric and octahedral stress values. The total success of any of these constitutive models is a combination of their predictions in volumetric and octahedral stress spaces. A brief investigation of the test data reveals that, the magnitude of the octahedral stresses and strains in all of the tests were
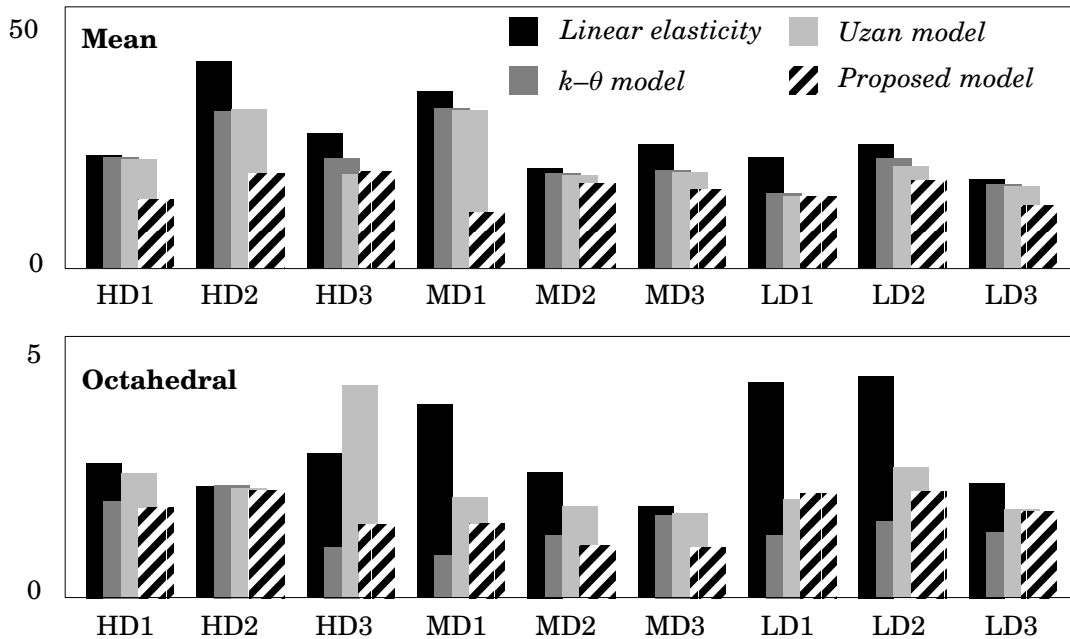
Figure 4.3. Distribution of Standard Error Between Predicted
and Measured Stress Values for Various Material Models.

relatively smaller than the volumetric stress and strain values. As these measurements were probably made with similar instruments, the octahedral measurements would be more polluted by experimental error. Therefore, one can intuit that the data fit for the volumetric response would be better. The values in Figure 4.3 were computed for $\lambda = 0.5$. However, for each specimen, there always was a value of λ such that the standard error of both the predicted mean and octahedral stress values were less for the proposed model, than for the other models. For example, the range of λ for the HD1 specimen for which the proposed model always does better is between 0.1 and 0.6.

Remark. In most cyclic triaxial tests the lateral strain ϵ_2 is not measured. The evaluation of the material parameters goes as follows. The resilient modulus M_r is measured for each level of applied stress and tabulated as the ratio $(\sigma_1 - \sigma_2)/\epsilon_1$. The material constants k, n, and m (of the Uzan-Witzcak model) are determined by minimizing the error function $e(k,n,m) \equiv \ln(M_r^{meas}) - \ln(k\theta^n\tau^m)$, where M_r^{meas} is the value of the measured ratio $(\sigma_1 - \sigma_2)/\epsilon_1$ and $\theta \equiv \frac{1}{3}|\sigma_1 + 2\sigma_2|$ and $\tau \equiv \sqrt{2}|\sigma_1 - \sigma_2|/3$ are evaluated from the measured applied stresses. This data fit can be done with linear least-squares. Unfortunately, the values of the material constants obtained by this procedure are not consistent with the constitutive model described by Eqn. (2.18). In fact, it is impossible to uniquely assess the material constants from triaxial test data without the lateral strain ϵ_2. Throughout this manuscript, when we refer to the $K-\theta$ or Uzan-Witzcak models we mean the model

Table 4.2. Material constants for various models in U.S. Customary units.

Materials	Linear Elasticity		K–θ Model			Uzan–Witzcak Model				Coupled Hyperelastic Model			
	E (ksi)	v	k (ksi)	v	n	k (ksi)	v	n	m	K (ksi)	G (ksi)	b (ksi)	c (ksi)
HD1	34.9	.34	14.2	.33	.29	14.8	.33	.22	.07	24.1	7.6	4.6E+06	6200
HD2	28.2	.38	2.2	.43	.82	4.4	.43	.41	.34	18.1	5.4	2.8E+06	8900
HD3	44.6	.40	6.3	.41	.64	.41	.42	2.0	−1.1	26.9	6.4	12.0E+06	16870
LD1	31.0	.36	3.7	.36	.70	.54	.36	1.2	−.38	16.8	2.7	5.5E+06	8600
LD2	26.0	.36	6.0	.36	.49	1.9	.35	1.2	−.59	16.2	2.6	3.7E+06	6600
LD3	27.5	.36	8.3	.36	.39	5.9	.36	.63	−.23	21.6	6.3	1.1E+06	4250
MD1	33.9	.38	3.8	.39	.69	24.0	.40	−.25	.67	24.9	2.0	9.2E+06	11200
MD2	28.8	.40	13.7	.29	.40	4.9	.40	.78	−.37	28.6	6.0	2.0E+06	5100
MD3	29.8	.40	3.6	.41	.67	2.5	.41	.95	−.27	29.5	6.8	1.8E+06	5800

implied by Eqn. (2.18) and not the ad hoc model that results from fitting the resilient modulus data as described in this paragraph and then using the resulting constants in Eqn. (2.18). The data set used in this study included a measurement of ϵ_2 and the constants for all of the material models were found by the procedure described in this section.

4.3 The Values of the Material Constants

The values of the material constants of linear elastic model, the $K–\theta$ model, the *Uzan-Witzcak* model, and the coupled hyperelastic model — each obtained by the procedure outlined in this section — are given in Table 4.2. Unless otherwise indicated, all of the values shown in these tables are obtained for $\lambda = 0.5$.

The values in Table 4.2 are in U.S. Customary Units and the conversion of the constant k of the $K–\theta$ and *Uzan-Witzcak* models is not so obvious (see Eqn. (2.3)). The

value of k in SI units (kPa) can be computed by multiplying its value in U.S. Customary Units (psi) by $6.895^{(1+n+m)}$.

4.4 Conclusions

As the results indicate, the coupled hyper elastic model described in Chapter 3 does a better job in predicting the measured stress values than the K– and *Uzan–Witzcak* models. Furthermore, it is observed that the coupled hyperelastic model displays a welcome sensitivity to the weight parameter λ of the nonlinear least squares procedure unlike the other models described earlier. Using this parameter, one can take into account the possible differences of the accuracy of the volumetric and deviatoric strain measurements if desired. The fact that the coupled model yields a better fit to the test data using same number material constants (four) as the *Uzan–Witzcak* model indicates that the simple idea of coupling the volumetric deviatoric responses of the material within the context of hyperelasticity is indeed a fruitful one. This coupling is also present in both the K– and *Uzan–Witzcak* models, yet in a more subtle way. Nevertheless, the coupled hyperelastic model somehow makes a better use of the flexibility provided by the four constants it uses. It also provides a welcome feature that one can interpret the meanings of these constants much more directly.

Chapter 5

A Projection Operator for No–Tension Elasticity

In this chapter a tensor–valued projection operator which operates on the stress tensor is proposed where the projected stress has principal values that are less than or equal to a preassigned value. Such a projection yields constitutive laws for materials with limited tensile/compressive strength. These constitutive models can also be viewed as *deformation plasticity* models in principal directions. Applications of the proposed class of constitutive models include stability and limit load analysis of structures such as tunnels or excavations into rock mass, masonry walls and pavements with compacted layers of granular materials which is the subject of this study. Researchers in the past have approached such problems using numerical (Zienkiewicz et. al, 1968) and analytic (Del Piero, 1989) methods and using elastic–perfectly plastic models that utilize well–known yield criteria such as Mohr–Coulomb all of which have fundamental differences with the proposed models.

The stress–update formulation and the derivation of the consistent tangent operator for the proposed models are provided for the finite element method. A robust implementation requires the derivatives of the projection operator with respect to strain to obtain the material tangent stiffness. The non–uniqueness of the spectral form of the projection operator in the case of coalescence of the principal values creates a fundamental difficulty. Aforementioned derivatives are obtained with careful consideration of the limit cases (Carlson, 1986) of the well known formulas for distinct principal values (Kato, 1976). A version of the proposed model with linear elastic behavior under compression and limit behavior under tension is implemented to a commercial finite element package (ABAQUS, 1994). Quadratic convergence rate of the Newton–Raphson solution method with this model for all possible cases (i.e. distinct, double and triple coalescence of principal values) is demonstrated with a few boundary value problems.

5.1 Preliminaries

Given the second–order symmetric tensor $\mathbf{S} : \mathbb{R} \to Sym(V_n)^\dagger$, we can write, through the spectral decomposition of $\mathbf{S}$,

$$\mathbf{S} = \sum_{i=1}^{n} s_i \mathbf{e}_i(\mathbf{S}) \otimes \mathbf{e}_i(\mathbf{S}) \tag{5.1}$$

where $\{s_1, s_2, ..., s_n\}$ is the spectrum of $\mathbf{S}$ and $\{\mathbf{e}_1(\mathbf{S}), \mathbf{e}_2(\mathbf{S}), ..., \mathbf{e}_n(\mathbf{S})\}$ is an orthonormal basis of eigenvectors of $\mathbf{S}$. The non–uniqueness of $\{\mathbf{e}_i(\mathbf{S})\}$ in the representation above when $\mathbf{S}$

$\dagger$ V_n denotes an n– dimensional normed vector space

has repeated eigenvalues is an obstacle when the derivatives of $\mathbf{S}$ are needed in spectral form. An alternative representation theorem that has recently found its way into computational mechanics (Simo 1991, Schreyer 1993) is based on eigenprojections. To wit,

$$\mathbf{S} = \sum_{i=1}^{p} s_i \mathbf{E}_i(\mathbf{S}) \tag{5.2}$$

where $\{s_1, s_2, ..., s_p\}$ is the set of *distinct* eigenvalues of $\mathbf{S}$ and $\mathbf{E}_i(\mathbf{S})$ is the eigenprojection corresponding to s_i. Unlike the basis $\{\mathbf{e}_i(\mathbf{S})\}$, the eigenprojections are unique and can be expressed as (see, for example, Halmos 1958),

$$\mathbf{E}_i(\mathbf{S}) = \begin{cases} \displaystyle\prod_{\substack{j=1 \\ j \neq i}}^{p} \frac{\mathbf{S} - s_j \mathbf{I}}{s_i - s_j}, & p > 1, \\ \mathbf{I}, & p = 1, \end{cases} \tag{5.3}$$

where the integer p is the number of distinct eigenvalues of $\mathbf{S}$. It can be shown that the eigenprojections have the following properties

$$\mathbf{E}_i(\mathbf{S})\mathbf{E}_j(\mathbf{S}) = \begin{cases} \mathbf{E}_i(\mathbf{S}), & i = j, \\ \mathbf{0}, & i \neq j, \end{cases} \tag{5.4}$$

$$\sum_{i=1}^{p} \mathbf{E}_i(\mathbf{S}) = \mathbf{I} \tag{5.5}$$

Since we are concerned with the stress tensor, we will restrict our attention to 3–dimensional space (i.e. $\mathbf{S} : \mathbb{R} \to Sym(V_3)$), therefore $p \leq 3$. Let $\mathbf{F} : Sym(V_3) \to Sym(V_3)$ be a tensor–valued function defined as

$$\mathbf{F}(\mathbf{S}) \equiv \sum_{i=1}^{p} f(s_i)\mathbf{E}_i(\mathbf{S}) \tag{5.6}$$

where the function $f: \mathbb{R} \to \mathbb{R}$, needs to be sufficiently smooth, as we shall see below, if the continuity and differentiability of $\mathbf{F}(\mathbf{S})$ is a requirement. Depending on the distinct eigenvalues of $\mathbf{S}$, we can equivalently state,

$$\mathbf{F}(\mathbf{S}) \equiv \begin{cases} f(s_1)\mathbf{E}_1(\mathbf{S}) + f(s_2)\mathbf{E}_2(\mathbf{S}) + f(s_3)\mathbf{E}_3(\mathbf{S}), & s_1 \neq s_2 \neq s_3 \neq s_1, \\ f(s_1)\mathbf{E}_1(\mathbf{S}) + f(s)[\mathbf{I} - \mathbf{E}_1(\mathbf{S})], & s_1 \neq s_2 = s_3 = s, \\ f(s)\mathbf{I}, & s_1 = s_2 = s_3 = s. \end{cases} \tag{5.7}$$

In what follows, we present two essential theorems , the proofs of which are omitted for brevity, due to Carlson and Hoger (Carlson 1986). Note that these theorems also hold for functions $f: \mathbb{R} \to \mathbb{R}$ that are smoother than what is stated below.

THEOREM. If $f \colon \mathbb{R} \to \mathbb{R}$, is three times continuously differentiable, the function $\mathbf{F} \colon Sym(V_3) \to Sym(V_3)$ defined in Eqn. (5.7) is continuous.

THEOREM. If the function f, is seven times continuously differentiable on $\mathbb{R}$, the function $\mathbf{F(S)}$ is continuously differentiable on $Sym(V_3)$ and the derivative of $\mathbf{F}$ with respect to its argument is,

$$
\frac{\partial \mathbf{F(S)}}{\partial \mathbf{S}} = \begin{cases}
[\Omega_1 + \Omega_2 + \Omega_3]\, \mathbf{S}^2 \oplus \mathbf{S}^2 \\[6pt]
-[(s_1+s_2)\Omega_3 + (s_2+s_3)\Omega_1 + (s_1+s_3)\Omega_2]\,(\mathbf{S}^2 \oplus \mathbf{S} + \mathbf{S} \oplus \mathbf{S}^2) \\[6pt]
+[s_1 s_2 \Omega_3 + s_1 s_3 \Omega_2 + s_2 s_3 \Omega_1]\,(\mathbf{S}^2 \oplus \mathbf{I} + \mathbf{I} \oplus \mathbf{S}^2) \\[6pt]
+\big[(s_1+s_2)^2\Omega_3 + (s_1+s_3)^2\Omega_2 + (s_2+s_3)^2\Omega_1\big]\, \mathbf{S} \oplus \mathbf{S} \\[6pt]
+[\omega_1 + \omega_2 + \omega_3 - s_1 s_2(s_1+s_2)\Omega_3 - s_2 s_3(s_2+s_3)\Omega_1 \\[3pt]
\quad - s_1 s_3(s_1+s_3)\Omega_2]\,(\mathbf{S} \oplus \mathbf{I} + \mathbf{I} \oplus \mathbf{S}) \\[6pt]
+\big[(s_1 s_2)^2\Omega_3 + (s_1 s_3)^2\Omega_2 + (s_2 s_3)^2\Omega_1 \\[3pt]
\quad -(s_1+s_2)\omega_3 - (s_1+s_3)\omega_2 - (s_2+s_3)\omega_1\big]\,\mathbf{1}, \quad s_1 \neq s_2 \neq s_3 \neq s_1, \qquad (5.8)\\[12pt]
\dfrac{1}{(s_1-s)^3}\Big\{\, [(s_1-s)(f'(s_1)+f'(s)) - 2(f(s_1)-f(s))]\, \mathbf{S} \oplus \mathbf{S} \\[6pt]
\quad +[(s_1+s)(f(s_1)-f(s)) - (s_1-s)(sf'(s_1)+s_1 f'(s))]\,(\mathbf{S} \oplus \mathbf{I} + \mathbf{I} \oplus \mathbf{S}) \\[6pt]
\quad +\big[(s_1-s)(s^2 f'(s_1)+s_1^2 f'(s)) \\[3pt]
\quad\quad - 2s_1 s(f(s_1)-f(s))]\mathbf{1}\,\Big\}, \quad s_1 \neq s_2 = s_3 = s, \\[12pt]
f'(s)\,\mathbf{1}, \quad s_1 = s_2 = s_3 = s,
\end{cases}
$$

where the scalars ω_i and Ω_i are given by,

$$
\omega_i = \frac{f(s_i)}{(s_i - s_j)(s_i - s_k)}
$$

$$
\Omega_i = \frac{1}{(s_i - s_j)^2 (s_i - s_k)^2}\big[f'(s_i) - (s_i - s_j)(\omega_i + \omega_k) - (s_i - s_k)(\omega_i + \omega_j)\big] \qquad (5.9)
$$

with the indices $i \neq j \neq k \neq i \in \{1, 2, 3\}$.

The non–commutative operation $\oplus$ in Eqn. (5.8) operates on two 2nd–order tensors and yields a 4th–order tensor, with components

$$(\mathbf{A} \oplus \mathbf{B})_{ijkl} = \tfrac{1}{2}(A_{ik}B_{jl} + A_{il}B_{jk}) \tag{5.10}$$

When this product is contracted with another 2nd–order tensor it yields,

$$(\mathbf{A} \oplus \mathbf{B}) : \mathbf{X} \equiv \mathbf{A}Sym(\mathbf{X})\mathbf{B} \tag{5.11}$$

or in component form,

$$(\mathbf{A} \oplus \mathbf{B})_{ijkl}\, X_{kl} \equiv \tfrac{1}{2}A_{ik}(X_{kl} + X_{lk})B_{lj} \tag{5.12}$$

where the summation convention is implied on repeated indices. Also, the 4th–order identity tensor $\mathbf{1}$ is,

$$\mathbf{1}_{\;ijkl} = (\mathbf{I} \oplus \mathbf{I})_{ijkl} = \tfrac{1}{2}(\delta_{ik}\delta_{jl} + \delta_{il}\delta_{jk}) \tag{5.13}$$

Upon denoting $\mathcal{F} \equiv \partial \mathbf{F}(\mathbf{S})/\partial \mathbf{S}$, inspection of Eqn. (5.8) indicates that $\mathcal{F}$ possesses both major and minor symmetries

$$\mathcal{F}_{ijkl} = \mathcal{F}_{klij} = \mathcal{F}_{jikl} = \mathcal{F}_{ijlk} \tag{5.14}$$

5.2 The Projection Operator

Let us define a function $g : \mathbb{R} \to \mathbb{R}$,

$$g(s) \equiv \tfrac{1}{2}[1 - \tanh(\beta s)] \tag{5.15}$$

where the scalar $\beta \in \mathbb{R}^+$. Note that the function is monotonic, that

$$\lim_{s \to -\infty} g(s) = 1 \;\; \text{and} \;\; \lim_{s \to +\infty} g(s) = 0 \tag{5.16}$$

and that $0 < g(s) < 1 \; \forall\, s \in \mathbb{R}$. The function $g(s)$, essentially a *smooth* switch function, is actually a specific form of the steady traveling wave solution for Burger's equation that describes the so–called *Burger's shock wave* [see, for example, Jeffrey 1995].

Let us also define, a function $f : \mathbb{R} \to \mathbb{R}$, such that

$$f(s) \equiv \int g(s)\mathrm{d}s = s - \frac{1}{2\beta}\ln\!\left[\tfrac{1}{2}(e^{2\beta s} + 1)\right]. \tag{5.17}$$

Note that, the function f is infinitely many times differentiable on $\mathbb{R}$. Taking the limit,

$$\lim_{s \to +\infty} f(s) = \frac{1}{2\beta}\ln(2) \tag{5.18}$$

and defining $s_{max} \equiv \ln(2)/2\beta$, we see that as $s \to -\infty$, $f(s) \to s + s_{max}$. Using the definition of s_{max} we can rewrite Eqn. (5.15) as
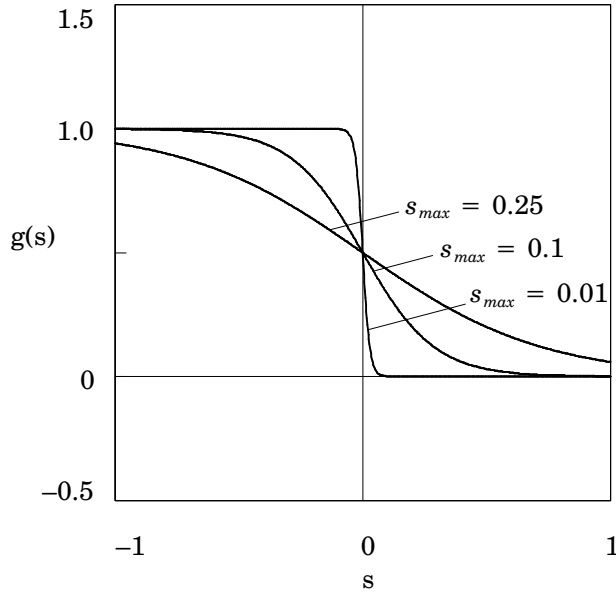
Figure 5.1. Effects of variation of scalar s_{max}.

$$f'(s) = g(s) = \left[2^{s/s_{max}} + 1\right]^{-1} \tag{5.19}$$

The function $g(s)$ is plotted in Figure 5.1 for various values of s_{max}. We can see that, from this graph, the smaller is the constant s_{max}, the steeper is the transition from left to right. Thus, we can control the shape of $g(s)$ by changing the value of s_{max}. Similarly, we can rewrite Eqn. (5.17) as

$$f(s) = s + \frac{s_{max}}{\ln(2)} \ln[2g(s)] \tag{5.20}$$

The variation of f, with respect to s is illustrated in Figure 5.2. Note that,

$$\lim_{s \to +\infty} f(s) = s_{max}. \tag{5.21}$$

and f is bounded from above, i.e.,

$$f(s) < s_{max}, \quad \forall\, s \in \mathbb{R}. \tag{5.22}$$

With these in mind, let us define the *no–tension projection operator* $\mathbf{F} : Sym(V_3) \to Sym(V_3)$ with (see Eqn. (5.7)),

$$\mathbf{F}(\mathbf{S}) = \sum_{i=1}^{p} f(s_i)\mathbf{E}_i(\mathbf{S}) \tag{5.23}$$

where $f : \mathbb{R} \to \mathbb{R}$ is given by Eqn.'s (5.19) and (5.20). The function $\mathbf{F}(\mathbf{S})$ is continuous and differentiable due to the theorems stated earlier because f is infinitely many times differ-
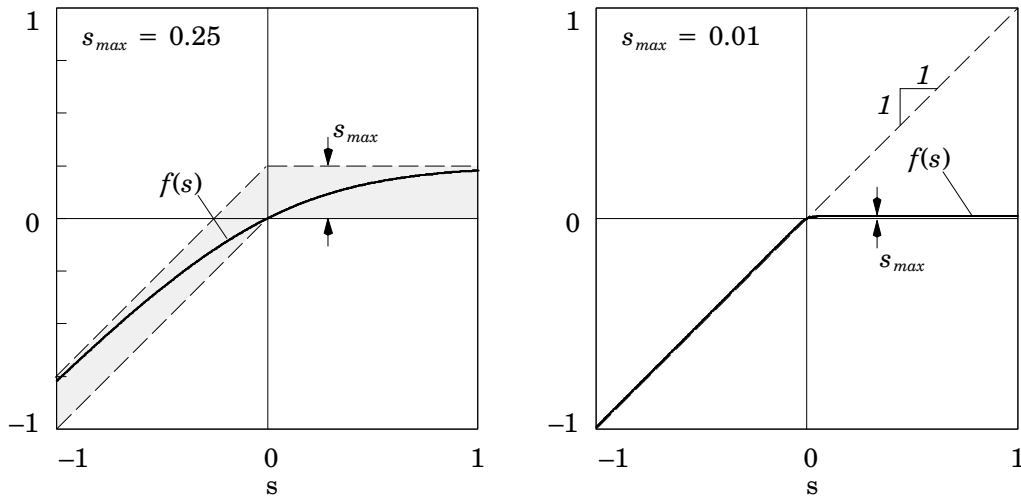
Figure 5.2. Function f.

entiable. The derivative of $\mathbf{F(S)}$ with respect to its argument can simply be obtained from Eqns. (5.8) and (5.9). Note that, $\mathbf{F(S)}$ is symmetric by definition.

5.3 No–Tension Elasticity

Consider a solid body $\mathcal{B}$ with boundary $\partial\mathcal{B}$, having normal vector field $\mathbf{n}$, subjected to applied tractions $\bar{\mathbf{t}}$ on $\partial\mathcal{B}_t \subset \partial\mathcal{B}$ and body forces $\mathbf{b}$ with prescribed displacements $\bar{\mathbf{u}}$ on $\partial\mathcal{B}_u \subset \partial\mathcal{B}$, subject to, $\partial\mathcal{B} = \overline{\partial\mathcal{B}_u \cup \partial\mathcal{B}_t}$ and $\partial\mathcal{B}_u \cap \partial\mathcal{B}_t = \emptyset$. Let $\mathbf{S}$ represent the stress tensor field and $\mathbf{E}$ the strain tensor field in the interior of the body. The equations governing the response of the body constitute the boundary value problem (see, for example, Hjelmstad 1997)

$$
\begin{aligned}
\text{div}\mathbf{S} + \mathbf{b} &= \mathbf{0} \quad \text{and} \quad \mathbf{S}^T = \mathbf{S} \quad &&\text{in } \mathcal{B} \\
\mathbf{E} &= \nabla^{(s)}\mathbf{u} = \tfrac{1}{2}\left(\nabla\mathbf{u} + \nabla\mathbf{u}^T\right) \quad &&\text{in } \mathcal{B} \\
\mathbf{Sn} &= \mathbf{t} \quad &&\text{on } \partial\mathcal{B}_t \\
\mathbf{u} &= \bar{\mathbf{u}} \quad &&\text{on } \partial\mathcal{B}_u
\end{aligned}
\tag{5.24}
$$

where the divergence is computed as $[\text{div}\mathbf{S}]_i = \partial S_{ij}/\partial x_j$ and the gradient as $[\nabla\mathbf{u}]_{ij} = \partial u_i/\partial x_j$. A superscript T indicates the transpose of the argument. To complete the statement of the boundary value problem we need only constitutive equations — the relationship between $\mathbf{S}$ and $\mathbf{E}$. Let us assume that the *elastic response* is characterized in terms of a strain energy density function $W : Sym(V_3) \to \mathbb{R}$ leading to a constitutive relation between an *intermediate* stress state ($\mathbf{S}^h$) and strain, i.e.,

$$
\mathbf{S}^h = \nabla W(\mathbf{E}).
\tag{5.25}
$$

Such a characterization is referred to as *hyperelasticity* (see, for example, Truesdell 1965). To obtain a no tension material, we project the *intermediate* (hyperelastic) stress ($\mathbf{S}^h$) with,

$$\mathbf{S} = \mathbf{F}(\mathbf{S}^h) = \mathbf{F}[\nabla W(\mathbf{E})] \tag{5.26}$$

where, $\mathbf{F} : Sym(V_3) \rightarrow Sym(V_3)$ is given by Eqn. (5.23). Thus Eqn. (5.26) is the constitutive relationship between the stresses and strains. It follows that, by the chain rule we can obtain the derivative of stress with respect to the strain,

$$\frac{\partial \mathbf{S}}{\partial \mathbf{E}} = \frac{\partial \mathbf{F}(\mathbf{S}^h)}{\partial \mathbf{S}^h} : \frac{\partial \mathbf{S}^h}{\partial \mathbf{E}} = \mathcal{F} : \nabla^2 W(\mathbf{E}) \tag{5.27}$$

where $\mathcal{F} \equiv \partial \mathbf{F}(\mathbf{S}^h)/\partial \mathbf{S}^h$. This 4th–order tensor ($\mathcal{F}$) can be computed by using Eqns. (5.8) and (5.9). Upon denoting $\mathcal{D} \equiv \partial \mathbf{S}/\partial \mathbf{E}$, we can write, in component form,

$$\mathcal{D}_{ijkl} = \mathcal{F}_{ijmn}\big[\nabla^2 W(\mathbf{E})\big]_{mnkl} \tag{5.28}$$

The 4th–order tensor $\mathcal{D}$ is called the *material tangent stiffness tensor*. Note that, for the current formulation, $\mathcal{D}$ always possesses minor symmetries but not the major symmetry over its indices in general, i.e.,

$$\mathcal{D}_{ijkl} = \mathcal{D}_{jikl} = \mathcal{D}_{ijlk} \neq \mathcal{D}_{klij} \tag{5.29}$$

Later on we shall discuss the consequences of this and other significant properties of $\mathcal{D}$.

5.4 Weak Formulation and Finite Element Discretization

In this section we present the standard variational formulation and the finite element discretization (Hughes 1987) of the boundary value problem given in Eqn. (5.24) along with the solution algorithm for the nonlinear material model in question. Let the U be space of admissible displacements given by,

$$U = \{\mathbf{u} : \mathcal{B} \rightarrow \mathbb{R}^3 \,|\, \mathbf{u} \in H^1(\mathcal{B}) \text{ and } \mathbf{u} = \overline{\mathbf{u}} \text{ on } \partial\mathcal{B}_u\}^\dagger. \tag{5.30}$$

Then, by defining the virtual work functional as,

$$G(\mathbf{S}, \mathbf{E}(\mathbf{u})) \equiv \int_{\mathcal{B}} (\mathbf{S} : \delta\mathbf{E} - \mathbf{b} \cdot \delta\mathbf{u})dV - \int_{\partial\mathcal{B}} (\mathbf{t} \cdot \delta\mathbf{u})dA \tag{5.31}$$

we see that if $G(\mathbf{S}, \mathbf{E}(\mathbf{u})) = 0$, for all variations ($\delta\mathbf{u}$) of $\mathbf{u} \in U$ then Eqn. (5.24) is satisfied. Note that due to the definition of the space of admissible displacements, $\delta\mathbf{u} = \mathbf{0}$ on $\partial\mathcal{B}_u$ for all $\mathbf{u} \in U$ and for the same reason we can write the domain of the second integral as the whole boundary ($\partial\mathcal{B}$).

$^\dagger H^1$ denotes a Hilbertian Sobolev space of order one.

The discretization of the weak form given in Eqn. (5.31) can be achieved by decomposing the domain into *finite elements* for which the strain-displacement matrix $\mathbf{B}_m$ allows the computation of the strain in element m from the nodal displacement $\mathbf{U}$ as

$$\boldsymbol{\epsilon}_m(\mathbf{x}) = \mathbf{B}_m(\mathbf{x})\mathbf{U} \tag{5.32}$$

where the element strain vector $\boldsymbol{\epsilon}_m$, following the standard notation for 3–dimensions, is defined as,

$$\boldsymbol{\epsilon}_m \equiv [\mathbf{E}_{11},\ \mathbf{E}_{22},\ \mathbf{E}_{33},\ 2\mathbf{E}_{12},\ 2\mathbf{E}_{13},\ 2\mathbf{E}_{23}]_m^T \tag{5.33}$$

Denoting the element stress vector $\boldsymbol{\sigma}_m$ in a similar fashion,

$$\boldsymbol{\sigma}_m \equiv [\mathbf{S}_{11},\ \mathbf{S}_{22},\ \mathbf{S}_{33},\ \mathbf{S}_{12},\ \mathbf{S}_{13},\ \mathbf{S}_{23}]_m^T \tag{5.34}$$

we get the discrete version of the weak formulation as,

$$\mathbf{R}(\mathbf{U}) \equiv \overset{M}{\underset{m=1}{\mathbf{A}}} \int_{\mathcal{B}_m} \mathbf{B}_m^T \boldsymbol{\sigma}_m(\mathbf{U})\, dV - \mathbf{P} = \mathbf{0} \tag{5.35}$$

where $\mathbf{A}$ is the standard assembly operator, M is the number of elements, $\mathcal{B}_m$ is the region occupied by element m and $\mathbf{P}$ are the work equivalent nodal loads. The element integrals in Eqn. (5.35) are generally carried out with numerical quadrature. This equation can be solved for $\mathbf{U}$ with an iterative method like Newton–Raphson. To wit, linearizing $\mathbf{R}(\mathbf{U})$ about a deformed state $\mathbf{U}^{(k)}$ we get,

$$\mathbf{R}^{(k+1)} = \mathbf{R}(\mathbf{U}^{(k+1)}) \approx \mathbf{R}(\mathbf{U}^{(k)}) + \partial_\mathbf{u}\mathbf{R}(\mathbf{U}^{(k)})d\mathbf{U}^{(k+1)} = \mathbf{0} \tag{5.36}$$

$$d\mathbf{U}^{(k+1)} = -\left[\partial_\mathbf{u}\mathbf{R}^{(k)}\right]^{-1}\mathbf{R}^{(k)}$$

where the Jacobian of the problem (global stiffness matrix) is,

$$\partial_\mathbf{u}\mathbf{R}^{(k)} \equiv \mathbf{K}_t(\mathbf{U}^{(k)}) = \overset{M}{\underset{m=1}{\mathbf{A}}} \int_{\mathcal{B}_m} \mathbf{B}_m^T(\mathbf{x})\mathbf{D}_m(\mathbf{U}^{(k)},\mathbf{x})\mathbf{B}_m(\mathbf{x})\, dV \tag{5.37}$$

Here, $\mathbf{D}_m(\mathbf{U},\mathbf{x})$ is the material tangent stiffness matrix for element m, which depends upon the displaced state $\mathbf{U}$ and varies with the spatial coordinates $\mathbf{x}$. Consistent with the notation of Eqn.'s (5.33) and (5.34) this matrix is given by,

$$\mathbf{D}_m = \begin{bmatrix} \mathcal{D}_{1111} & \mathcal{D}_{1122} & \mathcal{D}_{1133} & \mathcal{D}_{1112} & \mathcal{D}_{1113} & \mathcal{D}_{1123} \\ \mathcal{D}_{2211} & \mathcal{D}_{2222} & \mathcal{D}_{2233} & \mathcal{D}_{2212} & \mathcal{D}_{2213} & \mathcal{D}_{2223} \\ \mathcal{D}_{3311} & \mathcal{D}_{3322} & \mathcal{D}_{3333} & \mathcal{D}_{3312} & \mathcal{D}_{3313} & \mathcal{D}_{3323} \\ \mathcal{D}_{1211} & \mathcal{D}_{1222} & \mathcal{D}_{1233} & \mathcal{D}_{1212} & \mathcal{D}_{1213} & \mathcal{D}_{1223} \\ \mathcal{D}_{1311} & \mathcal{D}_{1222} & \mathcal{D}_{1333} & \mathcal{D}_{1312} & \mathcal{D}_{1313} & \mathcal{D}_{1323} \\ \mathcal{D}_{2311} & \mathcal{D}_{2322} & \mathcal{D}_{2333} & \mathcal{D}_{2312} & \mathcal{D}_{2313} & \mathcal{D}_{2323} \end{bmatrix} \tag{5.38}$$

Box 5.1. Solution Algorithm

1. Compute iterative strain

   $$\mathbf{E}_m^{(k)} = \mathbf{E}_m^{(k-1)} + \nabla^{(s)}\!\left(\Delta\mathbf{u}_m^{(k)}\right)$$

2. Compute iterative hyperelastic stress

   $$\mathbf{S}_m^{h,(k)} = \nabla W(\mathbf{E}_m^{(k)})$$

3. Compute eigenvalues of hyperelastic stress, projection operator
   $\mathbf{F}$ and iterative projected stress

   $$\mathbf{S}_m^{(k)} = \mathbf{F}\!\left(\mathbf{S}_m^{h,(k)}\right)$$

4.[†] Assemble the global residual vector and check for convergence

   Eqn. (5.35) $\rightarrow \mathbf{R}^{(k)}$

   IF: $\left\|\mathbf{R}^{(k)}\right\|_{L_2} \leqq TOL$ THEN Exit

5. Compute material tangent stiffness tensor and matrix

   $$\mathfrak{D}^{(k)} = \mathfrak{F} : \nabla^2 W(\mathbf{E}_m^{(k)}) \rightarrow \mathbf{D}_m^{(k)}$$

6.[†] Assemble the global stiffness matrix and compute increment to
   displacement

   Eqn. (5.37) $\rightarrow \mathbf{K}_t^{(k)}$

   $$\Delta\mathbf{U}^{(k+1)} = -\left[\mathbf{K}_t^{(k)}\right]^{-1}\mathbf{R}^{(k)}$$

7.[†] Update displacements

   $$\mathbf{U}^{(k+1)} = \mathbf{U}^{(k)} + \Delta\mathbf{U}^{(k+1)}$$

8. Set index $k+1 \rightarrow k$ and go to step 1.

[†] Denotes a global level computation

where we have made use of the minor symmetries of the material tangent stiffness tensor $\mathfrak{D}$ which is given by Eqn. (5.28). The algorithm of the procedures outlined above for the no–tension material is presented in Box 5.1. Note that this algorithm can be enhanced, if necessary, with line search and arc–length continuation methods (see, for example, Crisfield 1991).

Remarks. As we have mentioned earlier, the material tangent stiffness tensor $\mathfrak{D}$ does not possess major symmetry over its indices with the exception of triple coalescence of

principal stress values. As a consequence, we can conclude that the constitutive relationship can not be derived from a stored strain energy density function (see, for example, Truesdell 1965). Therefore, the response of the no–tension material under applied loading will be *path–dependent*. Note that in compression, however, as $s_i^h \to -\infty$, we see that $\mathbf{F}(\mathbf{S}^h) \to \mathbf{S}^h$. Therefore, the response of the material will approximately be equal to that of the underlying hyperelastic material, in the limit. Thus, the response of the no–tension material will be *nearly* path independent under large compressive stress regimes in all three principal directions. Furthermore, if the material is loaded such that all the principal stress values remain equal throughout the loading history, the response will be path independent.

The material tangent stiffness is positive definite for all admissible displacement (strain) states. This leads to a unique constitutive relationship. However, as $s_i^h \to +\infty$. the material tangent stiffness becomes *nearly* singular and this will cause numerical ill–conditioning. Consider, for example, two distinct strain states ($\mathbf{E}^1$ and $\mathbf{E}^2$) which yield two distinct hyperelastic stress states ($\mathbf{S}^{h,1}$ and $\mathbf{S}^{h,2}$) with all positive eigenvalues ($s_i^{h,1}$ and $s_i^{h,2}$) with,

$$e_i^1 >> \hat{a} \quad \text{and} \quad e_i^2 >> \hat{a}, \quad i \in \{1, 2, 3\}. \tag{5.39}$$

for some $\hat{a} > 0$, where e_i^1 and e_i^2 denote the principal strains corresponding to the strain tensors $\mathbf{E}^1$ and $\mathbf{E}^2$, respectively. Thus, from Eqn. (5.26), the projected stress for these two strain states will be $\mathbf{S}^1 \approx \mathbf{S}^2 \approx \mathbf{T}$ where $\mathbf{T}$ is a symmetric second–order tensor whose spectral radius is $\varrho[\mathbf{T}] \leq s_{max}$. Physically, this corresponds to a material that has (nearly) failed. This aspect of the proposed model may cause computational complications, particularly when the constant s_{max} is chosen to be very small.

In addition to these remarks, note that, the first minor symmetry of the material tangent stiffness tensor (i.e. $\mathfrak{D}_{ijkl} = \mathfrak{D}_{jikl}$) satisfies the classical requirement of the balance of angular momentum.

5.5 Examples

To illustrate response of the no–tension material, the stresses due to prescribed displacements in a unit cube (see Figure 5.3) are obtained. The cube is composed of no–tension material with material constant $s_{max} = 0.001$ MPa. For this example, the hyperelastic stress–strain relationship is chosen to be,

$$S_{ij}^h = [\nabla W(\mathbf{E})]_{ij} = \lambda E_{kk} \delta_{ij} + 2\mu E_{ij} \tag{5.40}$$

which is the standard linear elastic constitutive model and λ and μ are the Lamé Constants. For this example, we have chosen $\lambda = 1430$ MPa and $\mu = 360$ MPa which correspond to a Young's modulus of 1000 MPa and a Poisson's ratio of 0.4. Note that, the prescribed displacements require $E_{22} = E_{33} = E_{12} = E_{13} = E_{23} = 0$ and $E_{11} = \epsilon(t)$.
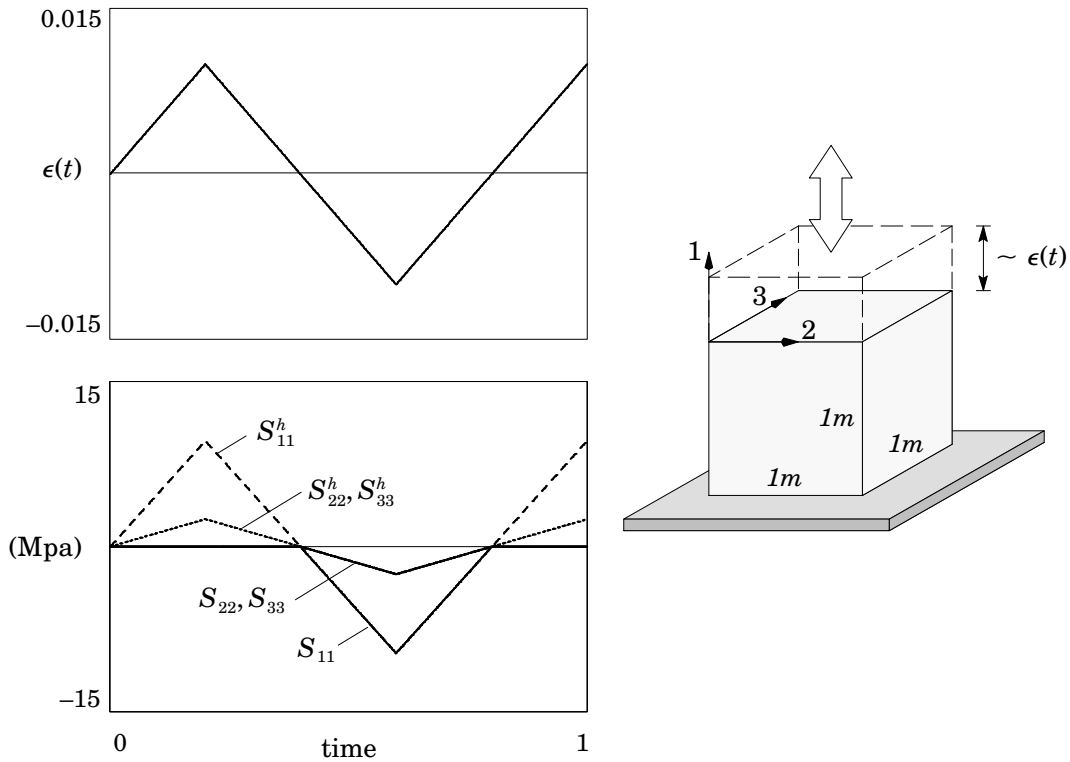
Figure 5.3. Unit cube, imposed displacements and resultant stresses.

As Figure 5.3 indicates the response of the *no–tension* cube under prescribed displacements (or strain) is identical to that of the *hyperelastic* (linear elastic in this case) cub when the resultant stresses are compressive. However, unlike the *hyperelastic* cube, the resultant stresses are zero (or 0.001 MPa to be exact) for the *no–tension* cube in tension. The reason that there are components of stress in directions 2 and 3 is, of course, due to the non–zero Poisson's Ratio.

To assess the asymptotic convergence rate of the algorithm shown in Box 5.1, we have devised a simple boundary value problem in which a block of no–tension material, embedded in a linear elastic material, is analyzed under various loadings. The dimensions of this structure and the applied load cases are shown in Figure 5.4. The underlying hyperelastic model for the no–tension block is again linear elasticity and the material constants for both the surrounding linear elastic material and the no–tension block are $\lambda = 1430$ MPa and $\mu = 360$ MPa. The additional material constant for the no–tension block is chosen as $s_{max} = 0.001$ MPa.
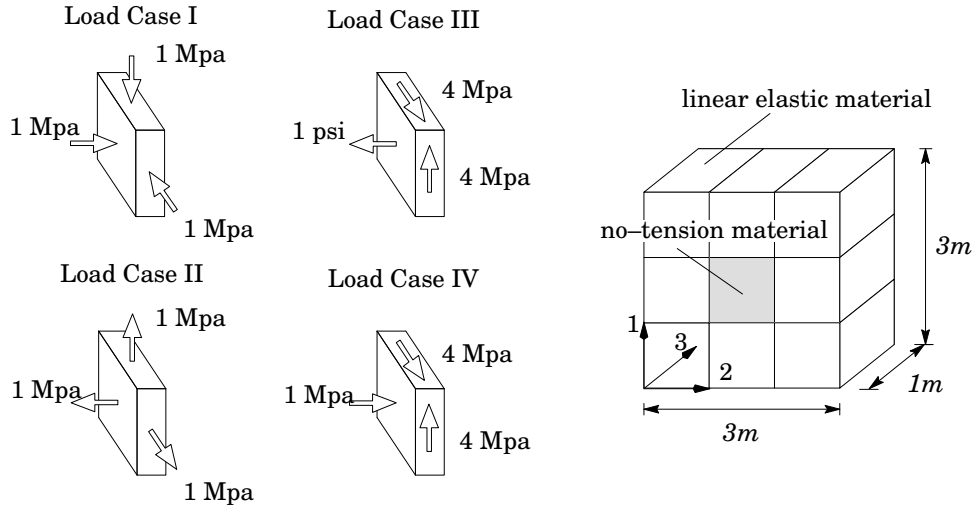
Figure 5.4. Finite element mesh and load cases.

The load cases are chosen so that all possible coalescence of the principal stress values can be observed (see Table 5.1): In cases I and II, three principal stresses in the no–tension block coalesce with negative and positive (s_{max}) values respectively; in case III there is a double coalescence with two principal stresses equal to s_{max} and finally in case IV, all principal stress values are distinct. Note that, in all loading cases except case I, there is at least one tensile principal stress equal to s_{max} in the no–tension block.

As we have mentioned earlier, the material tangent stiffness matrix is unsymmetrical. Finite element computations with an unsymmetrical stiffness matrix require more storage and more operations than those with a symmetric stiffness matrix. We can symmetrize the material tangent stiffness matrix as follows

$$\overline{\mathbf{D}}_m \;=\; \tfrac{1}{2}\bigl(\mathbf{D}_m + \mathbf{D}_m^T\bigr) \tag{5.41}$$

and use $\overline{\mathbf{D}}_m$ instead of $\mathbf{D}_m$ to form the global stiffness matrix $\mathbf{K}_t$. While this choice can mean substantial savings of computational resources in a given iteration, it generally destroys the quadratic convergence rate of the Newton iteration. However, if the number

Table 5.1. Resultant Stresses (MPa).

LCI		LCII		LCIII		LCIV	
s_i	s_i^h	s_i	s_i^h	s_i	s_i^h	s_i	s_i^h
−.999	−1.00	.001	1.00	−1.29	−1.88	−1.29	−1.88
−.999	−1.00	.001	1.00	0.00	0.91	−0.30	−1.09
−.999	−1.00	.001	1.00	0.00	1.62	0.00	1.62
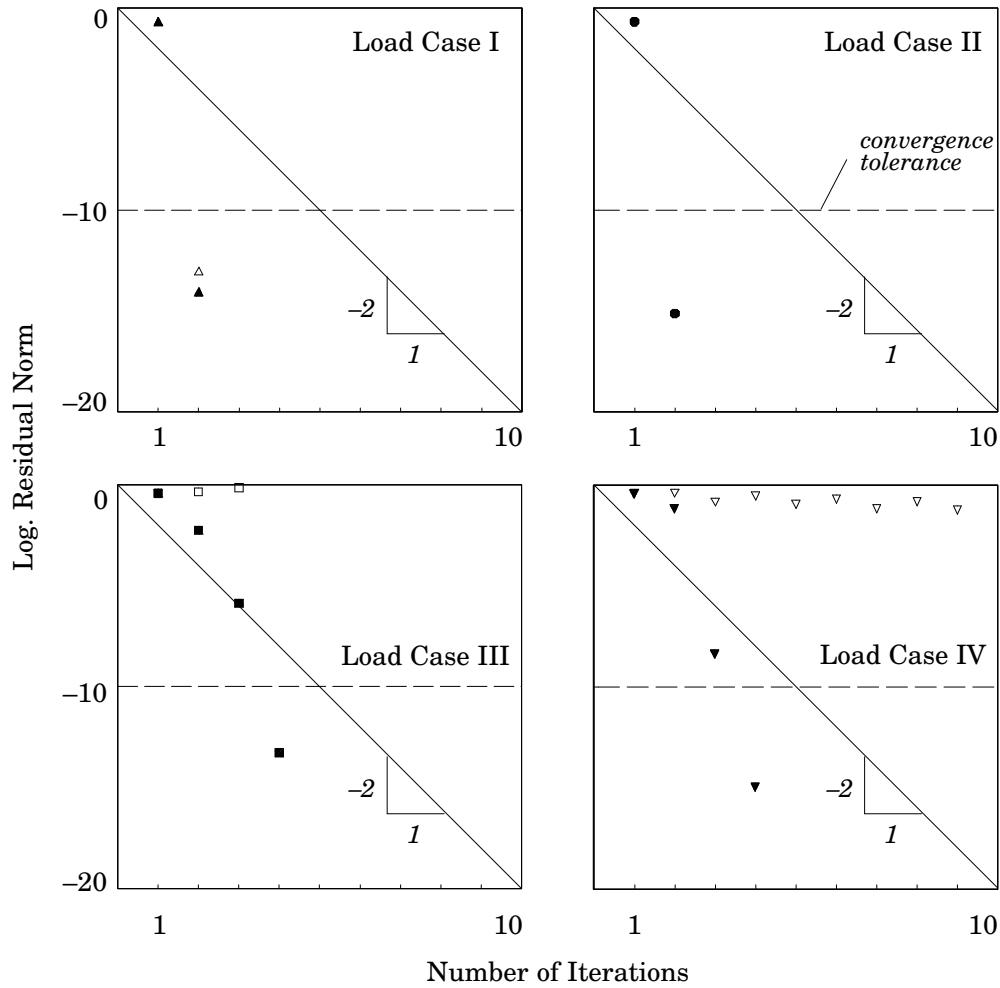
Figure 5.5. Residual norm for load cases (*Solid symbols correspond the unsymmetrical formulation*).

of elements in a finite element mesh is quite high, it may still be possible to obtain reduced or comparable total computation time due to reduced storage requirements of a symmetrical stiffness matrix.

We have implemented the algorithm outlined in Box 5.1, in the commercial finite element package ABAQUS (1994) with the help of user defined subroutine UMAT. The program ABAQUS supports both symmetric and unsymmetric tangent formulations. The residual norm versus the number of iterations for all the load cases is presented in Figure 5.5. The abscissae in this figure are $\log\left[\|\mathbf{R}\|_{L_\infty}\right]$. Since the optimal convergence rate for the Newton's Method is quadratic, we have plotted the *slope of optimal convergence* to aid the eye. The solid symbols correspond to the unsymmetrical formulation and others corre-

spond to the symmetrical formulation we have mentioned earlier. In Load Cases I and II, the convergence rate for both formulations are very close. This is due to the fact that during Newton's iterations, all the principal stresses remain equal (or nearly equal) and therefore the material stiffness matrix is nearly symmetric. In Load Cases III and IV however, there was no convergence for the symmetrical formulation. For all the load cases, optimal (*quadratic*) convergence rate is observed for the unsymmetrical formulation. It may be possible to obtain convergence, though with suboptimal rate, for Load Cases III and IV for the symmetrical formulation via line search and other techniques. Such issues, however, will not be investigated in the present work.

5.6 Simulations

In what follows, we present two boundary value problems where the no–tension model is used. In both problems, the response of the structures are compared to the response of the same structures for which the no–tension material is replaced with a linear elastic material. The results indicate that the overall response of the structures with and without the no–tension material differ significantly.

5.6.1 Cantilever beam with no–tension core

The first structure is a prismatic cantilever beam with a no–tension material core under bending. The beam is analyzed under two loading cases: A distributed load acting either upward or downward, applied at the free end as shown in Figure 5.6. The finite element mesh consists of 2400 elements each of which are unit cubes. The material surrounding the core is linear elastic and the material constants are chosen as $\lambda = 143$ MPa and $\mu = 36$ MPa. The core is chosen to have one of the following models: (a) linear elasticity with material constants having the same values as the sorrounding material, (b) no–tension material having the same values for its elastic constants as the surrounding material and the additional constant being $s_{max} = 0.01$ kPa, (c) a very soft linear elastic material with a Young's Modulus of 0.001 kPa and a Poisson's Ratio of zero value.

The bending stress and strain values at the center of the beam (i.e., 150 cm. from either end) along the centerline of the cross–section for these analyses are presented in Figure 5.7. As this figure shows, for the upward loading (Load Case II), the response of the beam with the no–tension core (b) is almost the same as the fully linear elastic beam (a). This is not surprising because the no–tension core is under compression in this case. However, when the load was reversed (Load Case I), the response of the beam with the no–tension core (b) resembles to that of the beam with the very soft core (c), in which case the no–tension core is under tension. In addition to these cross–sectional results, we have obtained the vertical tip displacement at the center of free end of the beam. The displacements were recorded as 1.743, 1.787, 1.920 centimeters under upward loading for linear elastic core, no–tension core and very soft core, respectively and −1.743, −1.904, −1.920 centimeters under downward loading in the same order.
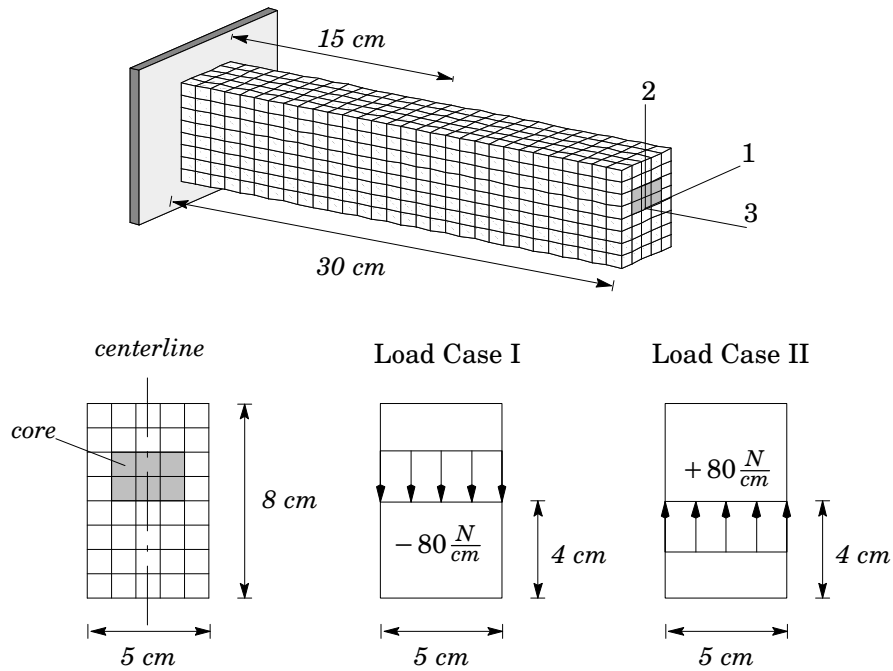
Figure 5.6. Cantilever beam with no–tension core.

In all the analyses for the beam with the no–tension core, we have used the unsymmetrical tangent stiffness matrix and have observed optimal convergence rate for the Newton–Raphson Method outlined in Box 5.1.

5.6.2 Three Dimensional Pavement Analysis

The second problem is the 3–dimensional finite element analysis of a flexible pavement system (for details of this boundary value problem see Figures 6.1 and 6.2 in Chapter 6).

The top layer of the system is 20 cm of asphalt concrete, the second layer is 112 cm of high density crushed rock and the bottom layer is natural soil extending to a depth of 9 m. The asphalt concrete layer is assumed to be linear elastic with Young's modulus $E = 1380$ MPa and Poisson's ratio of $\nu = 0.35$. The natural soil is also assumed to be linearly elastic with Young's modulus $E = 40$ MPa and Poisson's ratio of $\nu = 0.45$. The second layer is modeled using one of the following models: (a) linear elasticity with $E = 240$ MPa and $\nu = 0.34$, (b) no–tension elasticity with the same elastic material constants and $s_{max} = 7$ kPa (1 psi) (note that these values are for the HD1 material discussed in Chapter 4)..

The variation of the bending stress and the vertical strain through the depth of the top and second layers directly under one of the central wheels are shown in Figure 5.8.
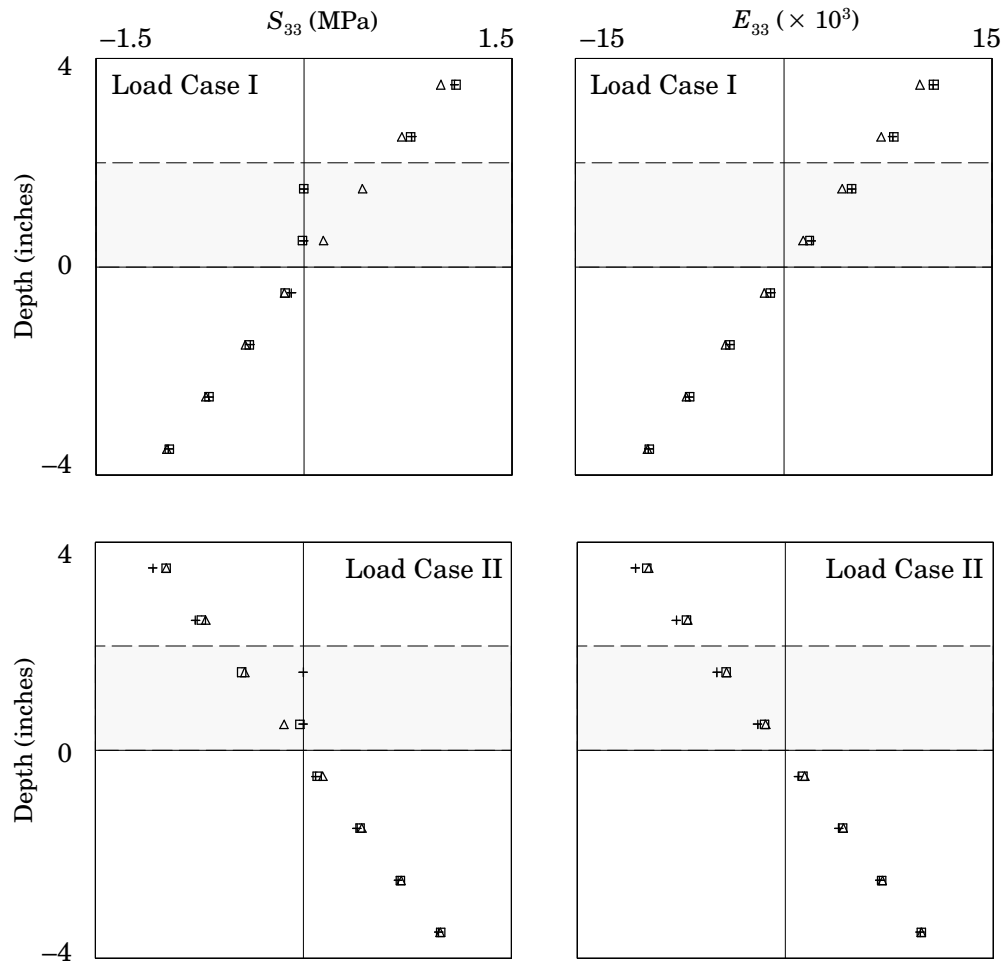
Figure 5.7. Bending stress and strain along the centerline of the can-
tilever beam: □ No–tension core, + very soft core,   linear elastic core.

Note that the scale on the stresses changes between the first and second layer. The values presented are at element center points. The two different models (a and b) are plotted using different symbols, as noted in the figure legend. Clearly, the no–tension model predicts significantly larger bending stress which is an important design parameter in pavements, at the bottom of the asphalt layer. Also, the variation of the vertical strain, another important design parameter, through the depth is different between the two models. This results in a significantly different deflection basin and the difference is reflected in the maximum surface displacement values which are recorded as 0.93 and 1.00 centimeters for the linear elastic and no–tension models respectively.

The loading is applied in two steps with the gravity loads induced by the weight of materials first followed by the applied gear loads. Equilibrium under gravity loads is iter-
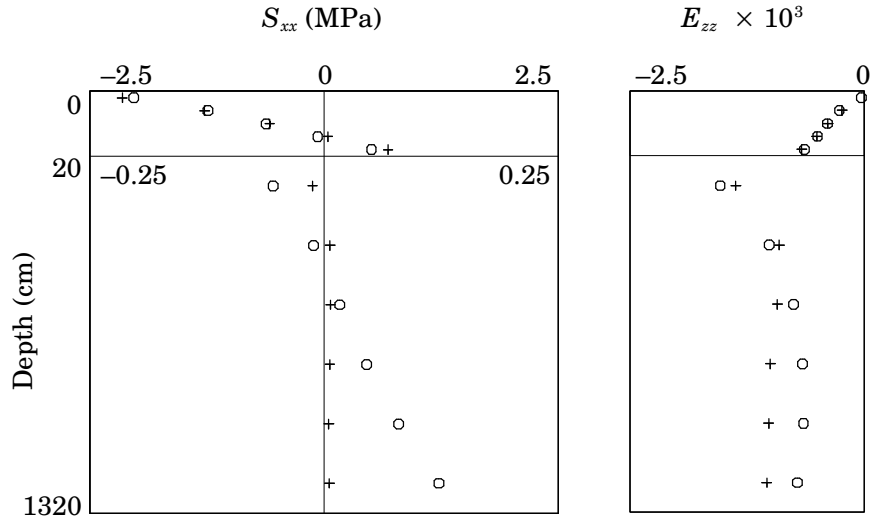
Figure 5.8. Bending stress and vertical strain under the wheel: ○ Linear elasticity, + no–tension elasticity.

ated to convergence prior to application of the wheel loads. The wheel loads are applied incrementally using ABAQUS' automatic incrementation procedure in which the load increment is increased or decreased according to the various convergence characteristics throughout the analysis (ABAQUS, 1994). For the no–tension model the number of iterations required per each increment of the wheel loading and the normalized residual norm ($R_{k,n}$) per each iteration is shown in Table 5.2. The normalized residual norm is given by

$$R_{k,n} = \left[\|\mathbf{R}\|_{L_\infty} / \eta \overline{\mathbf{P}} \right]_{k,n} \tag{5.42}$$

where $\overline{\mathbf{P}}$ is the absolute value of the average load and η is the load factor at the kth iteration of the nth load increment. As the results indicate, optimal convergence rate is attained throughout the analysis.

5.7 Conclusions

A tensor–valued projection operator that operates on the stress tensor is proposed. The resulting (stress) tensor has principal values with magnitude less than or equal to a value value defined a priori. It is demonstrated that the projection operator can be applied to a stress tensor that is described by any hyperelastic constitutive model. Therefore, the relationship between this modified stress and the strain yields a constitutive law that is useful obtaining or approximating the response of materials with very small or no strength under tension.

Table 5.2. Normalized residual norm for 3–D pavement analysis.

	Load Factor								
Gravity	*Wheel Loading* →								
1.00	0.05	0.10	0.18	0.29	0.46	0.62	0.79	0.96	1.00
$4.4E+01$	$2.7E-02$	$3.3E-05$	$8.3E-05$	$9.9E-04$	$5.4E-03$	$1.3E+01$	$4.6E-02$	$7.3E-03$	$8.8E-04$
$4.6E-01$	$8.7E-05$	$8.2E-09$	$4.2E-08$	$2.0E-05$	$1.3E-03$	$1.1E-01$	$5.3E-03$	$2.9E-03$	$2.2E-05$
$4.8E-03$	$4.2E-09$		$3.1E-13$	$1.1E-08$	$1.5E-05$	$2.2E-02$	$9.7E-04$	$6.8E-05$	$1.5E-07$
$1.6E-09$				$4.9E-13$	$1.0E-08$	$6.9E-03$	$8.4E-05$	$1.1E-06$	$5.2E-12$
					$5.4E-13$	$1.5E-03$	$6.6E-07$	$3.6E-11$	
						$2.5E-04$	$3.9E-11$		
						$6.2E-06$			
						$4.3E-09$			

It is demonstrated that using this constitutive law, the resilient response of the granular layers of pavements can be analyzed. The fact that the granular materials can not develop any tensile stresses is the motivation behind this approach. The same constitutive model has useful applications in the so–called "*no–tension*" design an analysis of various structures such as concrete dams, retaining walls and masonry and rock structures such as tunnels (see, for example, Bazant 1996) For these structures the limit loads under proportional loading are important in determining the safety. For example, a solution for these types of structures based on elastic behavior under compression but allowing no tension can obtained using the model described earlier. Such a solution will yield an upper bound for the loads the structure can safely withstand (see, for example, Zienkiewicz 1968). It appears that various algorithms have been proposed in the literature for "*no–tension*" elasticity but without the exact material tangent stiffness tensor, these algorithms suffer serious convergence problems (ABAQUS 1994).

Chapter 6

Finite Element Analysis of a Pavement System

In this chapter, the response of three–layered airport pavement under applied loading is analyzed with the finite element method. The constitutive models presented earlier are used to represent the behavior of the granular layer in this pavement system. Important design parameters such as the bending stress vertical strain at the bottom of the top layer are obtained to compare the predictions of various constitutive models used for the granular layer. The variation of pressure and volumetric strain, octahedral shear stress and strain through the depth of the granular are presented as well.

6.1 Description of the Pavement System

6.1.1 The Geometry and the Loading

The pavement system consist of a layer of asphalt concrete on a layer of high density crushed rock, on top of natural soil as shown in Fig. 6.1. It is subjected to a loading representative of a B777–200 type aircraft tridem gear (FAA 1995). The footprint of the loading is also shown in Fig. 6.1. The 55 cm × 35 cm rectangular tire prints are assumed to have a uniform pressure loading of 1.5 MPa. The loading is applied to the center of a 32 m × 32 m region.
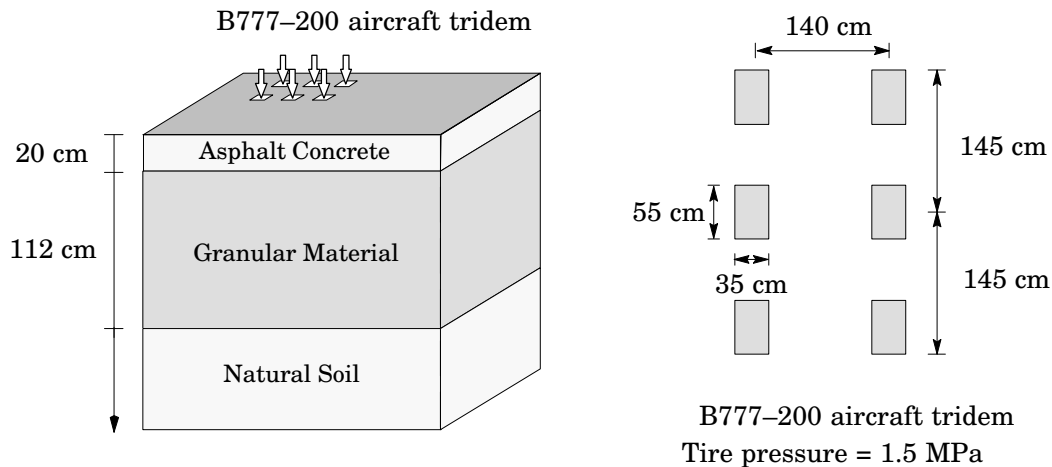
Figure 6.1. Flexible pavement system and applied loading
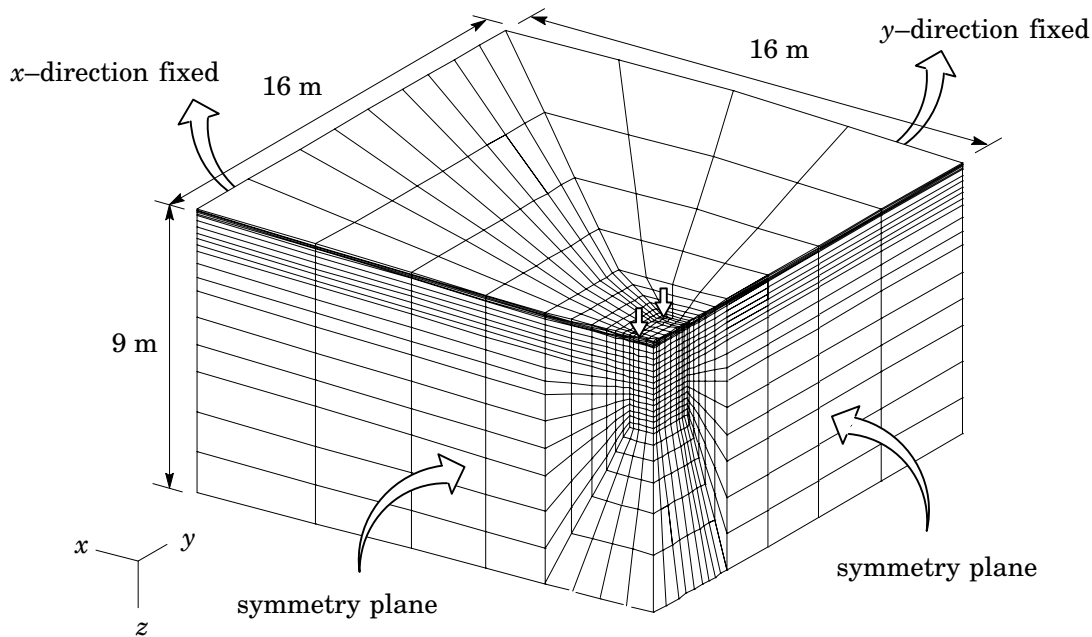
Figure 6.2. Finite element mesh and boundary conditions

6.1.2 The Finite Element Mesh

The finite element mesh, consisting of 3536 8–node hexahedron elements and 4206 nodes, is shown in Fig. 6.2. The lateral remote boundaries were truncated at a distance of 16 meters away from the center of the tridem and the total depth of the pavement system was taken as 9 meters. Owing to the symmetry of the model and loading, only a quarter of the region was included in the finite element model. The extent of the model region was selected so that the results were insensitive to the remote boundary conditions (Hjelmstad 1997B). Displacements were restrained only in the normal direction at the remote boundaries.

6.1.3 Materials

The top layer of the system is 20 cm of asphalt concrete, the second layer is 112 cm of high density crushed rock, designated as HD1 by Allen (1973), and the bottom layer is natural soil extending to a depth of 9 m. In the various analyses, the asphalt concrete layer is assumed to be linear elastic with Young's modulus $E = 1380$ MPa and Poisson's ratio of $v = 0.35$. The natural soil is also assumed to be linearly elastic with Young's modulus $E = 40$ MPa and Poisson's ratio of $v = 0.45$. The second layer was modeled using one of the following models: (a) Linear Elasticity (b) K– model (c) *Uzan–Witczak* model (d)

71

Table 6.2. Material constant values of various constitutive models for the granular layer.

| Constitutive Models | | | | | |
K–θ	Uzan–Witzcak	AD	MD	No–Tension Elasticity	Linear Elasticity
$K = 170 MPa$	$K = 180 MPa$	$K = 170 MPa$	$K = 170 MPa$	$E = 240 MPa$	$E = 240 MPa$
$v = 0.33$	$v = 0.33$	$G = 50 MPa$	$G = 50 MPa$	$v = 0.34$	$v = 0.34$
$n = 0.29$	$n = 0.22$	$b = 3200 GPa$	$b = 3200 GPa$	$s_{max} = 7\ kPa$	
	$m = 0.07$	$c = 43 GPa$	$c = 43 GPa$		
		$a = 10000$	$a = 1000$		
		$\sigma_o = 0\ kPa$			

AD model (described in Chapter 3) (e) MD model (also described in Chapter 3) and finally (f) the no–tension elasticity model described in Chapter 5. The values of the material constants for the high density crushed rock material were established by fitting the given model using a weighted nonlinear least-squares curve fitting technique, to the laboratory test data measured by Allen (1973) (see Chapter 4 for details). The values of the material constants of these model are shown in Table 6.2.. The densities of the materials are taken to be 0.0024 kgf/cm³ for the asphalt concrete, 0.0022 kgf/cm³ for the crushed rock, and 0.0017 kgf/cm³ for the natural soil.

6.2 Results

The variation of the bending stress through the depth of the first (asphalt) layer directly under one of the central wheels is shown in Figure 6.3. The variation of the bending stress and the vertical strain through the depth of the second (granular) layer are shown in Figure .6.4 and Figure 6.5 respectively. Note that the scale on the stresses changes between the first and second layer. Finally the variation of pressure, octahedral shear stress, volumetric strain, and octahedral shear strain are displayed in Figures 6.6, 6.7, 6.8 and 6.9, respectively. The values presented are at element center points. The six different models are plotted using different symbols, as noted in the figure legend. The affect of the nonlinearity is evident in these results.
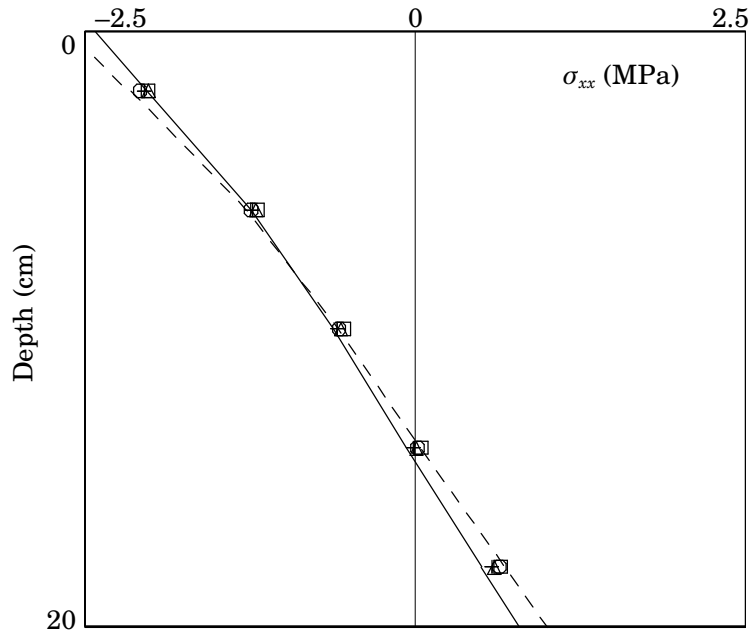
Figure 6.3. Bending stress in the asphalt layer under the wheel: ○ K–Θ model, + Uzan-Witczak model, ▵ *MD* model, □ *AD* model, — Linear Elasticity, – – – No–Tension Elasticity.
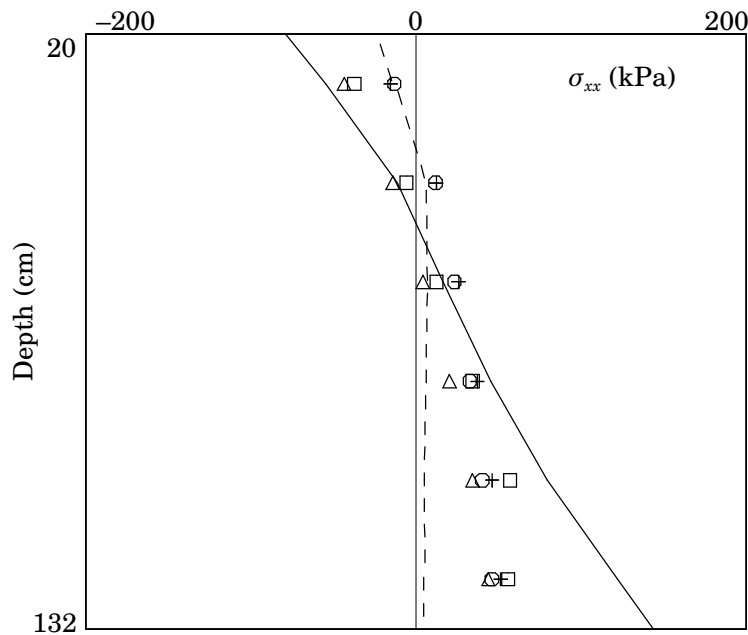
Figure 6.4. Bending stress in the granular layer under the wheel: ○ K–Θ model, + Uzan-Witczak model, ▵ *MD* model, □ *AD* model, — Linear Elasticity, – – – No–Tension Elasticity.
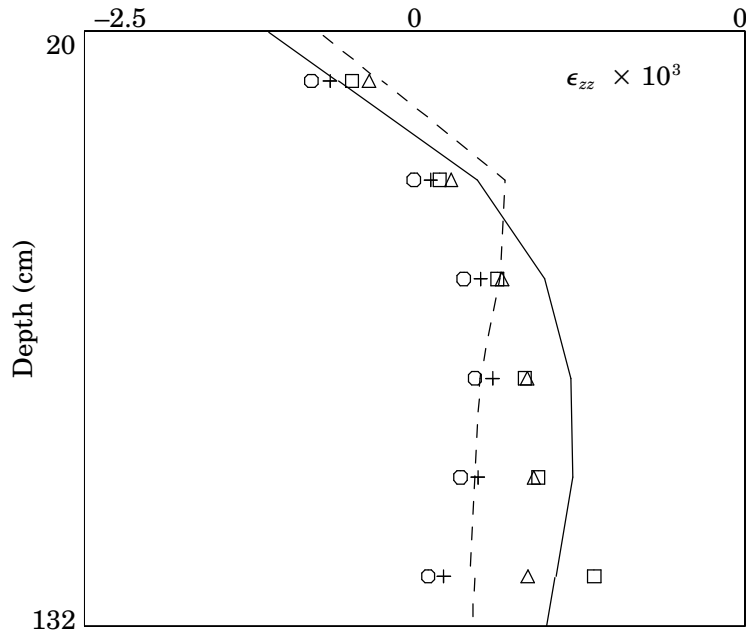
Figure 6.5. Vertical strain in the granular layer under the wheel: ○ K–Θ model, + Uzan-Witczak model, *MD* model, □ *AD* model, —— Linear Elasticity, – – – No–Tension Elasticity.
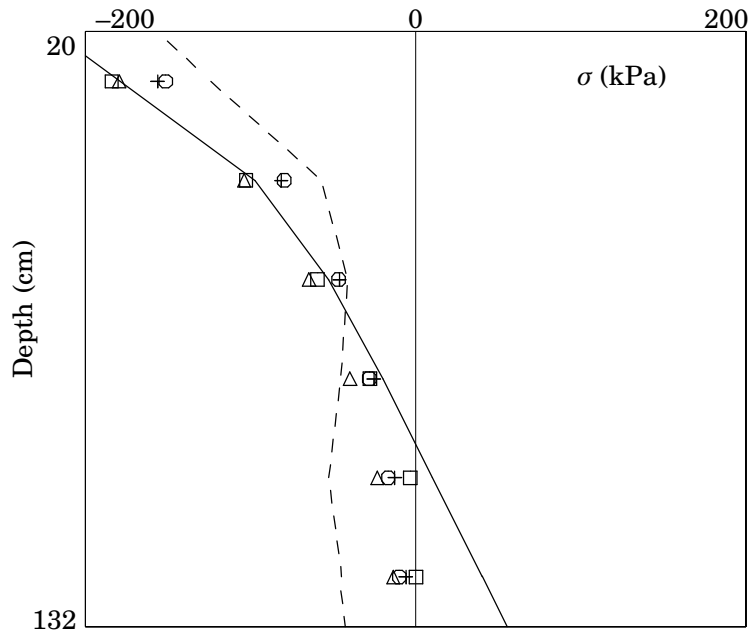
Figure 6.6. Pressure in the granular layer under the wheel: ○ K–Θ model, + Uzan-Witczak model, *MD* model, □ *AD* model, —— Linear Elasticity, – – – No–Tension Elasticity.

6.3 Conclusions

In this chapter, an airport pavement containing a granular layer is analyzed under applied (wheel) loading. In the analysis, the constitutive model governing the behavior of the granular layer is assumed to be one of the following six models : a) Linear Elasticity (b) K– model (c) *Uzan–Witczak* model (d) *AD* model (described in Chapter 3) (e) *MD* model (also described in Chapter 3) and finally (f) the *no–tension elasticity* model described in Chapter 5. It is observed that for all these models (except the Linear Elastic model) the bending stress at the bottom of the first (asphalt) layer is approximately 25 percent more than what is predicted by the Linear Elastic model. The value of this bending stress is an important parameter to be considered when designing pavements. Therefore, since we have also established (in Chapter 4) that all of these nonlinear models yield better fits to experimental data than linear elasticity, one could expect that using Linear Elastic constitutive models to represent the resilient behavior of the granular layers in pavements may yield inaccurate results and designs based on this assumption may prove suboptimal. However, interestingly another important design parameter – vertical strain at the top of the granular layer – turned out to be not so significantly different for any of the models.
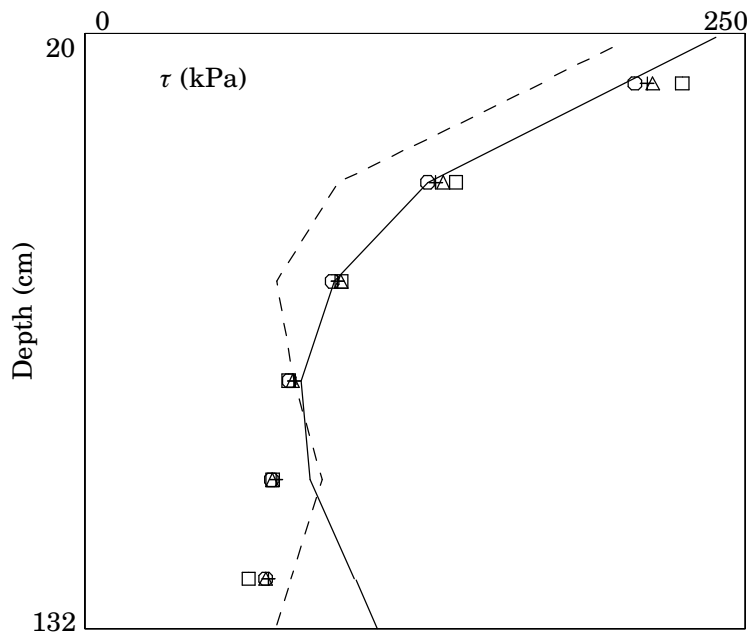
Figure 6.7. Octahedral shear stress in the granular layer under the wheel: ○ K–Θ model, + Uzan-Witczak model, MD model, □ AD model, —— Linear Elasticity, − − − No–Tension Elasticity.

It is also observed that the critical response (i.e. the bending stress at the bottom of the first layer and the vertical strain at the top of the granular layer) of the pavement predicted by all the models (except the Linear Elastic model) were nearly identical. However, as this study alone is not a conclusive one regarding the question "which model one should choose to represent the behavior of the granular layers ?", it is important to point out that for some other pavement configurations (e.g. different thickness for each layer, more layers of different constituents, etc.) it is possible that the nonlinear models may yield significantly different results. This possibility is evident from the fact that even though the response of the top layer was nearly identical for all the nonlinear constitutive models, the response of the granular layer (e.g. pressure, volumetric strain, octahedral shear stress and octahedral shear strain) differed significantly among them. Supporting this argument is the fact that the *K–* and *Uzan–Witzcak* models yielded no hydrostatic tension. This is entirely due to the magnitude of the loading, the geometry of the structure and the particular values of the material constants used in the analysis but not due to any provision in the formulation of these two models that systematically tries to eliminate the built up of hydrostatic tension. Therefore, for higher load levels, one could expect that the *K–* and *Uzan–Witzcak* models will yield tensile hydrostatic pressure within the granular layer, whereas, models like *AD, MD* and *No–Tension Elasticity* will nonetheless try to reduce the tensile hydrostatic pressure within the granular layer.
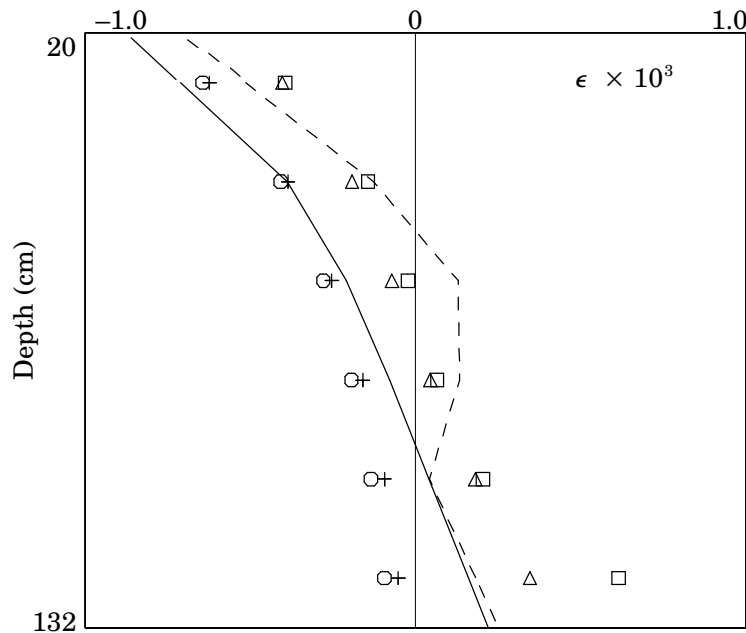
Figure 6.8. Volumetric strain in the granular layer under the wheel: ○ K–Θ model, + Uzan-Witczak model, *MD* model, □ *AD* model, — Linear Elasticity, – – – No–Tension Elasticity.
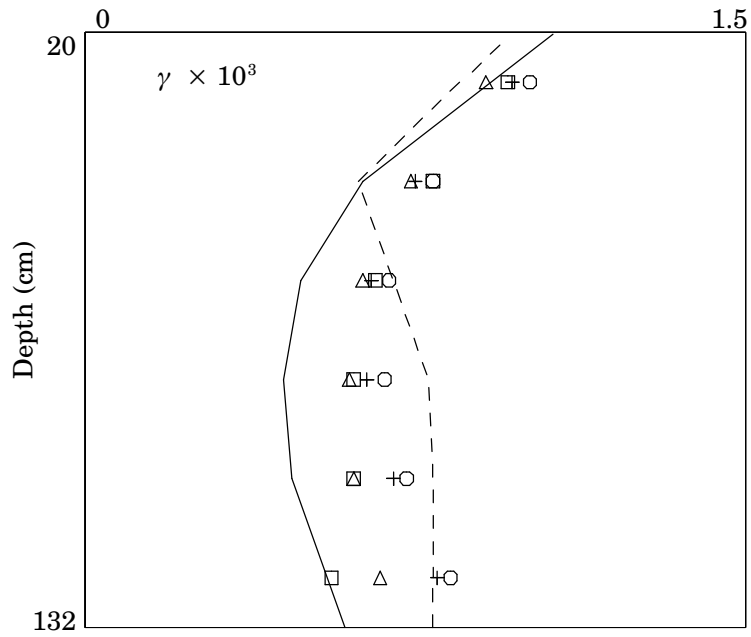
Figure 6.9. Octahedral shear strain in the granular layer under the wheel: ○ K–Θ model, + Uzan-Witczak model, △ *MD* model, □ *AD* model, — Linear Elasticity, – – – No–Tension Elasticity.

Chapter 7

Closure

The conclusions reached in this study have ben presented in the end of every chapter relevant to the topic of each of them, so they will not be repeated here. A few remarks and suggestions for future research will be made instead.

The constitutive models investigated or proposed in this study are calibrated using cyclic triaxial test data alone. The material constants of each of these models can only be determined from experiments in which the lateral strain measurements are made. Unfortunately such experimental data is very scarce. Furthermore, cyclic triaxial tests alone will not be helpful in fully understanding the resilient response; they can not simulate the stress/strain conditions within the granular layers of pavements where dilation may occur. For this, experiments are needed in which a well instrumented pavement, or a laboratory size model of a pavement is loaded repeatedly with actual wheel or compaction loads.

Built–up of residual stresses within the granular layers of pavements during shakedown is inevitable. This is actually what causes shakedown. The fact that pavements, or their granular layers, respond elastically after a relatively few number of load repetitions is an indication of how quickly this process takes place. The presence of residual stresses within the granular layer may well have important implications regarding the overall response of a pavement. The magnitude and the distribution of the residual stresses can be obtained using plasticity models that take into account the shakedown behavior. Such a plasticity model can be formulated with yield criteria in terms of principal stresses. The mathematical machinery needed to achieve such a model is very likely, similar to the ones used in formulating the *no–tension elasticity* model described in Chapter 5. Furthermore, the combination of a plasticity model of this sort and the coupled hyperelastic model presented in Chapter 3 can yield a model which accurately models the response of the granular materials during and after the shakedown. The use of plasticity models provide a natural setting in eliminating tensile stresses from building up in the finite element solutions.

The coupled hyperelastic model can also be used in combination with the no–tension model, as the latter one is applicable to any hyperelastic constitutive model. This combination will yield accurate representation of the portions of the granular layers that are under compression and will approximate failure conditions in the remaining portions.

Furthermore, the coupled hyperelastic model itself can be improved easily be introducing different forms of coupling and different terms to the strain energy density function. As demonstrated in Chapter 4, the coupled model yielded significantly better fits to the experimental data than any of the other models. This was interpreted as an indication of the correctness of the assumption that the volumetric and deviatoric response of granular materials are coupled. As intuition alone is insufficient for developing constitutive models., specific experiments are needed to achieve a coupled hyperelastic model that one can use to determine the specific form and the terms of the strain energy density function.

Bibliography

ABAQUS. (1994). Standard User's Manual, Version 5.4, Volumes 1 & 2. Hibbitt, Karlsson, and Sorensen, Inc. Pawtucket, RI.

Allen, J. J. (1973). *The effects of non–constant lateral pressures on the resilient response of granular materials.* Ph.D. Dissertation, Department of Civil Engineering, University of Illinois, Urbana, IL.

Bathe, K. J. (1982). *Finite element procedures in engineering analysis.* Prentice-Hall, Englewood Cliffs, N.J. pp. 335–345.

Bazant. (1996). *Is No–Tension Design of Concrete Structures Always Safe? — Fracture Analysis,* J. Structural Eng, **122**, pp 2–10.

Boussinesq, J. (1885). *Application des potentiels a l'etude de l'eequilibre et du mouvement des solids elastiques*. Gauthier–Villars, Paris.

Boyce, J. R. (1980). *A nonlinear model for the elastic behavior of granular materials under repeated loading*. Proceedings of the International Symposium on Soils Under Cyclic and Transient Loading, Swansea.

Brown, S. F. and Pappin, J. W. (1981). *Analysis of pavements with granular bases*. Transportation Research Record **810**. pp. 17–23.

Burmister, D. M. (1945). *The general theory of stresses and displacements in layered soil systems, I, II, and III*. Journal of Applied Physics, **16**. pp. 84–94 (I), 126–127 (II), 296–302 (III).

Carlson D. E. and Hoger, A. (1986). *The derivative of a tensor–valued function of a tensor*. Quart. Appl. Math.*, **XLIV**, No. 3, 409–423.

Chen, W. F. and A. F. Saleeb, (1994) *Constitutive Equations for Engineering Materials, Volumes 1 & 2*, Revised Edition, Elsevier.

Crisfield, M. A. (1991). *Non–linear finite element analysis of solids and structures. Volume 1: Essentials*. John Wiley & Sons. pp. 132–134, 154–155.

De Jong, D. L., Peatz, M. G. F. and Korswagen, A. R. (1972). *Computer program BISAR: Layered systems under normal and tangential loads,* Koninklijke Shell–Laboratorium, Amsterdam, External Report AMSR.0006.73.

Del Piero, G. (1989). *Constitutive equation and compatibility of the external loads for linear elastic masonry–like materials*. Meccanica, **24**, 150–162.

Appendix I

Desai, C. S. and H. J. Siriwardane, (1984) *Constitutive Laws for Engineering Materials, With Emphasis on Geologic Materials,* Prentice-Hall, Inc., Englewood Cliffs, New Jersey.

Domaschuk, L., Valiappan, P., (1975). *Nonlinear settlement analysis by finite elements*. Journal of the Geotechnical Engineering , ASCE, **101**(GT7), 601–614.

Duncan, J. M., Monismith, C. L. and Wilson, E. L. (1968). *Finite element analyses of pavements*. Highway Research Record **228**. pp. 18–33.

FAA. (1995). Advisory Circular (AC) No: 150/5320–16. *Airport pavement design for the Boeing 777 airplane.* Federal Aviation Administration, U.S. Department of Transportation, Washington D.C.

Fletcher, R. (1987). *Practical methods of optimization*, Second Edition, John Wiley & Sons. New York.

Guterl, F. (1997), *Riddles in the Sand*, Discover Magazine, November, pp. 104–114.

Halmos, P. R. (1958). *Finite–dimensional vector spaces*. 2nd Ed., D. Van Nostrand, Princeton NJ.

Harichandran, R. S., Yeh, M. S. and Baladi, G. Y. (1971). *MICH–PAVE: A nonlinear finite element program for analysis of pavements*. Transportation Research Record **345**. pp. 15–31.

Harr, M. E. (1977), *Mechanics of Particulate Media — A Probabilistic Approach*, McGraw Hill Book Company, Inc., New York.

Heath, M. T. (1997). *Scientific computing. An introductory survey*. McGraw-Hill. New York.

Hicks, R. G. and Monismith, C. L. (1971). *Factors influencing the resilient properties of granular materials*. Transportation Research Record **345**. pp. 15–31.

Hjelmstad, K. D. (1997A). *Fundamentals of structural mechanics.* Prentice Hall, Upper Saddle River, New Jersey.

Hjelmstad, K. D., J. Kim, and Q. H. Zuo. (1997B). *Finite element procedures for three dimensional pavement analysis*. Aircraft/Pavement Technology: In the Midst of Change (F. V. Hermann, ed.). Proceedings of the ASCE 1997 Airfield Pavement Conference. August 17–20, 1997. Seattle, Washington. pp. 125–137.

Huang, Y. H. (1993). *Pavement analysis and design.* Prentice Hall, Englewood Cliffs, NJ.

Hughes, T. J. R. (1987). *The Finite Element Method.* Prentice-Hall, Englewood Cliffs, N.J..

Izumi, H. K., Kamemura K. and Sato S., (1976). *Finite element analysis of stresses and movements in excavations*. Numerical Methods in Geomechanics, ASCE, 701–712.

Jeffrey, A. (1995). *Handbook of Mathematical Formulas and Integrals.* Academic Press, Inc., San Diego, CA. pp. 394–395.

Appendix I

Kato, T. (1976). *Perturbation Theory for Linear Operators*. 2nd Ed., Springer, Berlin–Heidelberg–New York.

Ko, H. Y., Scott, R. F., (1967). *Deformation of sand in shear.* Journal of the Soil Mech. Foundations Div., ASCE, **93**(SM5), 283–310.

Kooperman, S., Tiller, G. and Tseng, M. (1986). *ELSYM5, Interactive microcomputer version, User's Manual*. Report No. FHWA–TS–87–206, Federal Highway Administration, Washington, D.C.

Lade, P. V., Nelson R. B., (1987). *Modelling the elastic behavior of granular materials*, Int. J. Num. Anal. Methods Geomech., **11**, 521–542.

Lade, P. V., (1988). *Effect of voids and volume changes on the behavior of frictional materials.* Int. J. Num. Analytical Methods Geomech., **12**, pp 331–370.

May, R. W. and Witczak, M. W. (1981). *Effective granular modulus to model pavement responses*. Transportation Research Record **810**. pp. 1–9.

Raad, L. and Figueroa, J. L. (1980). *Load response of transportation support systems*. Transportation Engineering Journal, ASCE, **16** (TE1). pp. 111–128.

Schreyer, H. L. and Zuo, Q. H. (1995). *Anisotropic yield surfaces based on elastic projection operators*. J. Applied Mech., **v. 62**, pp. 780–785.

Simo, J. C. and Taylor, R. L. (1991). *Quasi–incompressible finite elasticity in principal stretches. Continuum basis and numerical algorithms*. Comp. Meth. Appl. Mech Eng*.,* v. **85**. 273–310.

Sokolnikoff, I. S., (1983) *Mathematical Theory of Elasticity,* Krieger Publishing Company, Inc., Malabar, Florida, Reprint Edition, pp. 339–343.

Truesdell, C. and Noll, W. (1965). *The Non–linear Field Theories of Mechanics*, Encyclopedia of Physics*,* **III** / **3**, Springer, Berlin.

Tutumluer, E. (1995). *Predicting behavior of flexible pavements with granular bases*. Ph.D. Thesis. Georgia Institute of Technology.

Uzan, J. (1985). *Characterization of granular materials*. Transportation Research Record **1022**. pp. 52–59.

Warren, H. and Dieckman, W. L. (1963). *Numerical computation of stresses and strains in a multiple–layer asphalt pavement system.* International Report, Chevron Research Corporation, Richmond, CA.

Westergaard, H. M., (1947) *New Formulas for Stresses in Concrete Runways of Airports*, Proceedings, **113**, ASCE.

Witczak, M. W. and Uzan, J. (1988). *The universal airport pavement design system. Report I of V: Granular material characterization*. University of Maryland, Department of Civil Engineering, MD.

Appendix I

Zienkiewicz, O. C., Valiappan, S. and King, I. P. (1968). *Stress analysis of rock as a "no tension" material.* Géotechnique. **18: 50**. 56–66.

Appendix

I. A Brief Overview of ABAQUS UMAT

User subroutines in *ABAQUS* provide an extremely powerful and flexible tool for analysis. The user–defined subroutine *UMAT* enables one to implement material behavior that are not found in *ABAQUS* material library. The use of *UMAT* requires great care. It must perform the intended function without interfering with other functions and without overwriting unintended arrays of *ABAQUS*.

The interface card for the user–subroutine *UMAT* is as follows.

```
 subroutine umat (stress, statev, ddsdde,
&          sse, spd, scd, rpl, ddsddt, drplde,
&          drpldt, stran, dstran, time,
&          dtime, temp, dtemp, predef, dpred,
&          cmname, ndi, nshr, ntens, nstatv,
&          props, nprops, coords, drot,
&          pnewdt, celent,dfgrd0, dfgrd1, noel,
&          npt, layer, kspt, kstep, kinc )
 include 'ABA_PARAM.INC'

 character*8 cmname
 dimension stress(ntens), statev(nstatv),
&          ddsdde(ntens, ntens),
&          ddsddt(ntens), drplde(ntens),
&          stran(ntens), dstran(ntens), time(2),
&          predef(*), dpred(*),
&          props(nprops), coords(3), drot(3, 3),
&          dfgrd0(3, 3), dfgrd1(3, 3)
```

The variables and arrays to be defined by this subroutine are *<ddsdde>* and *<stress>*. The variables and arrays that may be defined optionally are *<statev>*, *<sse>*, *<spd>* and *<scd>*. All the remaining argument variables are passed in for data and overwriting them will cause an error.

The two–dimensional array *<ddsdde>* is the material stiffness matrix. In other words, it is the Jacobian matrix of the constitutive model. The size of this array (per gauss point) is defined by the variable *<ntens>*. This integer–valued variable is generally different for each type of element. For 3–dimensional elements its value is usually 6, for axisymmetric elements it is 5. It also defines the size of the *<stress>* in which the stresses are stored. The subroutine must define every element of *<ddsdde>* regardless of symmetry. If it is

unsymmetrical, user can request in the input file, unsymmetrical storage and solver. This is achieved by specifying in the input file at the header,

```
*HEADING, UNSYMM, ... etc.
```

and in the material definition,

```
*USER MATERIAL, UNSYMMETRIC, ... etc.
```

However, since this will invoke the unsymmetric solver in *ABAQUS* and force *ABAQUS* to use unsymmetric storage the computations will take more time. Note that, *ABAQUS* assumes symmetric storage and solver by default.

The one–dimensional arrays *<stran>* and *<dstran>* contain the strain and incremental strain array respectively. Since the stresses must be computed using the total strain values, for elastic constitutive models, we need to add these two arrays to get the current iterative value of the strain.

The array *<props>* passes the information specified by user in input file. The contents of this array are usually the material parameters. The size of *<props>* is defined by the integer–valued variable *<nprops>* which is also specified in the input file. For example,

```
*USER MATERIAL, CONSTANTS = 7
10000, .35, .22, .7, 50000., 1., 0.
```

where 7 defines the value of *<nprops>* and the seven values in the second card above are the values of the material constants which will be stored in the array *<props>*. For example in our implementation of the *K–* and *Uzan–Witzcak* models these values are *k, , m, n, E, damping_factor*, *secant_switch* (for details see Appendix II).

The use of one dimensional array *<statev>* is optional. One can use this array to store solution dependent values for each gauss point. This array is overwritten after every load increment but *not* at every equilibrium iteration. The size of *<statev>* is defined by the integer–valued variable *<nstatev>* which can be specified in input file via card,

```
*USER MATERIAL, UNSYMMETRIC, ... etc.
... etc.
*DEPVAR
20
```

The value 20 above is the size of *<statev>* array. Thus, *ABAQUS* will reserve space for storing 20 entries for every gauss point. In our implementation of the *K–* and *Uzan–Witzcak* models, we have used this array to store the resilient moduli of every gauss point so that we could use visualization tools (such as *ABAQUS–POST* or *PATRAN*) to plot the resilient modulus distribution for any desired load increment. The values stored in *<statev>* can be output via card in input file

```
*EL FILE
SDV
```

If needed, one can create debug output for user–defined subroutines. This output can be written to *FORTRAN* unit 7 to appear on the .msg file, or to *FORTRAN* unit 6 to appear on the .dat file. *FORTRAN* units 15 through 18 may also be used to read or write other user–specified information. *ABAQUS* manual warns that the use of other *FORTRAN* units may interfere with *ABAQUS* file operations. In our implementation we have chosen unit 7 (.msg file) to write the debug output.

The source code for the *K–* and *Uzan–Witzcak* models discussed in Chapter 2 can be found in Appendix II as an example. The UMAT subroutine for all the other models presented in this manuscript are omitted for brevity.

II. UMAT Source Code for *K–* and *Uzan–Witzcak* Models.

```
      subroutine umat (stress, statev, ddsdde,
     &           sse, spd, scd, rpl, ddsddt, drplde,
     &           drpldt, stran, dstran, time,
     &           dtime, temp, dtemp, predef, dpred,
     &           cmname, ndi, nshr, ntens, nstatv,
     &           props, nprops, coords, drot,
     &           pnewdt, celent,dfgrd0, dfgrd1, noel,
     &           npt, layer, kspt, kstep, kinc )

      include 'ABA_PARAM.INC'

c  Argument variables

      character*8 cmname
      dimension stress(ntens), statev(nstatv),
     &          ddsdde(ntens, ntens),
     &          ddsddt(ntens), drplde(ntens),
     &          stran(ntens), dstran(ntens), time(2),
     &          predef(*), dpred(*),
     &          props(nprops), coords(3), drot(3, 3),
     &          dfgrd0(3, 3), dfgrd1(3, 3)

c  Local variables

      dimension tot_stran(ntens)
      logical   singular

c  Unnamed common block for storing <c_bar> values
      dimension c_bar_old(50000,8,1)
      common c_bar_old

c  **PROLOGUE******UZAN MODEL for SOLID AXY AND PSTN ELEMENTS***********
c  *                                                                 *
c  *    ABAQUS stress & strain notation:                             *
c  *                                                                 *
c  *         stress(1) = S11 = Srr   stran(1) = E11  = Err           *
c  *         stress(2) = S22 = Szz   stran(2) = E22  = Ezz           *
c  *         stress(3) = S33 = Soo   stran(3) = E23  = Eoo           *
c  *         stress(4) = S12 = Srz   stran(4) = 2 * E12 = Erz        *
c  *         stress(5) = S13 = Sro   stran(5) = 2 * E13 = Ero        *
c  *         stress(6) = S23         stran(6) = 2 * E23              *
c  *                                                                 *
c  *                                                                 *
c  *    MATERIAL MODEL DESCRIPTION:                                  *
c  *                                                                 *
c  *      Let [S] denote stress tensor   (3x3)                       *
c  *          [E] denote strain tensor   (3x3)                       *
c  *          [I] denote identity tensor (3x3)                       *
c  *                                                                 *
c  *                                                                 *
c  *------Then constitutive relationship is given by,               *
c  *                                                                 *
c  *         [S] = c_bar * [ alpha  * tr[E] * [I] + [E] ]            *
c  *         Sij = c_bar * [ alpha  * tr[E] * dij + Eij ]            *
```

Appendix II

```
c  *                                                              *
c  *          where,                                              *
c  *             dij: Kronecker delta ( 1 if i=j , 0 if i/=j )    *
c  *                                                              *
c  *             Mr: Resilient Modulus => <res_mod>               *
c  *                                                              *
c  *          c_bar = res_mod / (1 + dnu)                         *
c  *                                                              *
c  *                Mr =  dk * abs(theta)^dn  * (TAUoct)^dm       *
c  *                                                              *
c  *             c_bar = {dk_bar * alpha_bar^dn * (abs(tr[E]))^dn *
c  *                                  *  (gamma_oct)^dm }^ dmu    *
c  *                                                              *
c  *               dk_bar = dk / (1 +dnu)                         *
c  *                                                              *
c  *          dnu: Poisson's Ratio => <props(1)>                  *
c  *                                                              *
c  *           dk: Material param. => <props(2)>                  *
c  *                                                              *
c  *           dn: Material param. => <props(3)>                  *
c  *                                                              *
c  *           dm: Material param. => <props(4)>                  *
c  *                                                              *
c  *            E: Young's Modulus => <props(5)>                  *
c  *                                                              *
c  *         damp: Damping factor  => <props(6)>                  *
c  *                                                              *
c  *       switch: Secant Switch   => <props(7)>                  *
c  *                                                              *
c  *                 switch =  0. => use secant matrix            *
c  *                 switch =/ 0. => use tangent matrix           *
c  *                                                              *
c  *         alpha: dnu / (1 - 2dnu)                              *
c  *                                                              *
c  *     alpha_bar: (1 + dnu) / 3(1 - 2dnu)                       *
c  *                                                              *
c  *           dmu: 1 / (1 - dn - dm)                             *
c  *                                                              *
c  *      singular: a logical flag to mark singularity            *
c  *                                                              *
c  *         tr[E]: 1st invariant of E => <treps>                 *
c  *               tr[E] = Err + Ezz + Eoo                        *
c  *                                                              *
c  *         theta: 1st invariant of stress tensor                *
c  *               theta = Srr + Szz + Soo                        *
c  *                                                              *
c  *        TAUoct: Octahedral shear stress (also an invariant)   *
c  *               TAUoct = {(1/3) * tr[Sd*Sd]} ^ 0.5             *
c  *                                                              *
c  *     gamma_oct: Octahedral shear strain                       *
c  *               (also an invariant)   => <gamma_oct>           *
c  *               gamma_oct = {(1/3) * tr[Ed*Ed]} ^ 0.5          *
c  *                                                              *
c  *          [Sd]: Deviatoric stress tensor                      *
c  *               [Sd] = [S] - 1/3 theta [I]                     *
```

```
c  *                                                                        *
c  *         [Ed]: Deviatoric strain tensor                                 *
c  *               [Ed] = [E] - 1/3 tr[E] [I]                               *
c  *                                                                        *
c  *                                                                        *
c  *------Material tangent stiffness [C]                                    *
c  *                                                                        *
c  *             C     = d([S]) / d([E])                                    *
c  *             Cijkl = d([Sij]) / d([Ekl])                                *
c  *                                                                        *
c  *       thus, with summation implied over repeated                       *
c  *             indices, i;j;k;l = {1,2,3}                                 *
c  *                                                                        *
c  *             Sij = Cijkl Ekl                                            *
c  *                                                                        *
c  *             Cijkl =  c_bar { dik * djl                                 *
c  *                            +  A dij * dkl                              *
c  *                            +  B Eij * dkl                              *
c  *                            +  C dij * Ekl                              *
c  *                            +  D Eij * Ekl }                            *
c  *                                                                        *
c  *       where,                                                           *
c  *             A = alpha * ( dmu * x + 1)                                 *
c  *             B = D * alpha * (tr[E])                                    *
c  *             C = dmu * dm / (3*gamma_oct^2)                             *
c  *             D = dmu * x / (tr[E])                                      *
c  *             x = dn - dm * ( tr[E]/ 3gamma_oct) ^2                      *
c  *                                                                        *
c  *       Or in matrix notation,                                           *
c  *                                                                        *
c  *             vec(S) = mat(C) * vec(E)                                   *
c  *                                                                        *
c  *       where,                                                           *
c  *             vec(S): Stress vector => <stress>                          *
c  *             vec(E): Strain vector => <tot_stran>                       *
c  *             mat(C): Material tnagent dtiffness matrix => <ddsdde>  *
c  *                                                                        *
c  *                                                                        *
c  *                         1   1   1    0   0   0                         *
c  *                         1   1   1    0   0   0                         *
c  *                         1   1   1    0   0   0                         *
c  *             mat(dijdkl) =                                              *
c  *                         0   0   0    0   0   0                         *
c  *                         0   0   0    0   0   0                         *
c  *                         0   0   0    0   0   0                         *
c  *                                                                        *
c  *                                                                        *
c  *                         1   0   0    0   0   0                         *
c  *                         0   1   0    0   0   0                         *
c  *                         0   0   1    0   0   0                         *
c  *             mat(dikdjl) =                                              *
c  *                         0   0   0    .5  0   0                         *
c  *                         0   0   0    0   .5  0                         *
c  *                         0   0   0    0   0   .5                        *
c  *                                                                        *
```

```
c   *                                                                      *
c   *                         E11 E11 E11  0   0   0                       *
c   *                         E22 E22 E22  0   0   0                       *
c   *                         E33 E33 E33  0   0   0                       *
c   *           mat(Eijdkl) =                                              *
c   *                         E12 E12 E12  0   0   0                       *
c   *                         E13 E13 E13  0   0   0                       *
c   *                         E23 E23 E23  0   0   0                       *
c   *                                                                      *
c   *                                                                      *
c   *                         E11 E22 E33   E12 E13 E23                     *
c   *                         E11 E22 E33   E12 E13 E23                     *
c   *                         E11 E22 E33   E12 E13 E23                     *
c   *           mat(dijEkl) =                                              *
c   *                          0   0   0    0   0   0                      *
c   *                          0   0   0    0   0   0                      *
c   *                          0   0   0    0   0   0                      *
c   *                                                                      *
c   *                                                                      *
c   *                             | E11 |                                  *
c   *                             | E22 |                                  *
c   *                             | E33 |                                  *
c   *           mat(EijEkl) = |     | * [E11 E22 E33 E12 E13 E23]          *
c   *                             | E12 |                                  *
c   *                             | E13 |                                  *
c   *                             | E23 |                                  *
c   *                                                                      *
c   *-------NOTES:                                                         *
c   *                                                                      *
c   *          1- Modifications made for improving convergence             *
c   *             characteristics of model are as follows.                 *
c   *             if stran = dstran = 0, instead of returning              *
c   *             the material stiffness, we shall return                  *
c   *             a material secant stiffness, based on the                *
c   *             user supplied property <e> (<props(5)>). This            *
c   *             is achieved by setting A = alpha B=C=D=0 and             *
c   *             c_bar = e / ( 1 + dnu ).                                 *
c   *                                                                      *
c   *             This is done to avoid the singularity of the             *
c   *             global stiffness matrix. The singularity is              *
c   *             due to the fact that,                                    *
c   *                                                                      *
c   *             when  tr(E)=0 or gamma_oct=0                             *
c   *                                                                      *
c   *                Mr = (Mr)' = (Mr)'' = 0                               *
c   *                                                                      *
c   *             This causes problems usually at the first iteration      *
c   *             for equilibrium, since the material stiffness            *
c   *             matrix may have zero eigenvalues, and thus may           *
c   *             become singular. The method described above is           *
c   *             essentialy the following,                                *
c   *                                                                      *
c   *                       | E   FOR 1st iteration                        *
c   *                  Mr =|                                               *
c   *                       | Mr  FOR subsequent iters.                    *
```

```
c  *                                                              *
c  *         2- Another way of improving convergence is to use    *
c  *            a damping factor for the resilient modulus. To     *
c  *            wit, resilient modulus (or c_bar) is updated       *
c  *            as the following,                                  *
c  *                                                              *
c  *              Mr[E(i)] = damp * Mr[E(i-1)] + (1-damp) * Mr[E(i)]  *
c  *                                                              *
c  *            or equivalently,                                   *
c  *                                                              *
c  *              c_bar[E(i)] = damp * c_bar[E(i-1)]               *
c  *                            + (1-damp) * c_bar[E(i)]           *
c  *                                                              *
c  *            where i denotes the i-th iteration.                *
c  *            Note that damp = 1. defaults to the undamped       *
c  *            implementation.                                    *
c  *                                                              *
c  *            This option is allowed only with the secant        *
c  *            formulation. If the user request tangent           *
c  *            formulation the damping will be ignored.           *
c  *                                                              *
c  *         3- Syntax for the input file is,                      *
c  *                                                              *
c  *            *MATERIAL, NAME = <a name>                         *
c  *            *USER MATERIAL, (UN)SYMMETRIC, CONSTANTS = 7       *
c  *              <nu>, <k>, <n>, <m>, <E>, <damp>, <switch>       *
c  *            *DEPVAR                                            *
c  *               1                                              *
c  *                                                              *
c  *          4- Mr value can be output for each element via card  *
c  *             in input file,                                    *
c  *                                                              *
c  *              *EL FILE, POSITION=CENTROIDAL                    *
c  *               SDV1                                           *
c  *                                                              *
c  *             or,                                              *
c  *                                                              *
c  *              *EL PRINT, POSITION=CENTROIDAL                   *
c  *               SDV1                                           *
c  *                                                              *
c  *            Resilient modulus (Mr) will be computed at the     *
c  *            end of each load increment and stored in           *
c  *                                                              *
c  *                <statev(1)> : current resilient modulus value  *
c  *                                                              *
c  *            To make statev operational include in input file   *
c  *            **DEPVAR                                          *
c  *               1                                              *
c  *                                                              *
c  *            Also, note that the resilient modulus that is       *
c  *            computed and output is the actual resilient         *
c  *            modulus (i.e. the one used in updating the          *
c  *            stress) , but NOT the damped one which             *
c  *            might have been used in the secant material         *
c  *            matrix, if damping was requested by the user.       *
```

Appendix II

```
c   *                                                           *
c   ***************************************************END*PROLOGUE*****

c   ***********************************************************************
c   *     copyright  : E. Taciroglu, K. D. Hjelmstad -1997          *
c   *     references : 1- ABAQUS USER'S MANUAL, Ver. 5.4, Vol. II,     *
c   ***********************************************************************

c   Initialize Material Properties

      dnu    = props(1)
      dk     = props(2)
      dn     = props(3)
      dm     = props(4)
      e      = props(5)
      damp   = props(6)
      switch = props(7)

      alpha     = dnu / (1. - 2.*dnu)
      alpha_bar = (1. + dnu)/ ( 3. * (1. - 2. * dnu))
      dmu       = 1. / (1. - dn - dm)
      dk_bar    = dk / (1. + dnu)

c   Get total strain vector and strain invariants tr(E), gamma_oct

      tot_stran(1:ndi)  = stran(1:ndi) + dstran(1:ndi)
      tot_stran(ndi+1:) = (stran(ndi+1:) + dstran(ndi+1:)) / 2.

      treps = tot_stran(1) + tot_stran(2) + tot_stran(3)

      gamma_oct = 0.

      do i=1,ndi
         gamma_oct = gamma_oct + tot_stran(i)**2.
      end do
      do i=ndi+1,ntens
         gamma_oct = gamma_oct + 2.*tot_stran(i)**2.
      end do
      gamma_oct = gamma_oct - treps**2. / 3.
      gamma_oct = sqrt(gamma_oct/3.)

c   Update Resilient modulus

      c_bar = dk_bar * alpha_bar**dn * abs(treps)**dn * gamma_oct**dm
      c_bar = c_bar ** dmu
      res_mod = c_bar * (1. + dnu)

c   Select appropriate modulus value <c_bar> for <ddsdde> and <stress>

      singular = .true.
      do i=1,ntens
         if(tot_stran(i).ne.0.) singular = .false.
      end do

      if(singular) then
```

```
      c_bar = e / ( 1. + dnu)
   elseif (damp.ne.0.AND.switch.eq.0.) then
                          ! damping is not allowed with tangent formulation

      c_bar = damp * c_bar_old(noel,npt,1) + (1. - damp) * c_bar

   end if

c  Update <stress> vector

   stress(1:ndi) = c_bar * ( alpha * treps + tot_stran(1:ndi))
   stress(ndi+1:) = c_bar * tot_stran(ndi+1:)

c  Update tangent stiffnes matrix <ddsdde>

   if(switch.eq.0..OR.singular) then
      a = alpha               ! either actual secant was singular
      b = 0.                  ! or user wants secant
      c = 0.
      d = 0.
   else
      x = dn - dm * (treps/(3.*gamma_oct))**2.
      d = dmu * dm /(3.*gamma_oct**2.)
      a = alpha * (dmu * x + 1.)
      b = dmu * x / treps
      c = d * alpha * treps
   end if

   ddsdde = 0.

   do i=1, ndi
      ddsdde (i,i) = 1.
   end do
   do i=ndi+1 , ntens
      ddsdde (i,i) = 0.5
   end do

   do i=1, ndi
      do j=1,ndi
         ddsdde(i,j) = ddsdde(i,j)
&                 + a + b * tot_stran(i)
&                 + c * tot_stran(j)
&                 + d * tot_stran(i) * tot_stran(j)
      end do
   end do

   do i=1, ndi
      do j=ndi+1,ntens
         ddsdde(i,j) = ddsdde(i,j)
&                 + c * tot_stran(j)
&                 + d * tot_stran(i) * tot_stran(j)
         ddsdde(j,i) = ddsdde(j,i)
&                 + b * tot_stran(j)
&                 + d * tot_stran(j) * tot_stran(i)
      end do
   end do
```

```
      do i=ndi+1, ntens
         do j=ndi+1, ntens
            ddsdde(i,j) = ddsdde(i,j) + d * tot_stran(i) * tot_stran(j)
         end do
      end do

      ddsdde = c_bar * ddsdde

c  Debugging statements (will be written to .msg file)

      if(noel.eq.1121.AND.npt.eq.1) then

         write(7,*) ' **UMAT***********************DEBUG***'
         write(7,*) ' >>>> reporting gauss pt.',npt
         write(7,*)
         write(7,*) ' time(1)   = ', time(1)
         write(7,*) ' time(2)   = ', time(2)
         write(7,*) ' kstep     = ', kstep
         write(7,*) ' kinc      = ', kinc
         write(7,*) ' nu        = ', dnu
         write(7,*) ' k         = ', dk
         write(7,*) ' k_bar     = ', dk_bar
         write(7,*) ' n         = ', dn
         write(7,*) ' m         = ', dm
         write(7,*) ' e         = ', e
         write(7,*) ' damp      = ', damp
         write(7,*) ' switch    = ', switch
         write(7,*) ' alpha     = ', alpha
         write(7,*) ' alpha_bar = ', alpha_bar
         write(7,*) ' dmu       = ', dmu
         write(7,*) ' treps     = ', treps
         write(7,*) ' gamma_oct = ', gamma_oct
         write(7,*) ' c_bar     = ', c_bar
         write(7,*) ' c_bar_old = ', c_bar_old(noel,npt,1)
         write(7,*) ' res_mod   = ', res_mod
         write(7,*) ' statev(1) = ', statev(1)

         if(switch.eq.0.) then
            write(7,*) ' >>> using secant stiffness'
            if(singular) write(7,*) ' >>> (with user supplied <e>) '
         else
            write(7,*) ' >>> using tangent stiffness'
         end if

         if (damp.ne.0.AND.switch.eq.0.) then
            write(7,*) ' >>> stiffness has been damped'
            write(7,*) ' >>>  with, c_bar_old  ='
     &                 , c_bar_old(noel,npt,1)
         else
            write(7,*) ' >>> stiffness has NOT been damped'
         end if

         write(7,*) ' >>> stran :'
         do i=1, ntens
            write(7,100) i, stran(i)
         end do
```

94

```fortran
        write(7,*) ' >>> dstran :'
        do i=1, ntens
           write(7,200) i, dstran(i)
        end do

        write(7,*) ' >>> tot_stran :'
        do i=1, ntens
           write(7,300) i, tot_stran(i)
        end do

        write(7,*) ' >>> stress :'
        do i=1, ntens
           write(7,400) i, stress(i)
        end do

        write(7,*) ' >>> ddsdde :'
        do i=1,ntens
           write(7,500) (ddsdde(i,j), j=1,ntens)
        end do

        write(7,*) ' **END*************************DEBUG***'

      end if

c  Store current resilient modulus

      statev(1) = res_mod

c  Store <c_bar> value to <c_bar_old>

      c_bar_old(noel,npt,1) = c_bar

      return
 100  format(20x,' stran(',i1,') =', e12.4)
 200  format(20x,' dstran(',i1,') =', e12.4)
 300  format(20x,' tot_stran(',i1,') =', e12.4)
 400  format(20x,' stress(',i1,') =', e12.4)
 500  format(10x,6(x,f10.1))
      end
```

III. Data from the Allen–Thompson Experiment

Below is the experimental data from Allen–Thompson Tests (Allen, 1973). Stresses have *psi* units. The sign of the quantities in the tables below are omitted. The correct signs for the vertical stress, lateral stress, vertical strain and the lateral strain are, negative, negative, negative and positive, respectively.

Material Name: HD1

Vertical Stress	Lateral Stress	Vertical Strain	Lateral Strain
7.8	2.0	000401	.000074
11.7	2.0	.000530	.000200
15.9	2.0	.000654	.000310
10.3	5.0	.000300	.000036
14.6	5.0	.000451	.000071
21.1	5.0	.000603	.000160
34.5	5.0	.000869	.000360
44.3	5.0	.001070	.000540
23.5	8.0	.000635	.000046
39.4	8.0	.001000	.000290
55.2	8.0	.001220	.000440
21.7	11.0	.000499	.000071
42.8	11.0	.001000	.000180
64.3	11.0	.001300	.000390
24.7	15.0	.000468	.000073
45.6	15.0	.001070	.000130
59.3	15.0	.001400	.000190
73.8	15.0	.001600	.000330

Material Name: HD2

Vertical Stress	Lateral Stress	Vertical Strain	Lateral Strain
8.2	2.0	.000356	.000041
11.7	2.0	.000423	.000116
15.8	2.0	.000520	.000264
14.7	5.0	.000631	.000052
24.2	5.0	.000972	.000472
34.0	5.0	.001199	.000725
43.6	5.0	.001459	.000944
23.5	8.0	.000794	.000050
39.0	8.0	.001248	.000430
54.2	8.0	.001650	.000950
20.0	11.0	.000374	.000120
41.9	11.0	.000975	.000365
63.1	11.0	.001344	.000914
23.3	15.0	.000496	.000092
42.7	15.0	.000918	.000426

56.1	15.0	.001377	.000528
70.9	15.0	.001574	.000700

Material Name: HD3

Vertical Stress	Lateral Stress	Vertical Strain	Lateral Strain
8.1	2.0	.000334	.000072
11.8	2.0	.000435	.000119
15.6	2.0	.000510	.000167
10.3	5.0	.000201	.000060
14.7	5.0	.000368	.000145
24.3	5.0	.000652	.000180
33.8	5.0	.000786	.000324
44.4	5.0	.000987	.000523
12.2	8.0	.000134	.000047
23.1	8.0	.000418	.000167
39.8	8.0	.000769	.000229
54.2	8.0	.000987	.000373
21.6	11.0	.000334	.000096
42.0	11.0	.000786	.000252
62.5	11.0	.001037	.000314
23.5	15.0	.000201	.000096
42.8	15.0	.000601	.000310
57.4	15.0	.000886	.000343
71.1	15.0	.001003	.000376

Material Name: LD1

Vertical Stress	Lateral Stress	Vertical Strain	Lateral Strain
7.9	2.0	.000620	.000169
12.3	2.0	.000780	.000375
16.0	2.0	.000845	.000502
9.9	5.0	.000390	.000063
14.7	5.0	.000627	.000091
24.7	5.0	.001058	.000229
34.3	5.0	.001220	.000458
44.2	5.0	.001485	.000873
12.1	8.0	.000337	.000048
23.9	8.0	.000820	.000140
39.7	8.0	.001130	.000215
55.0	8.0	.001420	.000550
21.6	11.0	.000580	.000099
43.3	11.0	.001050	.000182
64.9	11.0	.001330	.000335
43.3	15.0	.000940	.000280
57.8	15.0	.001270	.000293
71.9	15.0	.001490	.000439

Material Name: LD2

Vertical Stress	Lateral Stress	Vertical Strain	Lateral Strain
8.0	2.0	.000661	.000119
11.2	2.0	.000780	.000225
15.0	2.0	.000949	.000405
9.6	5.0	.000626	.000059
14.3	5.0	.000864	.000121
24.5	5.0	.001169	.000303
33.3	5.0	.001356	.000630
42.9	5.0	.001644	.000993
11.8	8.0	.000254	.000065
22.8	8.0	.000720	.000194
38.4	8.0	.001356	.000391
53.2	8.0	.001593	.000753
20.8	11.0	.000492	.000135
42.0	11.0	.001153	.000221
63.1	11.0	.001559	.000369
23.4	15.0	.000492	.000099
42.2	15.0	.001085	.000208
56.1	15.0	.001322	.000246
69.8	15.0	.001559	.000309

Material Name: LD3

Vertical Stress	Lateral Stress	Vertical Strain	Lateral Strain
8.1	2.0	.000438	.000094
11.7	2.0	.000572	.000153
15.3	2.0	.000675	.000235
9.7	5.0	.000350	.000049
14.5	5.0	.000623	.000131
24.4	5.0	.000926	.000200
33.6	5.0	.001077	.000475
42.8	5.0	.001549	.000731
11.2	8.0	.000303	.000049
23.5	8.0	.000825	.000196
39.2	8.0	.001212	.000250
54.2	8.0	.001785	.000556
21.5	11.0	.000724	.000075
42.7	11.0	.001246	.000273
64.0	11.0	.001818	.000423
24.7	15.0	.000695	.000123
43.4	15.0	.001145	.000247
56.9	15.0	.001380	.000396
71.7	15.0	.001684	.000471

Material Name: MD1

Vertical Stress	Lateral Stress	Vertical Strain	Lateral Strain
8.0	2.0	.000470	.000230
11.8	2.0	.000740	.000400
15.9	2.0	.000845	.000550
9.9	5.0	.000378	.000049
14.5	5.0	.000612	.000096
24.4	5.0	.000920	.000477
34.2	5.0	.001148	.000700
43.5	5.0	.001268	.000830
11.7	8.0	.000301	.000038
23.1	8.0	.000720	.000200
39.0	8.0	.001148	.000500
54.7	8.0	.001384	.000730
21.6	11.0	.000540	.000072
42.6	11.0	.001050	.000477
64.0	11.0	.001280	.000617
24.4	15.0	.000422	.000048
44.3	15.0	.000980	.000146
58.8	15.0	.001148	.000316
73.2	15.0	.001283	.000436

Material Name: MD2

Vertical Stress	Lateral Stress	Vertical Strain	Lateral Strain
7.7	2.0	.000336	.000114
11.5	2.0	.000487	.000161
15.1	2.0	.000604	.000240
9.7	5.0	.000268	.000074
14.3	5.0	.000536	.000137
23.7	5.0	.000906	.000294
33.1	5.0	.001208	.000553
42.8	5.0	.001527	.001008
12.0	8.0	.000227	.000074
22.7	8.0	.000738	.000248
38.0	8.0	.001174	.000347
53.4	8.0	.001577	.000597
21.1	11.0	.000520	.000075
41.6	11.0	.001275	.000422
62.4	11.0	.001644	.000503
23.6	15.0	.000369	.000173
42.7	15.0	.001040	.000399
57.1	15.0	.001376	.000429
71.1	15.0	.001611	.000527

Material Name: MD3

Vertical Stress	Lateral Stress	Vertical Strain	Lateral Strain
7.6	2.0	.000385	.000107
11.9	2.0	.000544	.000118
15.3	2.0	.000653	.000166
9.3	5.0	.000218	.000091
14.4	5.0	.000436	.000141
23.5	5.0	.000812	.000245
33.3	5.0	.001106	.000462
42.8	5.0	.001407	.000718
11.5	8.0	.000167	.000046
22.6	8.0	.000616	.000179
38.5	8.0	.001105	.000278
54.1	8.0	.001575	.000570
21.8	11.0	.000436	.000146
42.2	11.0	.001122	.000325
63.3	11.0	.001608	.000732
23.8	15.0	.000410	.000065
42.1	15.0	.000955	.000248
57.6	15.0	.001306	.000430
71.0	15.0	.001608	.000584